A Parametric Model for Predicting Submarine Dynamic Stability in Early Stage Design

Lisa Minnick

A thesis submitted to the Faculty of

Virginia Polytechnic Institute and State University

in partial fulfillment of the requirements for the degree of

MASTER OF SCIENCE

in

Ocean Engineering

Dr. Alan J. Brown, Chairman
Dr. Craig Woolsey
Dr. Leigh McCue

April 21, 2006
Blacksburg, Virginia

Keywords: submarine, dynamic stability, design

A Parametric Model for Predicting Submarine Dynamic Stability in Early Stage Design

Lisa Minnick

ABSTRACT

The goal of this thesis is to develop a dynamic stability and control module that can be used in the concept exploration phase of design. The purpose of the module is to determine the hydrodynamic coefficients/derivatives and stability characteristics of a given design. Two tools, GEORGE and CEBAXI and LA_57, were used to model a submarine, calculate its hydrodynamic coefficients, and determine its stability in the horizontal and vertical plane. GEORGE was developed and used heavily at Naval Coastal Systems Laboratory (NSWCPC) in Panama City, FL and the CEBAXI and LA_57 program was developed partially at University of California State at Long Beach and at the Carderock Division of the Naval Surface Warfare Center (NSWCCD) and is in use at NSWCCD in Bethesda, MD. Both programs require the hull offsets and geometry of the control surfaces as input. The hull offsets were determined by assuming an idealistic teardrop shape and a method for sizing control surfaces was developed by using previous designs to determine sizing trends. ModelCenter software was used to integrate the methods to determine the offsets and control surface geometry with the stability programs. A design of experiments was performed to determine the influence of various input variables on the stability indices and response surface models were created. The response surfaces were implemented into a Total Ship Systems Engineering optimization process used in the senior ship design course at Virginia Tech.

Acknowledgements

I would like to express my sincere thanks and appreciation to the following:

Dr. Alan Brown, my chairman, for taking me on as one of his graduate students, for his support and feedback, and being a constant mentor throughout my undergraduate and graduate career.

Dr. Craig Woolsey, my committee member, for his support and willingness to take time to answer any questions I had, especially those relating to stability of underwater vehicles, and taking time to further explain concepts that I needed clarity on.

Dr. Leigh McCue, my committee member, for her support, helpful suggestions, and feedback throughout this whole process.

Jan Crane, my contact at NSWCPC, who was so gracious to answer all of my questions relating to GEORGE and helping me to troubleshoot the discontinuity in the GEORGE data.

Kurt Junghans, Dr. Joan Lewis, and Bowen Jeffries, of the Maneuvering and Controls Division of the Hydromechanics Department at NSWCCD for their hospitality and willingness to help me while I was on-site at NSWCCD using their in-house submarine stability program to collect data.

Dr. Thomas Fu of the Maneuvering and Controls Division of the Hydromechanics Department at NSWCCD for putting me in contact with Kurt Junghanas, Dr. Lewis, and Bowen. Jeffries and being willing to help me with whatever I needed.

Patrick Ryan and **David Cash**, my contacts at Northrop Grumman Newport News Shipyard, for their eagerness to help me, answer any general submarine questions I had, and provide with any other contacts that may be beneficial to me.

All of my **friends** who have been extremely supportive, especially **Tyson Scofield** and **Brook Sherman**, my officemates; **Jesse Panneton** and **Ingrid Shwaiko** for their support and hospitability while I was staying in Washington DC and working at NSWCCD and **Brian Cavanaugh** for his support and assistance while at NSWCCD; **Chris Bassler,** truly one of my best friends, for his endless support and encouragement and **Maria Dunn, James Dreher, Luisa Coppola, Brian Wolyniak, Roger Zalneraitis, Michael Schwandt, Brian Tesson, Jen Suehs, Aimee Schottler, Derek Dupuis, Christy Marr, Dara Ramey, Emily Rhode,** and **Sam Wright** for all their support.

Finally, **my family,** for their continuous support and love throughout this process and in everything that I embark on.

TABLE OF CONTENTS

TABLE OF FIGURES

APPENDIX A

APPENDIX B

TABLE OF TABLES

CHAPTER 1 INTRODUCTION

1.1 Motivation

The ship design process shown in Figure 1 consists of five main stages: Concept Exploration, Concept Development, Preliminary Design, Contract Design, and Detail Design. The concept exploration phase of the design process is detailed in Figure 2 and begins once a mission need has been determined. It involves translating the need into specific engineering terms and design variables, determining technology and design alternatives, and identifying the design space to be used for ship synthesis and optimization. The result is a baseline design that can be analyzed in greater detail during concept development. This thesis focuses on the concept exploration phase of the total design process.

Traditional approaches to submarine design have been guided primarily by experience, design lanes, and rules-of-thumbs. A Total Ship System Engineering (TSSE) approach has been developed at Virginia Tech to be used in early stage design for surface ships and a similar approach is being developed for submarines. The TSSE approach views the ship as a supersystem comprised of various systems, subsystems, and components functioning together to achieve a common objective [3]. The goal is to optimize the total ship over its lifecycle based on the objective attributes of cost, risk, and effectiveness. The current submarine synthesis model developed for this purpose takes into account a number of different design variables such as hullform, propulsion, and combat systems with measures of performance (MOPs) for speed, endurance, and diving depth. However, it does not consider dynamic stability and control.

Dynamic stability is a difficult aspect to include in early stage submarine design. It is dependent on the hydrodynamic coefficients and stability derivatives of the submarine which are functions of a submarine's hullform and control surfaces. These coefficients and derivatives are traditionally determined from analysis and model tests once detailed aspects of the design have been determined and set. In addition, the specifications of each control surface are generally considered during later stages of the design process and therefore not typically a part of the optimization process during concept exploration. The motivation for this thesis is to develop a dynamic stability module that will evaluate stability by considering hullform and control surface parameters early in the design process.

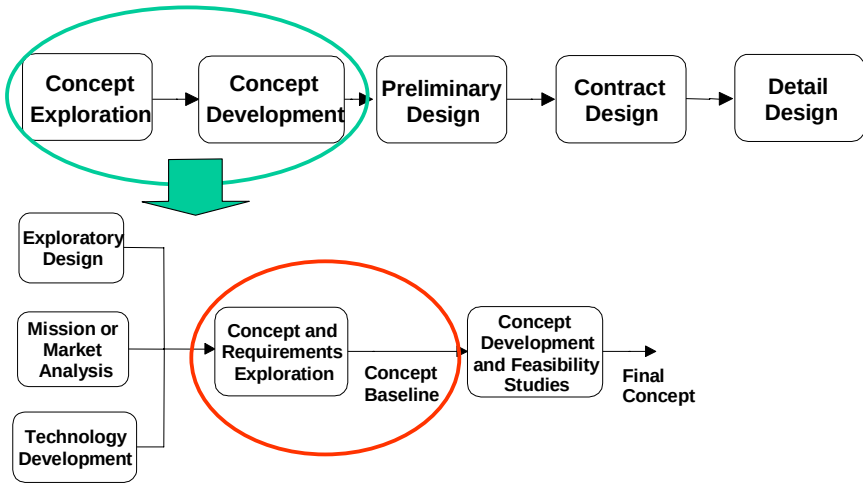

Figure 1. Design Process [1].

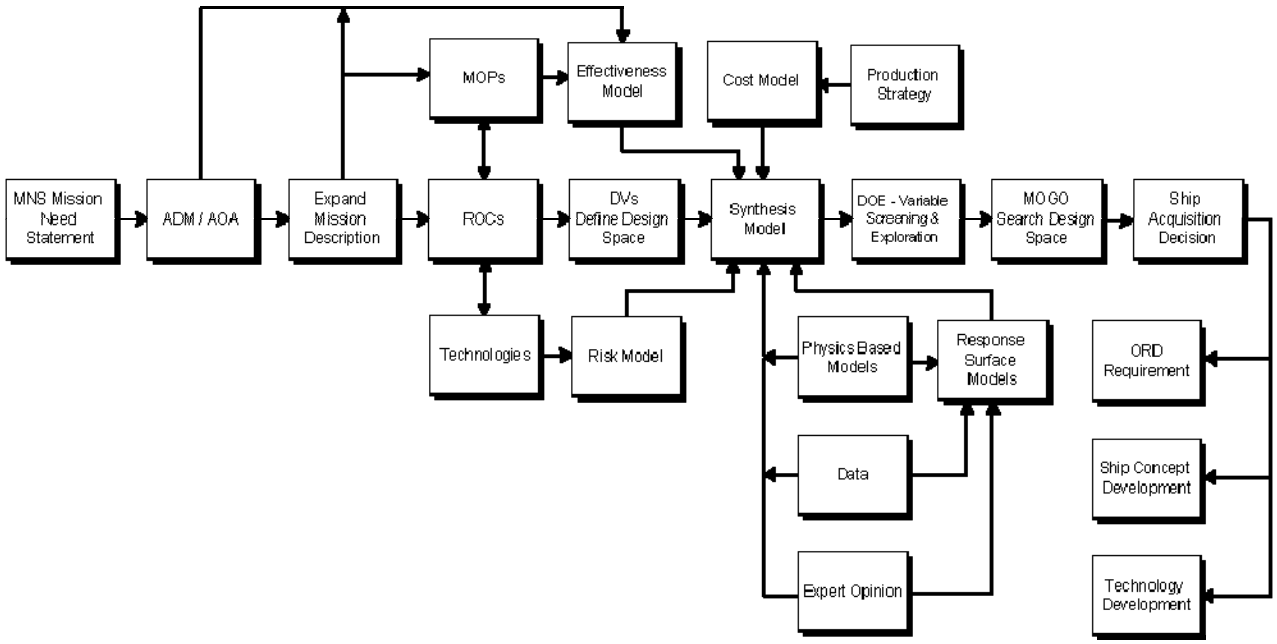

Figure 2. Concept Exploration [1].

1.2 Multi-Objective and Multi-Disciplinary Optimization of Submarines

In early stage design, the design space (i.e. the number of possible combinations and values of the various design variables, either continuous or discrete) is typically very large. Evaluating the performance of designs for even a small portion of this large design space can become prohibitive if the analyses are computationally expensive. Because of this, higher-fidelity codes are typically not used in the early stages of the design process. Major decisions regarding the basic elements of the design are already made before higher-fidelity codes begin to be used.

At Virginia Tech, during the concept exploration phase, a synthesis model is developed and an optimization process is used to aid in exploring the design space. The submarine synthesis model is used to balance and assess designs during optimization. Specific modules in the model (weights, hullform, space available, propulsion, etc.) are developed using FORTRAN, and are integrated and executed in ModelCenter (MC). A Multi-Objective Genetic Optimization (MOGO) is run in MC using a Darwin optimization plug-in. A flowchart for the synthesis model in MC is shown in Figure 3. Each box represents a design module and the lines connecting each module show how the inputs and outputs of the modules relate to one another. The process begins by generating a unique set of inputs that are provided to the individual modules. Within each module a number of functions are performed and outputs are generated. These outputs are then supplied to other modules that rely on those outputs as inputs and are also linked to the last four modules (feasibility, effectiveness, cost, and risk) where effectiveness, cost and risk are the attributes by which each design is measured. These attribute modules then produce their own outputs that are input to the optimizer, which works to maximize the effectiveness of the design while complying with constraints set by the feasibility module and minimizing cost and risk.

Multi-objective optimization of naval ships focuses on three primary objective attributes: life cycle cost, military effectiveness, and the technology risk associated with the design (cost, performance risk, and schedule). In order to carry out the optimization, quantitative objective functions are developed for each specified objective attribute. These functions are developed and described in more detail in Sections 1.2.1, 1.2.2, and 1.2.3.

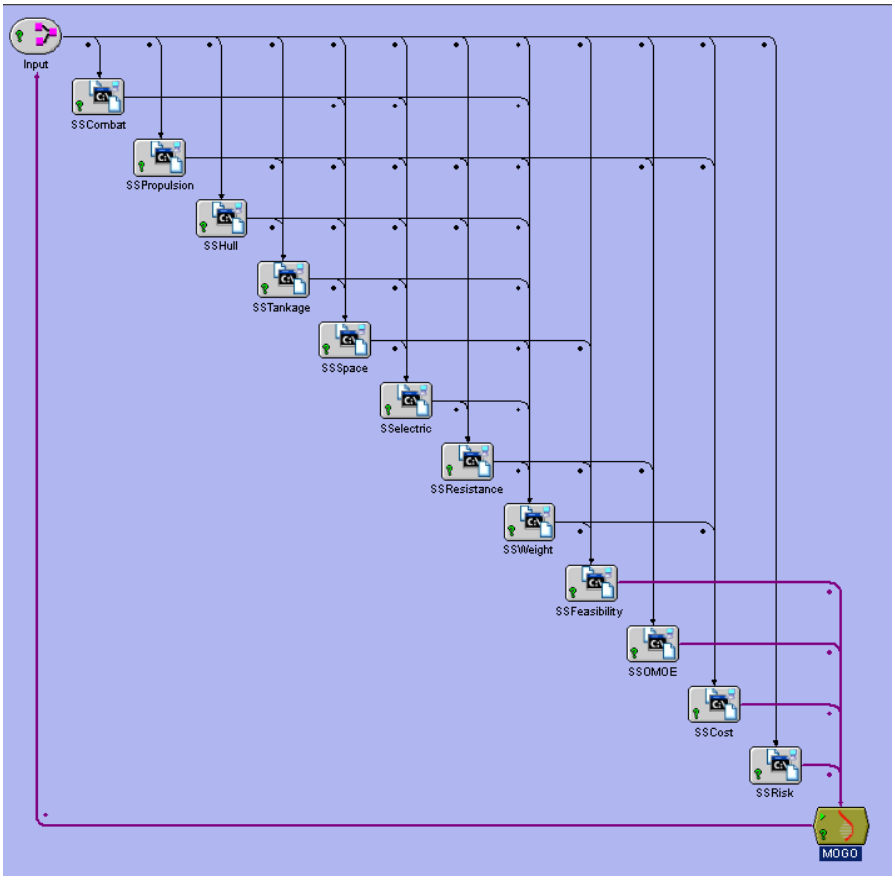

Figure 3. Submarine Synthesis Model in ModelCenter [1].

1.2.1 Overall Measure of Effectiveness (OMOE)

The OMOE is a single overall metric (0.0-1.0) that describes the ship's effectiveness over all assigned mission types. The OMOE value for each design is dependent on individual Measures of Performance (MOPs) and Values of Performance (VOP). Figure 4 shows the process used to develop an OMOE and OMOR (Overall Measure of Risk). The results of this process are OMOE and OMOR functions which represent two of the three objectives considered in this multi-objective optimization process.

MOPs are defined as specific ship or system performance metrics independent of mission. Once the required capabilities of the vessel have been identified from the mission need, MOPs are specified for the required mission capabilities. MOPs are only specified for capabilities that vary in the designs as a function of the design variables. Speed, range, and number of missiles are examples of possible MOPs. In addition, each MOP is given a threshold and goal value

corresponding respectively to the minimum and maximum level of performance. The goal value is typically determined by a technology limitation or as the point of diminishing marginal value.

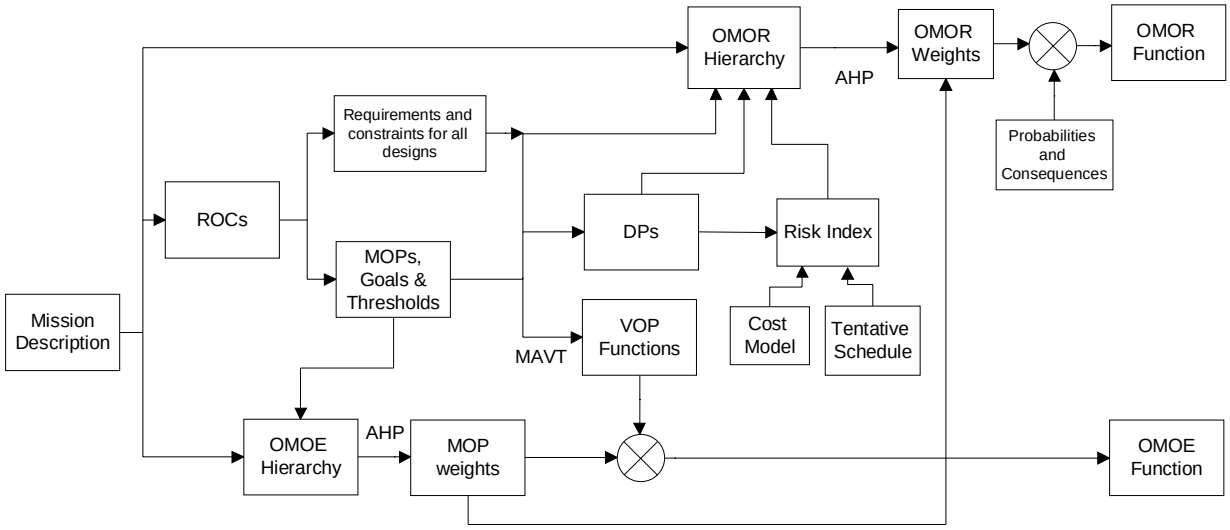

Figure 4. OMOE and OMOR Development Process [1].

An OMOE hierarchy is developed once the required missions for the submarine have been determined. It groups the MOPs defined to assess the submarine's ability to meet its mission requirements into various categories. An example of an OMOE hierarchy is shown in Figure 5. The hierarchy is developed using an Analytical Hierarchy Process (AHP) which involves pair-wise comparison questionnaires that solicit expert and customer opinion. From this hierarchy and process MOP weights are calculated for each MOP and used to develop the individual MOP value functions.

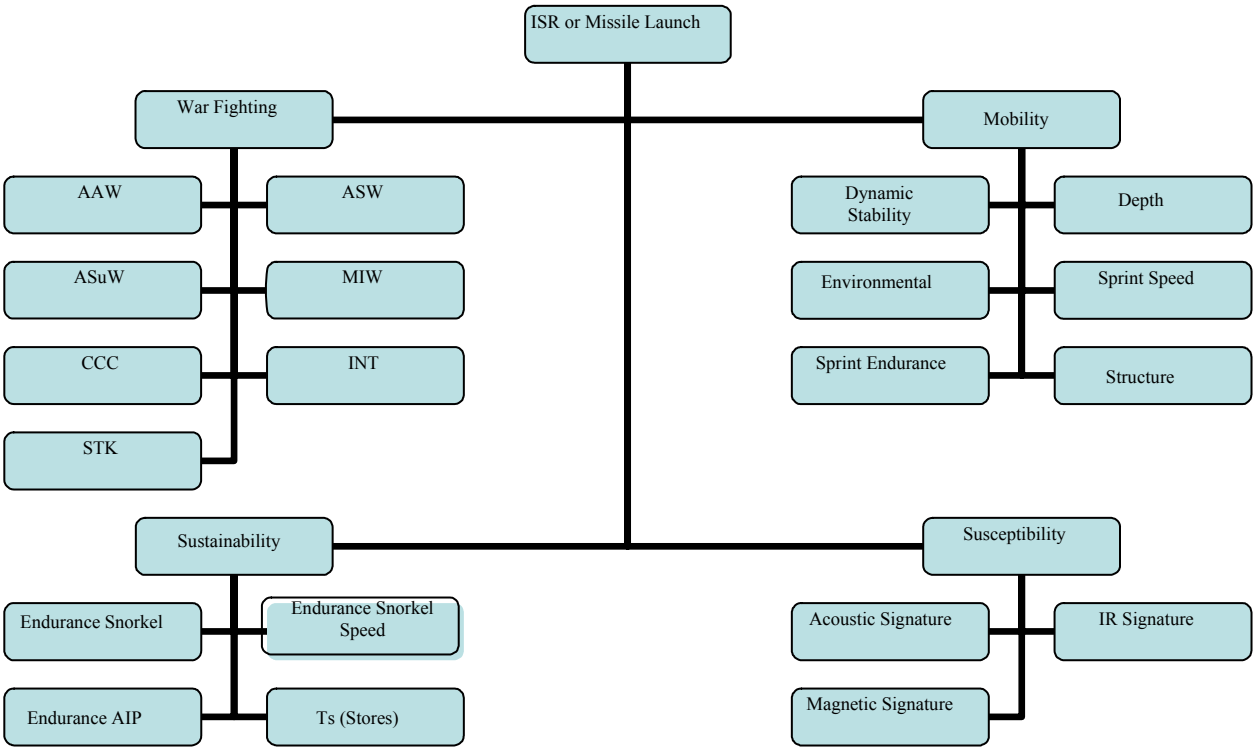

Figure 5. OMOE Hierarchy [1].

Each MOP has a corresponding VOP. A VOP is a figure of merit index ranging from zero to one specifying the value of a specific level of performance. A VOP function, typically an S-curve, is developed for each MOP and used in the ship synthesis model to calculate each VOP. The VOP value of zero corresponds to the MOP threshold while a value of one corresponds to the MOP goal. The MOP weights and VOP functions are combined into a single OMOE function shown in Equation 1:

$$OMOE = g\left[VOP_i\left(MOP_i\right)\right] = \sum_i w_i VOP_i\left(MOP_i\right) \tag{1}$$

1.2.2 Overall Measure of Risk (OMOR)

Three types of technology risk events are considered when calculating the OMOR: performance, cost, and schedule. Once the ship's missions, required capabilities, and technology

options have been defined these options and associated design variables are assessed for their contribution to overall risk. In addition, MOP weights, tentative ship and technology development schedules, and cost predictions are also considered. Risk events are identified with associated design variables, required capabilities, cost, and schedule. Like OMOE, AHP and a pair-wise comparison are performed to gather expert opinion and develop OMOR hierarchy weights. Previously calculated OMOE hierarchy weights associated with risk events are normalized to a total of 1.0 and reused in the OMOR calculations. After risk events have been identified a probability of occurrence, P_i, and consequence of occurrence, C_i, are estimated for each event using the guidelines outlined in Table 1 and Table 2. OMOR is then a function of the weights and probabilities and listed in Equation 2:

$$OMOR = W_{perf} \sum_i \frac{w_i}{\sum_i w_i} P_i C_i + W_{cost} \sum_j w_j P_j C_j + W_{sched} \sum_k w_k P_k C_k \tag{2}$$

Table 1. Event Probability Estimate [1].

Probability	What is the Likelihood the Risk Event Will Occur?
0.1	Remote
0.3	Unlikely
0.5	Likely
0.7	Highly likely
0.9	Near Certain

Table 2. Event Consequence Estimate [1].

Consequence Level	Given the Risk is Realized, What Is the Magnitude of the Impact?		
	Performance	Schedule	Cost
0.1	Minimal or no impact	Minimal or no impact	Minimal or no impact
0.3	Acceptable with some reduction in margin	Additional resources required; able to meet need dates	<5%
0.5	Acceptable with significant reduction in margin	Minor slip in key milestones; not able to meet need date	5-7%
0.7	Acceptable; no remaining margin	Major slip in key milestone or critical path impacted	7-10%
0.9	Unacceptable	Can't achieve key team or major program milestone	>10%

1.2.3 Cost

The components considered in the calculation of the Basic Cost of Construction (BCC) are shown in Figure 6. BCC is dependent on input variables, listed in Table 3, an inflation factor, labor costs, material costs, and total direct and indirect costs. The inflation rate is an average inflation rate based on the number of years between the initial costing and base year. The labor cost is determined using the ship work breakdown structure (SWBS) weights, complexity factors, and the man-hour rate. The material cost is a function of SWBS weights, material cost factors, inflation factor, battery type, propulsion propeller type, and manning and automation factor. The total direct cost is the sum of total labor cost and total material cost. The total indirect cost is determined by multiplying the total direct cost by the overhead rate. The BCC is then determined by summing the total direct and indirect cost and multiplying by one plus the profit margin.

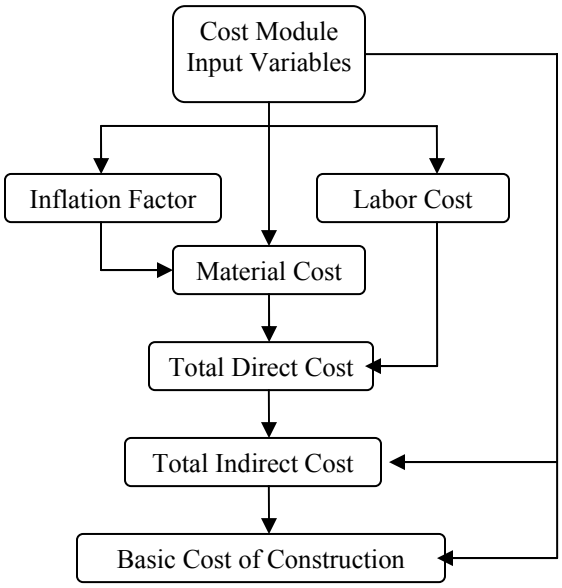

Figure 6. Cost Flowchart.

Table 3. Cost Module Input Variables [1].

Input Variable	Description
W1	SWBS 100 structure weight
W2	SWBS 200 propulsion weight
W3	SWBS 300 electrical weight
W4	SWBS 400 command and control weight
W5	SWBS 500 auxiliaries weight
W6	SWBS 600 outfit weight
W7	SWBS 700 ordnance weight
Yioc	Initial operational capability year
Rp	Shipbuilding rate per year after lead ship
Mh	Average man – hour rate (dollar/hr)
R	Average inflation rate
Yb	Base year (appropriation)
ovhd	Overhead rate
profit	Profit margin
PROPtype	Propulsion propeller type
BATtype	Battery type
PSYS	Propulsion system
Cman	Manning and automation factor

1.2.4 Multi-Objective Genetic Optimization (MOGO) and Results

The optimization is performed in MC based on the three objective attributes previously defined; cost, risk, and effectiveness. A flow chart for a MOGO is shown in Figure 7. Once the design space has been defined the optimizer randomly populates the first design generation with 200 balanced ships using the ship synthesis model. Each of these 200 designs has their own

unique set of design variables that are run through the synthesis model. The model balances each design using the individual modules and then calculates the design's objective attribute values. In addition, feasibility is checked by determining if the resulting design meets the set requirements and constraints. Penalties are given for infeasibility and niching or bunching up the design space. Each design is then ranked relative to one another based on its fitness, which is defined by its dominance in effectiveness, cost, and risk. A second design generation is then randomly selected from the first. Designs with a higher fitness have a higher probability of being selected. From the second generation, twenty-five percent are marked for crossover mutation or swapping of some design variable values. Randomly selected design variable values are then mutated, replaced with a new random value, and re-run through the ship synthesis model. This method allows for exploration across the entire design space and frontier. This is repeated until the maximum number of generations has been met, which is set at 1000, or until convergence occurs. Convergence is defined as the evaluation of 100 generations without any improvement. From the completed optimization a non-dominated frontier (NDF) is defined. Figure 8 shows a 2-D example of a NDF. The figure shows effectiveness vs. cost for given ranges of risk which are denoted by different colors. Each point represents a feasible ship design, denoting the design with the highest effectiveness for a given cost and risk. The "best" design for further analysis in concept development is then determined by the customer's preferences for cost, risk, and effectiveness. A customer typically looks for the "knees" in the curve which are defined as the top of a region where there is a substantial increase in effectiveness for only a small increase in cost. Run 44 circled in Figure 8 is an example of a "knee" in the curve.

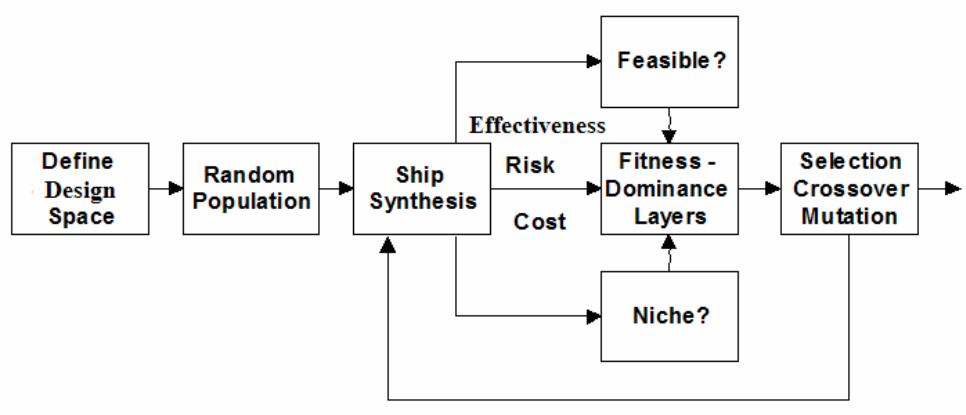

Figure 7. Multi-Objective Genetic Optimization [1].

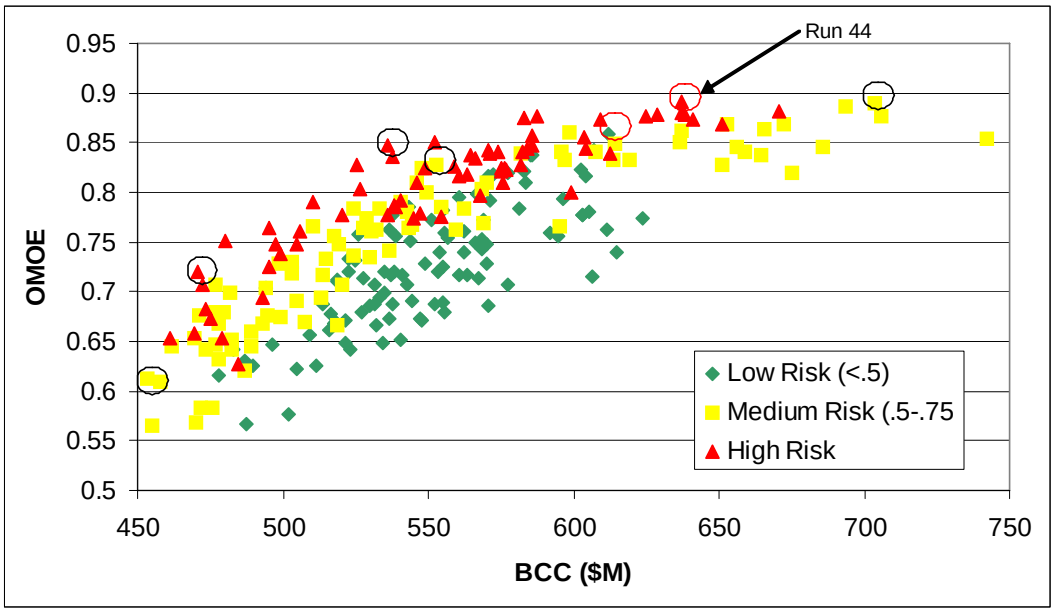

Figure 8. Example of Non-Dominated Frontier [1].

1.3 Submarine Dynamic Stability

The current submarine optimization does not consider dynamic stability and control. Development of a simplified method for the selection of control surfaces and stern configurations, preliminary sizing of the control surfaces, and assessment of vertical and horizontal stability are the primary objectives of this thesis.

The stability of a submarine is defined by its ability to return to an equilibrium state after a disturbance without corrective action. Maneuverability refers to the ability to carry out specific maneuvers. The more stable a vessel is, the more input is needed by the control surfaces to perform a specific maneuver. A balance of stability and maneuverability requires some type of tradeoff. A submarine's dynamic stability is a function of its hydrodynamic coefficients which are a function of the control surfaces present on the submarine and the shape of the submarine.

Figure 9 shows the various kinds of motional stability for submarines. For each case the submarine is assumed to be moving in a straight horizontal path at a constant depth until an instantaneous disturbance occurs. In Case I the final path is a straight line as it initially was, however, it does not retain the same direction or depth as the original path. This is called straight-line stability. Case II represents directional stability. In this case the final path is in the same direction as the initial path, but at a different depth. Therefore, it retains the straight line path and direction of the initial path and it is seen that to achieve directional stability a vessel

must also have straight line stability. Case III is similar to Case II in that the final path is the same that is reached in Case II, however, the vessel does not oscillate after the disturbance as in Case II. This is because the system in Case II is under-damped, having complex eigenvalues that cuase the system to oscillate at a damped frequency before returning to equilibrium. Finally, Case IV represents positional motion stability. In this case the submarine's final path is in the same direction and at the same depth as the initial path. Positional motion stability involves a combination of straight line and directional stability. It is important to note that straight line stability is determined from a second-order differential equation, directional stability from a third-order equation, and positional motion stability from a fourth-order differential equation.

The control surfaces of an underwater vehicle are designed to ensure stability in the horizontal and vertical planes and to provide sufficient control for maneuvering. This thesis only examines controls-fixed stability where the positions of the control surfaces are fixed and not varied. In the horizontal plane with the controls-fixed only straight-line stability can be achieved and as noted above will be determined from a second-order differential equation. Vertical stability can require both straight-line and directional stability. The scope of this thesis is to determine if a given submarine design has stability in both the horizontal and vertical planes.

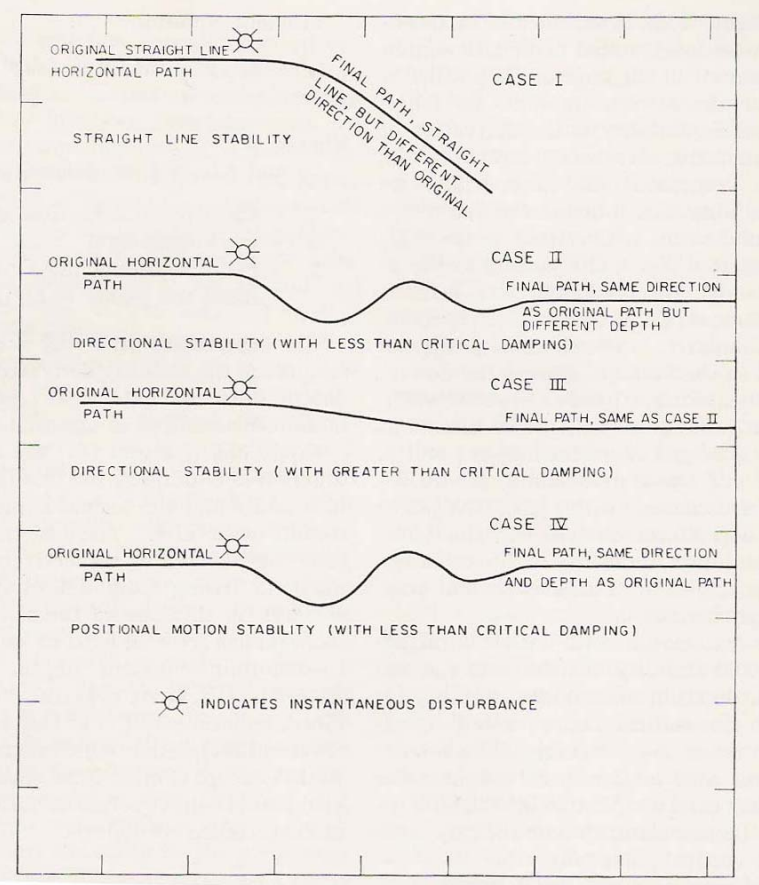

Figure 9. Various kinds of motion stability in the vertical plane [2].

1.4 Thesis Objectives

The primary objectives of this thesis are to:

- Investigate, document and summarize existing literature in evaluating submarine dynamic stability, specifically in early stage design.
- Develop a model to perform preliminary sizing of control surfaces for different control and stern configurations and calculate the hydrodynamic coefficients needed to determine the dynamic stability of a conventional submarine using two different tools.
- Compare the accuracy and effectiveness of the tools utilized.
- Use sensitivity analysis to refine and screen variable inputs to calculate dynamic stability.
- Develop flexible response surface models (RSMs) for estimating submarine dynamic stability in the early stages of design.
- Apply these RSMs to a submarine design optimization case study.
- Assess the results.

1.5 Thesis Outline

Chapter 1 provides an introduction and motivation for this thesis and provides a background on the TSSE design process used at Virginia Tech and submarine dynamic stability.

Chapter 2 summarizes the theory used to develop stability indices used in the analysis of submarine dynamic stability.

Chapter 3 describes the tools used for modeling and analyzing early stage dynamic stability and summarizes the information needed for each tool to calculate the derived stability indices.

Chapter 4 details the process and tools used to perform the sensitivity analysis and variable screening and to develop the response surface models.

Chapter 5 analyzes and discusses the results of the sensitivity analysis and the response surfaces that were created.

Chapter 6 provides a case study for the Conventional Guided Missile (SSG(X)) Submarine.

Chapter 7 presents results and conclusions.

CHAPTER 2 SUBMARINE DYNAMIC STABILITY AND CONTROL SURFACES

2.1 Dynamic Stability

2.1.1 Equations of Motion and Hydrodynamic Coefficients

Figure 10 defines the coordinate system used in this analysis. The origin is placed at the center of gravity (CG) of the submarine. The x-axis is the longitudinal axis and positive towards the bow. The y-axis is the lateral axis and positive starboard and the z-axis, determined by the right-hand rule, is positive downward. The three components of the hydrodynamic forces in the x, y, and z directions are denoted X, Y, and Z respectively while the hydrodynamic torques are denoted by L (roll), M (pitch), and N (yaw) respectively. The components of the velocity in the x, y, and z directions are u, v, w respectively and the angular velocities are p, q, and r as shown in Figure 10.

The hydrodynamic derivatives/coefficients are used to approximate the forces and moments acting on the vessel. This approach assumes that the motions of the body are small deviations from straight line motion. Based on this assumption the forces and moments acting on the body due to a small perturbation can be approximated as directly proportional to the associated small change in velocity. For example, for a small sway velocity, v, the resulting hydrodynamic force in the lateral direction acting on the body, Y, can be approximated by the product $Y_v v$, where Y_v represents the sensitivity of the lateral force to changes in sway velocity and is defined as the partial derivative of the lateral force with respect to the sway velocity evaluated at the nominal condition, $\frac{\partial Y}{\partial v}$, and v is the sway velocity encountered by the vessel. The partial derivative is the hydrodynamic derivative or hydrodynamic coefficient. The hydrodynamic coefficients are useful in determining a submarine's dynamic stability.

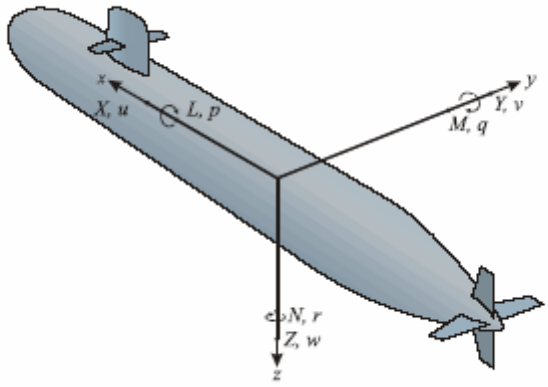

Figure 10. Coordinate Reference Frame Definition [12]

2.1.2 Stability in the Horizontal Plane [13][1]

Stability in the horizontal plane is a submarine's ability to maintain a set course with little variation in heading. A submarine that is dynamically stable in the horizontal plane will not need constant attention from the operator to continuously alter the rudder settings to achieve a straight line path. This section will discuss the equations of motion in the horizontal plane and derive a stability index useful to determining a vessel's dynamic stability in the horizontal plane.

The horizontal stability index is derived assuming straight line motion at a constant forward speed. Since only horizontal motions are of interest, motions in the vertical plane are ignored. Therefore, heave, pitch, and roll motions are set to zero, i.e. w=p=q=0. This reduces the six degree of freedom equations of motions to three degrees of freedom: surge, sway, and yaw as shown in Equations 3, 4, and 5.

$$X = m(\dot{u} - vr) \tag{3}$$

$$Y = m(\dot{v} + ur) \tag{4}$$

$$N = I_{zz}\dot{r} \tag{5}$$

Where: X = total surge force

Y = total sway force

[1] The derivation presented in this section was taken from Volume III of Principals of Naval Architecture.

N = total yaw moment

m = mass of submarine

u = surge velocity

$\dot{u}$ = surge acceleration

v = sway velocity

$\dot{v}$ = sway acceleration

r = yaw rate

$\dot{r}$ = yaw acceleration

I_{zz} = moment of inertia about the z-axis

The left hand side of Equations 3, 4, and 5, which represent the total force and moment in the given degree of freedom, are functions of the surge velocity and acceleration, sway velocity and acceleration, and yaw rate and acceleration:

$$X = F_x(u, \dot{u}, v, \dot{v}, r, \dot{r}) \tag{6}$$

$$Y = F_Y(u, \dot{u}, v, \dot{v}, r, \dot{r}) \tag{7}$$

$$N = F_N(u, \dot{u}, v, \dot{v}, r, \dot{r}) \tag{8}$$

A Taylor series expansion is performed to reduce Equations 6, 7, and 8 into useful mathematical form. An example of the Taylor series expansion for the total sway force is shown below:

$$Y = Y_o + (u-u_o)\frac{\partial Y}{\partial u} + (\dot{u}-\dot{u}_o)\frac{\partial Y}{\partial \dot{u}} + (v-v_o)\frac{\partial Y}{\partial v} + (\dot{v}-\dot{v}_o)\frac{\partial Y}{\partial \dot{v}} + (r-r_o)\frac{\partial Y}{\partial r} + (\dot{r}-\dot{r}_o)\frac{\partial Y}{\partial \dot{r}} \tag{9}$$

The zero subscript denotes values at the nominal condition (straight-line motion with constant forward speed) and each partial derivative is evaluated at this condition. Since the reference condition is constant forward speed, the accelerations are zero, therefore $\dot{u} = \dot{v} = \dot{r} = 0$. Due to port/starboard symmetry v_o=0, $\frac{\partial Y}{\partial u} = \frac{\partial Y}{\partial \dot{u}} = 0$, and Y_o=0. Based on these assumptions Equation 9 becomes:

$$Y = v\frac{\partial Y}{\partial v} + \dot{v}\frac{\partial Y}{\partial \dot{v}} + r\frac{\partial Y}{\partial r} + \dot{r}\frac{\partial Y}{\partial \dot{r}} \tag{10}$$

The same process is applied to the total surge force and yaw moment. For yaw, port/starboard symmetry dictates that $\frac{\partial N}{\partial u} = \frac{\partial N}{\partial \dot{u}} = 0$, therefore the total yaw moment can be represented as:

$$N = v\frac{\partial N}{\partial v} + \dot{v}\frac{\partial N}{\partial \dot{v}} + r\frac{\partial N}{\partial r} + \dot{r}\frac{\partial N}{\partial \dot{r}} \tag{11}$$

Similarly for surge, $\frac{\partial X}{\partial v} = \frac{\partial X}{\partial \dot{v}} = \frac{\partial X}{\partial r} = \frac{\partial X}{\partial \dot{r}} = 0$ because of port/starboard symmetry and the total surge force becomes:

$$X = \frac{\partial X}{\partial u}u + \frac{\partial X}{\partial \dot{u}}\dot{u} \tag{12}$$

Equation 12 shows that surge has been decoupled from sway and yaw and can be neglected for the remainder of the derivation. Substituting Equations 10 and 11 into Equations 3 and 5, rearranging, and applying the derivative notation yields:

$$-Y_v v + (m - Y_{\dot{v}})\dot{v} - (Y_r - mU)r - Y_{\dot{r}}\dot{r} = 0 \tag{13}$$

$$-N_v v - N_{\dot{v}}\dot{v} - N_r r + (I_{zz} - N_{\dot{r}})\dot{r} = 0 \tag{14}$$

These equations are the linearized equations of motion for the sway velocity and yaw rate. It is important to note that there are no added forces or moments due to the control surfaces since controls-fixed stability (zero-angle of attack) is assumed. Equations 13 can be non-dimensionalized by dividing through by $\frac{\rho L^2 V^2}{2}$ and Equation 14 can be non-dimensionalized by $\frac{\rho L^3 V^2}{2}$. The resulting equations are:

$$-Y'_v v' + (m' - Y'_{\dot{v}})\dot{v}' - (Y'_r - m')r' - Y'_{\dot{r}}\dot{r}' = 0 \tag{15}$$

$$-N'_v v' - N'_{\dot{v}}\dot{v}' - N'_r r' + (I'_{zz} - N'_{\dot{r}})\dot{r}' = 0 \tag{16}$$

The superscript prime denotes a non-dimensionalized term. $Y'_{\dot{v}}$ is defined as the virtual mass coefficient and acts like an added mass. It is the hydrodynamic force that is a result of the acceleration of the body through the fluid. Similarly, $N'_{\dot{r}}$ is the virtual moment of inertia coefficient.

Equations 15 and 16 are coupled in sway and yaw, solving this set of linear equations results in a second order linear homogeneous equation. The solution for v' and r' can be determined assuming the standard solution for a second order differential equation:

$$v' = ve^{\sigma t} \tag{17}$$

$$r' = re^{\sigma t} \tag{18}$$

The constants v and r can be determined from initial conditions and e =2.718. Equations 17 and 18 show that for stability the real part of the exponent σ needs to be negative. If the real part of sigma is positive then v' and r' will increase with increasing time and the initial equilibrium state will not be reached. If the real part of σ is negative then v' and r' will decrease with increasing time and the system will return to its initial state.

A relationship between σ and the stability derivatives can be derived by substituting the solutions obtained using Equations 17 and 18 into Equations 15 and 16 and looking at the resulting characteristic polynomial:

$$A\sigma^2 + B\sigma + C = 0 \tag{19}$$

Where the coefficients are defined as:

$$\begin{aligned} A &= (I'_{zz} - N'_{\dot{r}})(m' - Y'_{\dot{v}}) \\ B &= -(I'_{zz} - N'_{\dot{r}})Y'_{v} - (m' - Y'_{\dot{v}})N'_{r} \\ C &= Y'_{v}\,N'_{r} - (Y'_{r} - m')N'_{v} \end{aligned} \tag{20}$$

And σ is determined by the quadratic formula:

$$\sigma = \frac{\left(-B \pm \sqrt{B^2 - 4AC}\right)}{2A} \tag{21}$$

Routh stability criteria [9] requires that the coefficients A, B, and C have the same sign. Experimental data show that A and B are always positive, therefore C must be positive:

$$Y'_{v}\,N'_{r} - (Y'_{r} - m')N'_{v} > 0 \tag{22}$$

Or

$$Y'_{v}\,N'_{r} > (Y'_{r} - m')N'_{v} \tag{23}$$

Dividing through by Y'_{v} and $(Y'_{r} - m')$ yields,

$$\frac{N'_r}{(Y'_r - m')} - \frac{N'_v}{Y'_v} > 0 \tag{24}$$

The first term in Equation 24 is the ratio of the moment due to rotational motion to the force due to rotational motion which can also be seen as a measure of the point of action of the rotational force. The second term is the ratio of the moment due to the sway motion to the force due to sway or the point at which the force due to sway acts. Therefore, Equation 24 requires for stability that the force due to yaw rotational motion act at a point further forward than the force due to sway.

Equation 24 can be modified to represent a stability index,

$$G_H = 1 - \frac{N'_v (Y'_r - m')}{Y'_v N'_r} \tag{25}$$

As long as G_H is positive the submarine is stable. As the index approaches zero the damping ratio decreases, decreasing the stability of the submarine in the horizontal plane. As the index approaches one the submarine becomes more stable, increasing stability while decreasing the submarine's maneuverability characteristics. Based on previous designs and rules of thumb G_H should fall in the range of 0.15 to 0.30 to ensure a good tradeoff between stability and maneuverability.

2.1.3 Stability in the Vertical Plane

Stability in the vertical plane relates to a submarine's ability to maintain a steady depth without continuous activity of the hydroplanes. This characteristic is particularly important at deep submergence when little can be done to vary the external hydrodynamic forces acting on the submarine. Therefore, a submarine's innate dynamic stability plays an important role. This section will discuss the vertical equations of motion and derive a stability index useful in assessing the dynamic stability of a submarine in the vertical plane.

The vertical stability index is derived assuming straight line motion at a constant forward speed. Since only vertical motions are of interest, motions in the horizontal plane are ignored. Therefore, surge, sway and yaw motions are set to zero, i.e. x=y=r=0. This reduces the six degree of freedom equations of motions to three degrees of freedom: heave, roll, and pitch as shown in Equations 26, 27, and 28.

$$Z = m(\dot{w} - qU) \tag{26}$$

$$L = I_{xx}\dot{p} \tag{27}$$

$$M = I_{yy}\dot{q} \tag{28}$$

Where: Z = total heave force

L = total roll moment

M = total pitch moment

m = mass of submarine

U = constant forward velocity

$\dot{w}$ = heave acceleration

q = pitch velocity

$\dot{q}$ = pitch acceleration

$\dot{p}$ = roll acceleration

I_{xx} = moment of inertia about the x-axis

I_{yy} = moment of inertia about the y-axis

The left hand side of Equations 26, 27, and 28, which represent the total force and moment in the given degree of freedom, are functions of the heave velocity and acceleration, roll rate and acceleration, and pitch rate and acceleration:

$$Z = F_Z(w, \dot{w}, p, \dot{p}, q, \dot{q}) \tag{29}$$

$$L = F_P(w, \dot{w}, p, \dot{p}, q, \dot{q}) \tag{30}$$

$$M = F_q(w, \dot{w}, p, \dot{p}, q, \dot{q}) \tag{31}$$

A Taylor series expansion is performed to reduce Equations 29, 30, and 31 into a useful mathematical form. An example of the Taylor series expansion for the total heave force is shown below:

$$Z = Z_o + (w - w_o)\frac{\partial Z}{\partial w} + (\dot{w} - \dot{w}_o)\frac{\partial Z}{\partial \dot{w}} + (p - p_o)\frac{\partial Z}{\partial p} + (\dot{p} - \dot{p}_o)\frac{\partial Z}{\partial \dot{p}} + (q - q_o)\frac{\partial Z}{\partial q} + (\dot{q} - \dot{q}_o)\frac{\partial Z}{\partial \dot{q}} \tag{32}$$

The zero subscript denotes values at the nominal condition (straight-line motion with constant forward speed) and each partial derivative is evaluated at this condition. Since the reference condition is constant forward speed, the accelerations are zero, therefore $\dot{w} = \dot{p} = \dot{q} = 0$. In addition, $Z_o = q_o = w_o = 0$. Due to port/starboard symmetry $\frac{\partial Z}{\partial p} = \frac{\partial Z}{\partial \dot{p}} = 0$. Based on these assumptions Equation 32 becomes:

$$Z = w\frac{\partial Z}{\partial w} + \dot{w}\frac{\partial Z}{\partial \dot{w}} + q\frac{\partial Z}{\partial q} + \dot{q}\frac{\partial Z}{\partial \dot{q}} \tag{33}$$

The same process is applied to the total roll and pitch moments. For pitch, port/starboard symmetry dictates that $\frac{\partial M}{\partial p} = \frac{\partial M}{\partial \dot{p}} = 0$, therefore the total pitch moment can be represented as:

$$M = w\frac{\partial M}{\partial w} + \dot{w}\frac{\partial M}{\partial \dot{w}} + q\frac{\partial M}{\partial q} + \dot{q}\frac{\partial M}{\partial \dot{q}} \tag{34}$$

Similarly for roll, $\frac{\partial L}{\partial w} = \frac{\partial L}{\partial \dot{w}} = \frac{\partial L}{\partial q} = \frac{\partial L}{\partial \dot{q}} = 0$ because of port/starboard symmetry and the total roll moment becomes:

$$L = \frac{\partial L}{\partial p}p + \frac{\partial L}{\partial \dot{p}}\dot{p} \tag{35}$$

Equation 35 shows that roll has been decoupled from heave and pitch and can be neglected for the remainder of the derivation. Substituting Equations 33 and 34 into Equations 26 and 28, rearranging, and applying the derivative notation yields:

$$m(\dot{w} - qU) - Z_{\dot{w}}\dot{w} - Z_w w - Z_q q - Z_{\dot{q}}\dot{q} = 0 \tag{36}$$

$$I_{yy}\dot{q} - M_w w - M_{\dot{w}}\dot{w} - M_\theta\theta - M_q q - M_{\dot{q}}\dot{q} = 0 \tag{37}$$

The hydrostatic restoring moment, M_θ, defined as $M_\theta = W \cdot BG$, is added to Equation 37. BG is the distance between the center of gravity and center of buoyancy, W is the weight of the body, and θ is the angle of pitch. M_θ is independent of speed, however the other terms in Equation 37 (the hydrodynamic terms) are dependent on the speed squared. Therefore, the solution is speed dependent. At high speeds the hydrodynamic terms dominate and the hydrostatic term becomes negligible. In other words, M_θ approaches zero as speed increases. This high speed

approximation reduces the solution to a second-order differential equation and the process used in deriving the horizontal stability index can be used. The high speed approximation is used in this discussion because it essentially models dynamic stability at an infinite speed and it is assumed that if the vessel is stable at infinite speed then it will be stable at all speeds.

Equations 36 and 37 are the linearized equations of motion for the heave velocity and pitch rate. It is important to note that there are no added forces or moments due to the control surfaces since controls-fixed stability (zero-angle of attack) is assumed. Equations 36 can be non-dimensionalized by dividing through by $\frac{\rho L^2 V^2}{2}$ and Equation 37 can be non-dimensionalized by $\frac{\rho L^3 V^2}{2}$. The resulting equations are:

$$m'(\dot{w}'-q') - Z'_{\dot{w}}\,\dot{w} - Z'_{w}\,w - Z'_{q}\,q - Z'_{\dot{q}}\,\dot{q} = 0 \tag{38}$$

$$I'_{yy}\,\dot{q}'-M'_{w}\,w'-M'_{\dot{w}}\,\dot{w}'-M'_{q}\,q'-M'_{\dot{q}}\,\dot{q}' = 0 \tag{39}$$

The superscript prime denotes a non-dimensionalized term. Solving this set of linear equations results in a second order linear homogeneous equation. The solution for w' and q' can be determined assuming the standard solution for a second order differential equation:

$$w' = we^{\sigma t} \tag{40}$$

$$q' = qe^{\sigma t} \tag{41}$$

The constants w and q can be determined from initial conditions and e =2.718. Equations 40 and 41 show that for stability the real part of the exponent σ needs to be negative. If the real part of sigma is positive then w' and q' will increase with increasing time and the initial equilibrium state will not be reached. If the real part of σ is negative then v' and r' will decrease with increasing time and the system will return to its initial state.

A relationship between σ and the stability derivatives can be derived by substituting the solutions obtained using Equations 40 and 41 into Equations 38 and 39 and looking at the resulting characteristic polynomial:

$$A\sigma^2 + B\sigma + C = 0 \tag{42}$$

Where σ is determined by the quadratic formula:

$$\sigma = \frac{\left(-B \pm \sqrt{B^2 - 4AC}\right)}{2A} \tag{43}$$

Routh stability criteria [9] requires that the coefficients A, B, and C have the same sign. Experimental data show that A and B are always positive, therefore C must be positive, where C is defined as:

$$C = M'_q Z'_w - M'_w \left(Z'_q + m'\right) \tag{44}$$

Therefore,

$$M'_q Z'_w - M'_w \left(Z'_q + m'\right) < 0 \tag{45}$$

Or

$$\frac{M'_q}{\left(Z'_q + m'\right)} - \frac{M'_w}{Z'_w} > 0 \tag{46}$$

The first term in Equation 46 is the ratio of the moment due to rotational motion to the force due to rotational motion. The second term is the ratio of the moment due to heave motion to the force due to heave. Therefore, Equation 46 shows that stability requires the force due to pitch rotational motion to act at a point further forward than the force due to the heave motion. Equation 46 can be modified to represent a stability index similar to the horizontal stability index previously derived:

$$G_v = 1 - \frac{M'_w \left(Z'_q + m'\right)}{Z'_w M'_q} \tag{47}$$

As long as G_v is positive the submarine is stable in the vertical plane. As the index approaches one the submarine becomes more stable while as it approaches zero stability decreases. Based on previous designs and rules of thumb G_v should fall in the range of 0.50 to 0.70 to ensure a good tradeoff between stability and maneuverability.

2.1.4 Summary

A stability index for both the horizontal and vertical plane are derived to assess submarine dynamic stability in these planes. A submarine is stable in each plane as long as the value of the corresponding index is positive. As each index approaches zero the submarine becomes less stable and likewise as each index approaches one the submarine becomes more stable. The more stable the submarine the less agile and more difficult to perform some maneuvers, especially those that may need to be taken in emergency situations. Therefore, based on previous designs,

rules of thumb for acceptable ranges of these indices have been defined to allow for a tradeoff between stability and maneuverability. These indices will be used to assess dynamic stability in early stage design.

2.2 Control Surfaces

A submerged submarine has various hydrodynamic forces and moments acting on it at all times. The purpose of a submarine's control surfaces is to provide forces and moments to counteract and change the hydrodynamic forces and moments naturally acting on the hull. The control surfaces can initiate a change in the motion path which may be necessary to perform a specific maneuver or simply to keep the submarine on its intended path. Therefore, as previously discussed, the dynamic stability of a submarine is a function of its hydrodynamic coefficients which are in turn a function of its control surfaces and hullform.

2.2.1 Forward Planes

The forward planes are mainly used for diving purposes and are most useful at low speeds. At high speeds heave and pitch are typically coupled and can be controlled solely through the use of the aft planes. Therefore forward planes are most useful at periscope depth where low speed operations dominate. The forward planes can either be located on the sail, referred to as sail planes, or the body of the submarine, known as bow planes. There are advantages and disadvantages for each configuration.

The presence of forward planes provides a means for controlling the pitch angle and depth independently meaning the submarine can remain level while slowly changing depth. This is achieved by placing the forward planes at a neutral point where the net control force of the aft and forward planes is neutral causing a zero pitching moment. Sail planes therefore become beneficial because due to internal arrangement considerations the sail is often placed far enough forward on the hull that it located near the neutral point. In addition, the narrow beam of the sail allows for the sail planes to have a large aspect ratio and therefore large surface area which influences stability. It is beneficial for the span of any control surface not to exceed the maximum beam of the hull. This eliminates the need for retractable planes which are necessary for alongside operations when the control surface span exceeds the maximum beam of the hull.

To be most effective bow planes should be placed at mid-height of the hullform, parallel to the centerline. This ensures symmetric flow over both planes making each plane equally effective for rising and diving maneuvers. However, to have effective bow planes the span of

each plane needs to extend beyond the maximum beam. Therefore, bow planes need to be retractable which is useful at high speeds because it helps to reduce drag, but introduces the need for a complex control system and room in the bow for the planes to retract into. The presence of bow planes also affects the performance of the aft planes. The forward planes shed tip vortices which are not an issue with sail planes because they are located high enough above the centerline that they are not encountered by the aft planes. Therefore the location of the bow planes on the hull is altered to be closer to the keel rather than on centerline to help counteract this issue.

The forward planes are also useful in emergency situations. Since they produce a pitching moment as well as a rising and diving force they can be used if the aft planes become jammed. However, if bow planes are present and retracted when the aft planes jam then they are less effective than sail planes. Both bow plane and sail plane configurations will be considered in this thesis.

2.2.2 Aft Planes

Horizontal planes, often referred at as stabilizer fins are used to provide vertical plane stability and the vertical planes/rudders provide horizontal stability. Their sizes are also constrained by the maximum beam and diameter of the hullform. The horizontal planes require a large surface area for dynamic stability reasons but not for maneuvering. Therefore, flaps/elevators are added for maneuvering purposes. The proportion of flap area to fin area is used to determine the amount of tradeoff between stability and maneuverability.

The total area of the rudders is also important for stability reasons. The rudders are used for course keeping and providing horizontal stability. The whole surface is typically made to be moveable to allow for fast turning maneuvers. The upper rudder often has a larger span than the lower rudder due to dry dock considerations. The span of the lower rudder cannot fall below the submarine baseline while the upper rudder does not have this constraint. This offset can be beneficial though, asymmetric rudders help to counteract the roll moment generated by the sail.

The traditional stern configuration is a cruciform stern with the horizontal planes parallel to the centerline and upper and lower rudder located at 90˚ angles to the horizontal planes (see Figure 11). This configuration limits the span of the control surfaces and surface area of the planes. Therefore alternative stern configurations have been explored and used in designs. The most common alternate configuration is the x-stern where the planes are offset by 45˚from the cruciform configuration (see Figure 11). This configuration allows for larger surface areas which

is beneficial to stability and is useful in surfaced conditions. With a cruciform stern at surfaced conditions the upper rudder is useless since it is not longer submerged. The x-stern configuration still allows for a pair of surfaces to be submerged and used to control the submarine. One disadvantage of this configuration however, is that the forces generated in the horizontal and vertical planes are symmetric meaning there is little scope for independent adjustment of the stability and maneuvering characteristics of the submarine. Both cruciform stern and x-stern configurations are considered in this thesis.

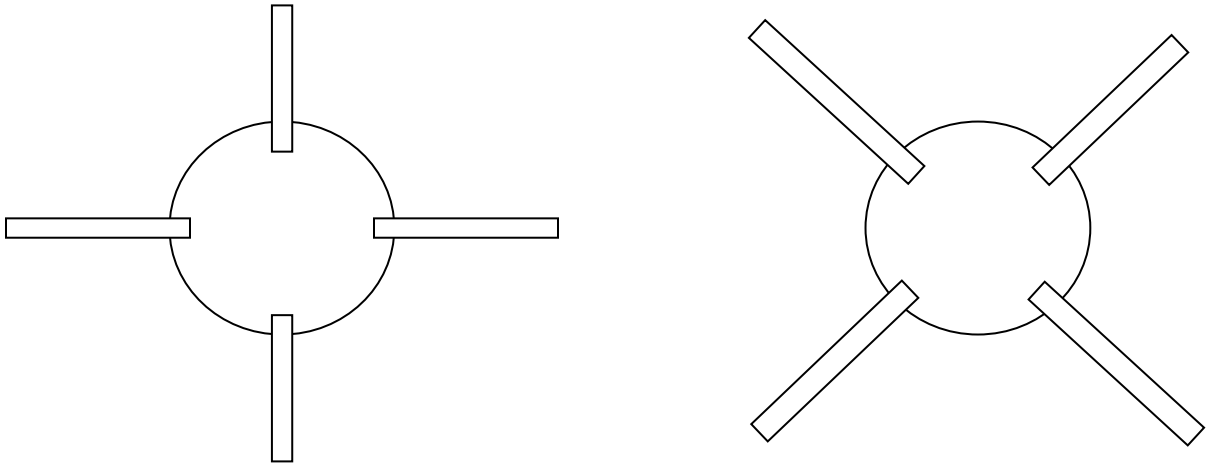

Cruciform Stern, Φ=0˚ X-Stern, Φ=45˚

Figure 11. Stern configurations.

2.2.3 Sail/Fairwater

The sail is completely undesirable for hydrodynamic reasons but very necessary to house radar, visual, and communication equipment. The presence of a sail generates high drag and lift forces. The lift force contributes to the sway and yaw forces and moments on the hull which affects the horizontal stability of the submarine. Therefore, the longitudinal location of the sail is important; if it is located too far forward then stability can be decreased.

The added complications of the drag and lift created by the sail are most seen when turning maneuvers are performed. A sway lift force is generated by the sail during a turn when the hull is in a drift direction. The force acts high above the centerline, creating a heeling moment which in a tight turn can build up and create a “snap roll” which is undesirable for the crew and equipment on board. Turning maneuvers also create a unique interaction between the vortices shed by the sail and the hull which can generate a force and moment on the hull in the vertical plane that can

cause pitch and a change in depth if no action is taken. All configurations analyzed in this thesis will include a sail.

CHAPTER 3 TOOLS USED FOR DETERMINING SUBMARINE DYNAMIC STABILITY

This chapter describes the tools used to calculate the hydrodynamic coefficients and stability indices for a given submarine design. Two different tools are discussed, a program named GEORGE used at the Naval Coastal Systems Laboratory (NCSL) and another program, CEBAXI and LA_57, used at the Naval Surface Warfare Center Carderock Division (NSWCCD). The theory behind each program is discussed with the inputs necessary to run each program.

3.1 GEORGE [10]

3.1.1 Overview

GEORGE is a computer program written in FORTRAN, developed in 1979 in collaboration with the Naval Coastal Systems Laboratory (NCSL) in Panama City, Florida. It is a compilation of methods used to analytically predict the hydrodynamic coefficients from geometric and mass distribution characteristics of an underwater vehicle. GEORGE can be used to analyze both free swimming and towed vehicles. It takes into account control surfaces if input; forward planes and fairwater, and horizontal and vertical (upper and lower) stern planes. It can also model a shroud. If no control surfaces are input then the coefficients calculated are the coefficients for the bare hull only.

The need for GEORGE arose as current research in the areas of design and simulation of towed, tethered, or free swimming vehicles required the calculation of hydrodynamic coefficients. This information is typically determined by model tests which can be both expensive and time consuming. Therefore, GEORGE has proven to be useful during the design phase of a vehicle when design requirements are constantly changing. It provides the designer with the ability to vary the design requirements and inputs and to see how the hydrodynamic coefficients vary without the need of model tests. It offers the assurance of vehicle dynamic stability that model tests provide at a much lower cost.

3.1.2 Input File

GEORGE requires a user defined input file to be run. The input file provides GEORGE with general vehicle information (length, displacement, operating speed etc), a definition of the hullform, and detailed geometry for the control surfaces. The input file also includes control integers which are used to tell the program what information to expect, what information is not needed for analysis, and what information the user wants in the output file. The user has the option to input weight and balance data such as location of center of gravity and buoyancy and moments of inertia or to prompt the program to determine this information by using its internal weight and balance subroutine. The submarine hullform is defined by dividing the hull into stations and defining the longitudinal location and body radius at each station as shown in Figure 12.

Due to this input format GEORGE is constrained to conventional submarine hullforms where providing the body radius at a particular station is sufficient information for defining the hullform. In addition, the input file allows the user to define which control surfaces are present on the vehicle. The user can specify if a sail is present, if forward planes are present and whether they are located on the sail or body, if a tail structure is present (includes horizontal and vertical tail planes), if there is a propulsor shroud, and if the vehicle is attached to a cable. Based on this information GEORGE is able to calculate the vehicle hydrodynamic coefficients.

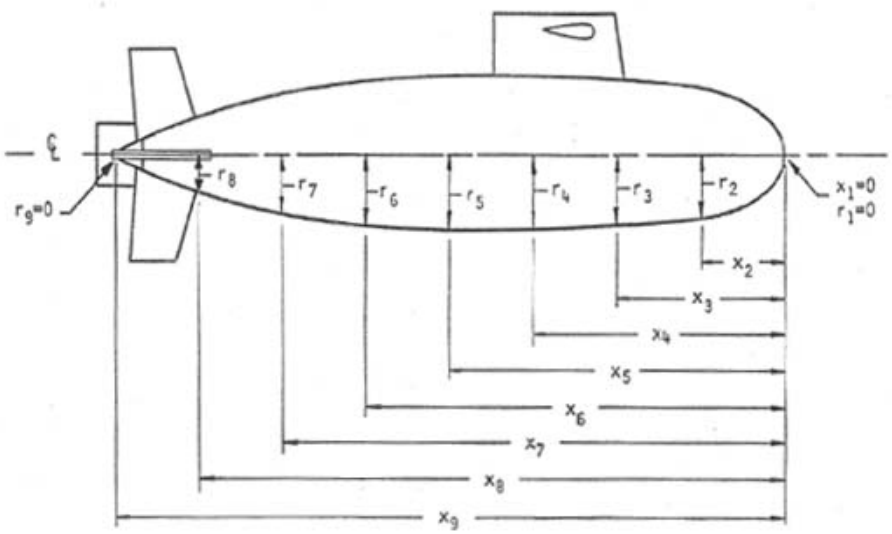

Figure 12. Body station definition [10].

3.1.3 Program Structure

Figure 13 is a block-diagram representation of the program. It shows that GEORGE consists of a main program with a number of subroutines embedded in it. The main program reads and writes the control integers and vehicle input and the weight and balance information. It calculates and writes the bare hull hydrodynamic information and total wind axis derivatives. It also computes the body axis derivatives from the wind axis data and writes the total body derivatives.

The subroutine SWTBAL computes the vehicle weight and balance data if not already input by the user. There is subroutine for each control surface which computes and writes the local stability derivatives for each specific control surface; SSAIL for the sail, SSFWP for the forward planes, STAIL for the horizontal and vertical tail planes, and SSHROUD for the propulsor shroud. The control integers defined in the input file determine which of these subroutines need to be run. Each control surface subroutine calculates the local hydrodynamic coefficients for its specific control surface based on geometry and then transforms the local coefficients from the local axis system to the vehicle axis system. These values of the coefficients are read into the main program and used in the calculation of the total body coefficients. In addition the SCABLE subroutine calculates the cable stability derivatives for towed vehicles. The ADDMASS subroutine computes the component added mass derivatives. The TFLONG and TFLAT subroutines calculate the longitudinal and lateral hydrodynamic transfer functions and roots of the characteristic equation respectively.

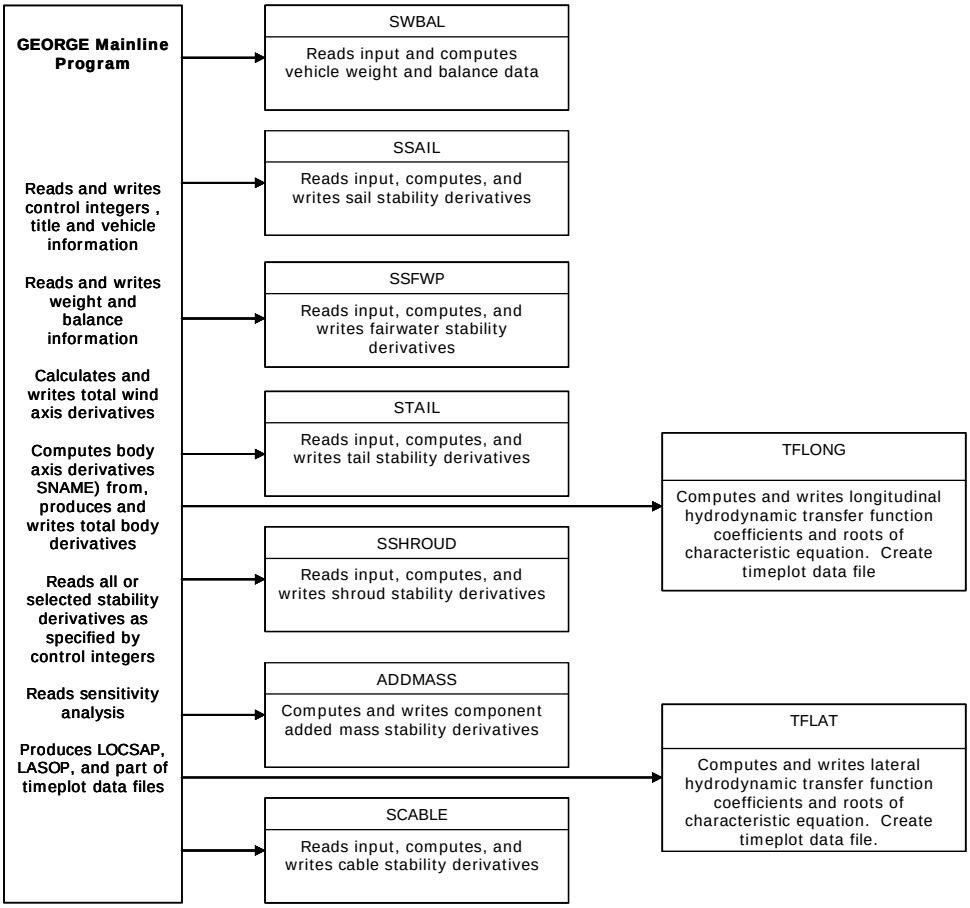

Figure 13. GEORGE Flowchart.

3.1.4 Output File

An output file is created each time GEORGE is run. The output file summarizes the information provided in the input file and provides the desired output information specified in the input file. Specifically, it details the input control integers, input vehicle information and hullform shape as well as the input geometry for each control surface specified. The output includes specific output for each subroutine (mainly the local axis hydrodynamic derivatives for each control surface) and the main program output. For the scope of this thesis the only output of interest are the non-dimensional total body hydrodynamic coefficient/derivatives.

3.2 CEBAXI and LA_57

In addition to GEORGE another submarine stability code was used to determine the stability characteristics of each design. This program is a combination of two codes and is used at the

Naval Surface Warfare Center, Carderock Division (NSWCCD) in Bethesda, Maryland by the Maneuvering and Controls Division of the Hydromechanics Department. These programs are written in FORTRAN and executed sequentially.

3.2.1 CEBAXI

CEBAXI was initially developed by Tuncer Cebeci in the Mechanical Engineering Department at California State University at Long Beach in February of 1978. Since 1978 it has been modified and used by NSWCCD. The program is designed to calculate the incompressible laminar and turbulent boundary layers on plane and axisymmetric bodies. It requires the hull offsets non-dimensionalized by the overall length as input and its output is necessary to run the LA_57 code. CEBAXI requires about 100 stations for the offsets with more stations concentrated along the nose and tail of the submarine to ensure proper approximations of the boundary layer and velocity profiles [7].

3.2.2 LA_57

LA_57 was developed in 1994 by the Maneuvering and Controls Division at NSWCCD. It computes the forces and moments acting on an appended body of revolution. The theory of the code focuses on a mathematical formulation that contains relevant viscous fluid physics, but is simple enough for rapid computation. It uses potential flow theory along the hull and lifting line theory for all appendages. Hull separation is represented by discrete vortices and vortices from the hull and appendages are tracked and interactions are computed. LA_57 requires less input than GEORGE. It uses the output from CEBAXI as input and also needs for each control surface the x-location measured from the nose, span, root chord, and tip chord. This code can model bow planes, sail planes, a fairwater, and different stern configurations [7].

3.3 Control Surfaces Database

To use GEORGE or CEBAXI and LA_57 to calculate the hydrodynamic coefficients of each submarine the geometry of the control surfaces needs to be known. Both programs require detailed information for the fairwater (sail), forward planes, and stern planes. If a fairwater is present, then GEORGE assumes that the forward planes are attached to the fairwater and symmetric about the longitudinal axis. Every configuration considered in this thesis has a fairwater, therefore when GEORGE is used to analyze stability only sail planes will be

considered. CEBAXI and LA_57 can model either bow planes or sail planes. GEORGE considers the stern planes in two categories: horizontal and vertical stern planes. The horizontal stern planes are assumed to be symmetric about the longitudinal axis and it is only necessary to model one plane. Separate information is required by GEORGE for the upper and lower vertical stern planes. CEBAXI and LA_57 require the user to model both the port and starboard horizontal stern planes and upper and lower vertical planes (rudders).

The need for specific information for each control surface causes some complications since these specifics are usually determined during detail design rather than in the concept exploration phase. In addition, the required dimensions of a control surface are typically derived from hydrodynamic equations of motion and model tests. However, in feasibility design where the goal is to arrive at a simplified baseline model to use in detail design, the size of the control surfaces can be determined based on ratios from previous successful designs. A control surface database of the required data was collected based on ten submarine designs that have been built by the US Navy. The purpose of the database was to determine sizing trends for the various control surfaces for use in scaling the control surfaces of each design that is run through the optimizer. A summary of the designs used to create the database is shown in Table 4.

Table 4. Summary of designs measured for control surface database.

Class	Skipjack	Permit	Sturgeon	Seawolf	LA	VA	George Washington	Ben Franklin	Lafayette	Ohio
Length, ft	252	278	292	353	360	377	381.5	425	425	560
Diameter, ft	31	32	32	40	33	34	33	33	33	42
L/D ratio	8.1	8.7	9.1	8.8	10.9	11.1	11.6	12.9	12.9	13.3

Since most submarine data is classified or difficult to obtain the dimensions of each control surface for each of these designs were determined from CAD models found on the webpage: www.combatindex.com [15]. Combatindex.com contains CAD models of numerous military craft developed to the best of the website's knowledge to be as accurate as possible. Since this information was needed only to have a ballpark idea of the size and location of the control surfaces on current vessels, perfect accuracy of the data was not the top priority. In addition, this information is only needed to aid in understanding the initial stability characteristics of each design. The specifics of the control surfaces are determined and adjusted during the concept development phase of the design process. Figure 14 and Figure 15 are top and side views of the

Los Angeles class submarine model measured to create the database. Appendix A shows more samples of the models used to create the database.

Figure 14. Top View of Los Angeles class submarine [15].

Figure 15. Side view of Los Angeles class submarine [15].

For each CAD model used to create the database the overall length and diameter were measured. For each control surface the span, root chord, tip chord, and longitudinal location measured from the nose of the submarine to the forward most point of the control surface were also measured. From these measurements, the average chord and aspect ratio were calculated as shown:

$$c = \frac{c_r + c_t}{2} \tag{21}$$

$$AR = \frac{b}{c} \tag{22}$$

Each of these values (span, root and tip chord, mean chord, and aspect ratio) were then non-dimensionalized by the overall model length. In addition, a control surface parameter, m, was calculated for every control surface on each vessel. The control surface parameter is defined as:

$$m = \frac{LD}{bc} \tag{23}$$

This is an area coefficient used in the past in an MIT submarine design course [6]. Based on this information trends were observed and relationships were determined to use to calculate the information needed by the stability programs.

The following sections give detailed information about the specific geometry needed by GEORGE and CEBAXI and LA_57 for each control surface and a description of the method used to determine these values.

3.3.1 Forward Planes

This section details the geometry of the forward planes that GEORGE and CEBAXI and LA_57 require as inputs.

3.3.1.1 GEORGE

Table 5 summarizes the control surface information needed by GEORGE for the forward planes.

Table 5. Summary of forward plane geometry needed for GEORGE.

Forward Planes	
Variable	**Description**
XNACSA	x-location of the aerodynamic center measured from the nose
ZACSAL	z-location of the aerodynamic center measured from the centerline
TRSAL	taper ratio
BSAL	span
BSALQC	span measured perpendicular to the body centerline at the aerodynamic center
SSAL	total planform area of both surfaces
YACSAL	y-location of the aerodynamic center
ARSAL	total aspect ratio of both surfaces
LAMDSA	sweep angle in degrees
DIHDSA	dihedral angle in degrees
IDSAL	incidence angle in degrees
FWDIA	fairwater thickness or body diameter at fwd plane quarter chord
NTACH	attached in a conventional or non-conventional manner
CL0SAL	zero angle of attack lift coefficient
CD0SAL	zero angle of attack drag coefficient
CM0SAL	zero angle of attack moment coefficient
DEDA	tail downwash angle with respect to change in vehicle angle of attack
DWD	tail downwash angle
TOCSAL	thickness to chord ratio
ANSWER	forward planes are fixed or movable

Figure 16 and Figure 17 provide a graphical definition of the forward plane geometry. The z-location of the aerodynamic center is negative if the aerodynamic center is above the centerline. Since the forward planes are assumed to be symmetric about the longitudinal axis only one plane

is modeled, however, the value provided for the planform area and aspect ratio should be the value for the two planes combined. For the scope of this thesis the dihedral and incidence angle is zero. The variable FWDIA is used for the calculations necessary to include the K_b-K_w effect which accounts for the interference factor between the body and the planes. If FWDIA is set to zero, the body diameter necessary for the K_b-K_w calculations is determined by the program, therefore, this value is always set to zero. NTACH refers to the attachment of the forward planes. Conventional attachment is defined as planes that are attached to the body on the body plane of symmetry. The forward planes are attached to the sail as shown in Figure 16 and Figure 17 rather than the body therefore the forward planes are considered to be attached in a non-conventional way. The forward planes are assumed to be NACA 0020 airfoils. Since this is a symmetric airfoil the zero angle of attack lift and moment coefficients are always zero and the thickness to chord ratio is 0.20. The variables DEDA and DWD refer to the velocity field produced by the forward planes that can affect the angle of attack of any control surfaces aft of the forward planes. Since only controls fixed stability is considered for the scope of this thesis the angle of attack for every control surface is set to zero and the downwash has no effect on planes aft of the forward planes, therefore these variables are always set to zero.

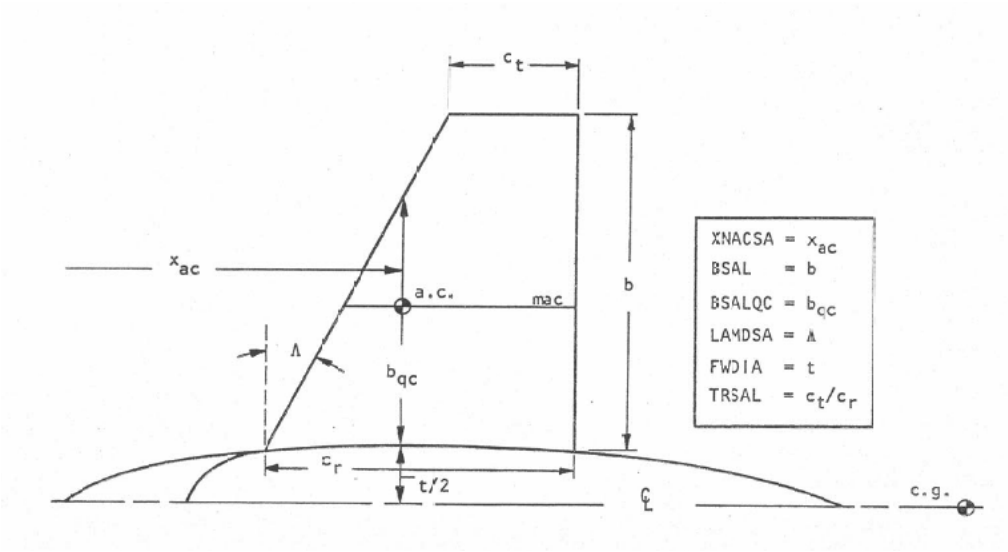

Figure 16. Forward plane attached to fairwater geometry, top view [10].

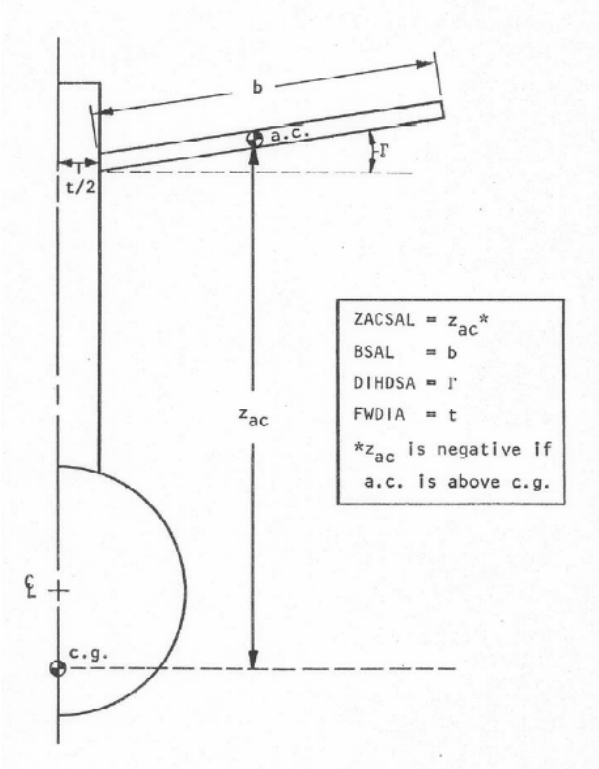

Figure 17. Forward plane attached to fairwater geometry, end view [10].

3.3.1.2 CEBAXI and LA_57

CEBAXI and LA_57 require the x-location, span, root chord, and tip chord of the forward planes be provided as input. The x-location of the forward planes is measured from the bow of the submarine. The user can decide if bow planes or sail planes will be modeled. If sail planes are modeled then the height of the sail planes above the centerline needs to be specified as well as the information previously noted.

3.3.2 Fairwater Geometry

This section details the fairwater/sail geometry required as inputs by GEORGE and CEBAXI and LA_57.

3.3.2.1 GEORGE

Table 6 summarizes the fairwater geometry needed by GEORGE.

Table 6. Summary of fairwater geometry needed for GEORGE.

Fairwater	
Variable	**Description**
XNACFW	x-location of the aerodynamic center measured from the nose
ZACFWP	z-location of the aerodynamic center measured from the centerline
TRFWP	taper ratio
BFWP	span
BFWPQC	span measured perpendicular to the body centerline at the aerodynamic center
SFWP	planform area
ARFWP	aspect ratio
LAMDFW	sweep angle in degrees
EFFFWP	fairwater efficiency
XOCHFW	x-distance from fairwater leading edge to fwd plane aerodynamic center divided by fairwater chord at fwd plane aerodynamic center
ZOBHFW	z-distance from hull to aerodynamic center of fwd plane divided by the exposed span of the fairwater
CL0FWP	zero angle of attack lift coefficient
CD0FWP	zero angle of attack drag coefficient
CM0FWP	zero angle of attack moment coefficient
TOCFWP	thickness to chord ratio

Figure 18 and Figure 19 provide a graphical definition of the fairwater geometry. The z-location of the aerodynamic center is negative if the aerodynamic center is above the centerline. For the scope of this thesis the dihedral and incidence angle is always zero. The efficiency of the fairwater is always assumed to be 1. Like the forward planes the fairwater is assumed to be a NACA 0020 airfoil. Therefore, the zero angle of attack lift and moment coefficients are always zero and the thickness to chord ratio is 0.20.

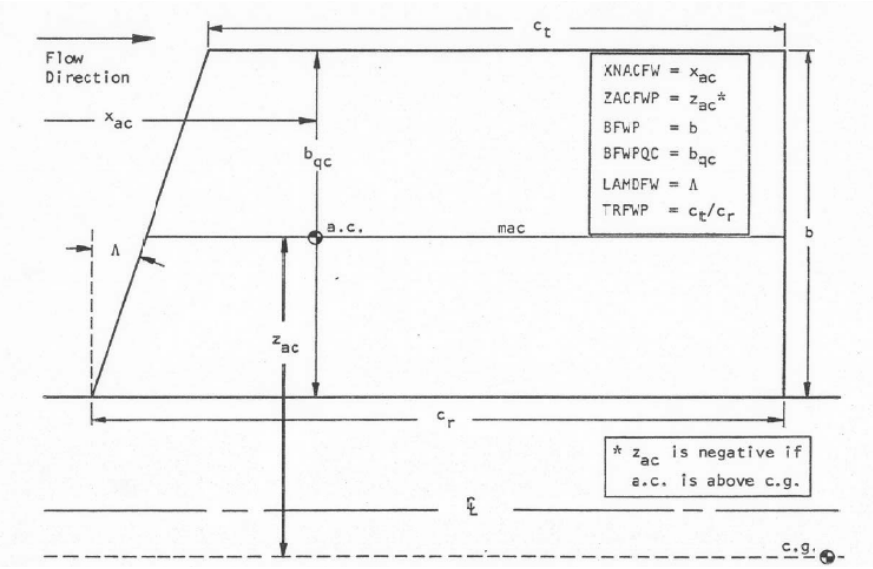

Figure 18. Fairwater geometry, side view (bow is to the left) [10].

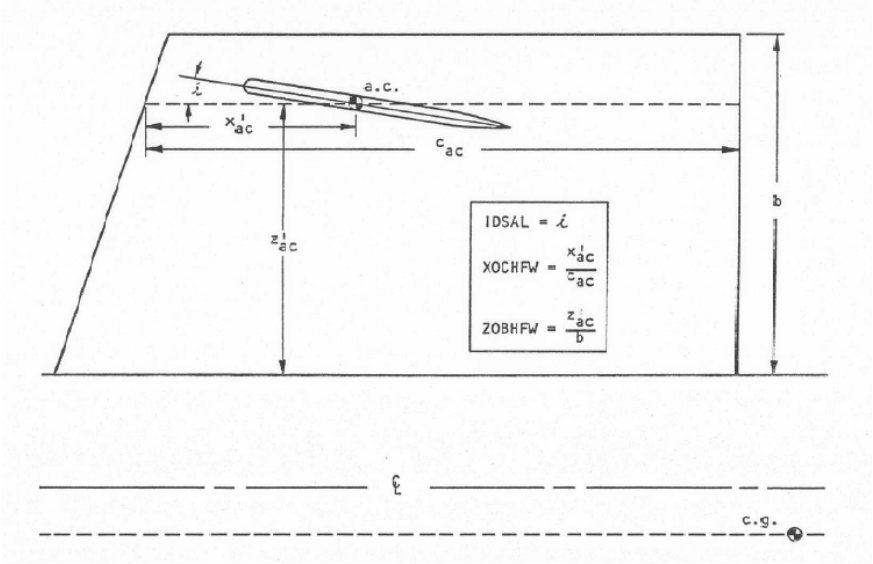

Figure 19. Fairwater geometry with forward planes attached, side view (bow is to the left) [10].

3.3.2.2 CEBAXI and LA_57

CEBAXI and LA_57 require the x-location, span, root chord and tip chord of the fairwater be provided. The x-location is measured from the bow of the submarine.

3.3.3 Horizontal Stern Planes

This section details the geometry of the horizontal stern planes required by GEORGE and CEBAXI and LA_57 as inputs.

3.3.3.1 GEORGE

Table 7 summarizes the geometry needed by GEORGE for the horizontal stern planes.

Table 7. Summary of horizontal stern plane geometry needed for GEORGE.

Horizontal Stern Planes	
Variable	**Description**
XNACTE	x-location of the aerodynamic center measured from the nose
ZACTE	z-location of the aerodynamic center measured from the centerline
TRTE	taper ratio
BTE	span
BTEQC	span measured perpendicular to the body centerline at the aerodynamic center
STE	planform area of both port and starboard horizontal planes
YACTE	y-location of aerodynamic center
ARTE	total aspect ratio of both surfaces
LAMDTE	sweep angle in degrees
DIHDTE	dihedral angle in degrees

Variable	Description
IDTE	incidence angle in degrees
EFFTE	horizontal plane efficiency
NTACH	attached in conventional or non-conventional manner
CL0TE	zero angle of attack lift coefficient
CD0TE	zero angle of attack drag coefficient
CM0TE	zero angle of attack moment coefficient
PHITE	angle of rotation
TOCTE	thickness to chord ratio

Figure 20 and Figure 21 provide a graphical definition of the horizontal stern plane geometry. The z-location of the aerodynamic center is negative if the aerodynamic center is above the centerline. Since the horizontal planes are assumed to be symmetric about the longitudinal axis only one plane is modeled however, the value provided for the planform area and aspect ratio should be the value for the two planes combined. For the scope of this thesis the dihedral and incidence angle is always zero. The efficiency of the horizontal planes is always assumed to be one. NTACH refers to whether the horizontal planes are attached in a conventional or non-conventional manner. Like the forward planes, conventional attachment is determined as planes that are attached to the body on the body plane of symmetry. Therefore the horizontal planes are always attached in a conventional manner. The horizontal planes are assumed to be NACA 0020 airfoils, therefore, the zero angle of attack lift and moment coefficients are always zero and the thickness to chord ratio is 0.20. The angle Φ is used to model different stern plane configurations; more detail is provided Section 3.2.4.

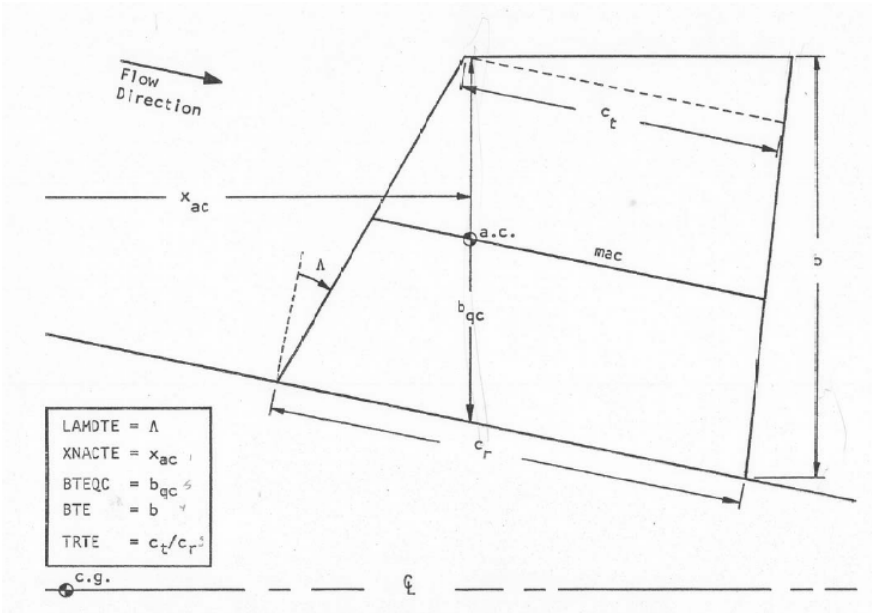

Figure 20. Horizontal stern plane geometry, top view [10].

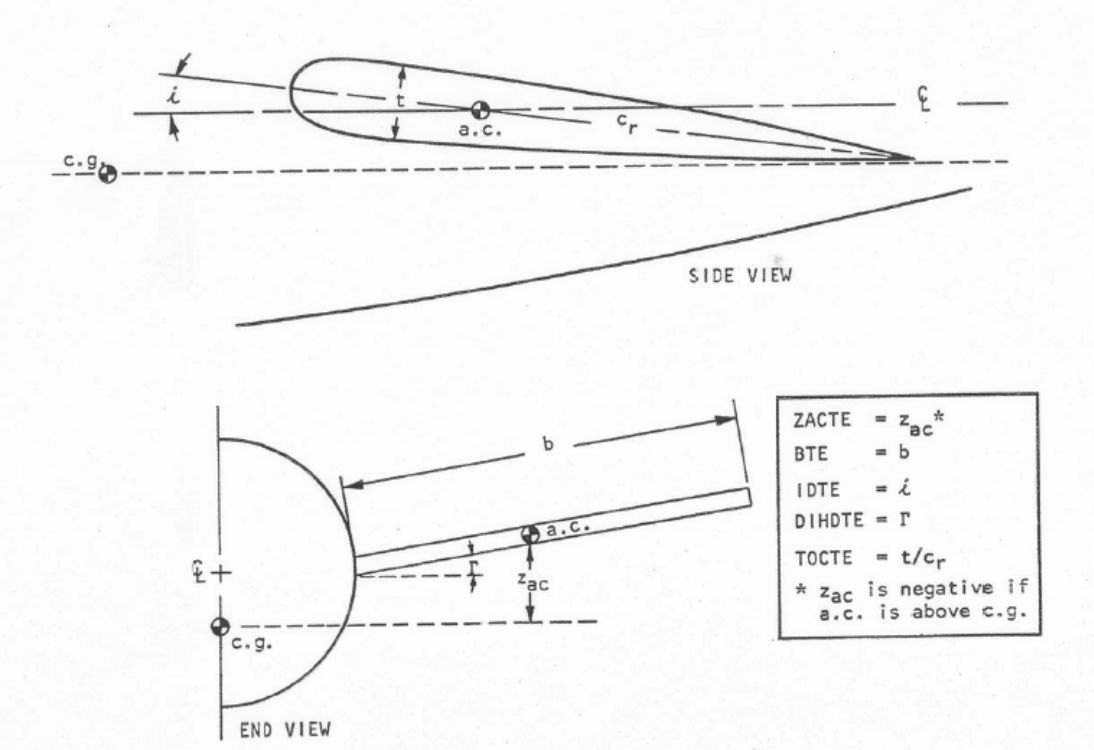

Figure 21. Horizontal stern plane geometry, side and end views [10].

3.3.3.2 CEBAXI and LA_57

CEBAXI and LA_57 require that information for both the port and starboard horizontal stern planes be input. For the purpose of this thesis the geometry of the port and starboard stern planes are assumed to be identical. The x-location, span, root chord, and tip chord of each plane is needed as input. The x-location is measured from the bow of the submarine and the span is measured from the centerline. In addition, the angle of each plane measured from the lower vertical is also needed. For a cruciform stern configuration the port and starboard planes are placed at -90 and 90 degrees respectively. Details for an x-stern configuration are provided in Section 3.3.4.2.

3.3.4 Vertical Stern Planes

This section details the input geometry for the vertical stern planes required by GEORGE and CEBAXI and LA_57.

3.3.4.1 GEORGE

Table 8 provides a summary of the geometry needed by GEORGE for the vertical stern planes.

Table 8. Summary of geometry for upper and lower vertical stern planes for GEORGE.

Upper Vertical Stern Plane	
Variable	**Description**
XNACUV	x-location of the aerodynamic center measured from the nose
ZACUVT	z-location of the aerodynamic center measured from the centerline
TRUVT	taper ratio
BUVT	span
BUVTQC	span measured perpendicular to the body centerline at the aerodynamic center
SUVT	planform area of both port and starboard horizontal planes
ARUVT	aspect ratio
LAMDUVT	sweep angle in degrees
EFFUVT	efficiency of upper vertical tail
CLOVT	zero angle of attack lift coefficient
CD0VT	zero angle of attack drag coefficient
CMOUVT	zero angle of attack moment coefficient
PHIUVT	angle of rotation
TOCUVT	thickness to chord ratio
Lower Vertical Stern Plane	
Variable	**Description**
XNACLV	x-location of the aerodynamic center measured from the nose
ZACLVT	z-location of the aerodynamic center measured from the centerline
TRLVT	taper ratio
BLVT	span
BLVTQC	span measured perpendicular to the body centerline at the aerodynamic center
SLVT	planform area of both port and starboard horizontal planes
ARVT	aspect ratio
LAMDLV	sweep angle in degrees
EFFLVT	efficiency of lower vertical tail
CL0VT	zero angle of attack lift coefficient
CD0VT	zero angle of attack drag coefficient
CM0VT	zero angle of attack moment coefficient
PHILVT	angle of rotation
TOCLVT	thickness to chord ratio

Figure 22 provides a graphical definition of the vertical stern plane geometry. The z-location of the aerodynamic center is negative if the aerodynamic center is above the centerline. Since it is typical that the geometry of the upper and lower vertical stern planes not identical due to dry dock requirements each plane is modeled separately. The efficiency of the vertical stern planes is always assumed to be one. The vertical stern planes are assumed to be NACA 0020 airfoils, therefore, the zero angle of attack lift and moment coefficients are always zero and the thickness to chord ratio is 0.20. The angle Φ is used to model different stern plane configurations. It is

local for each plane. When Φ is equal to zero for the vertical and horizontal stern planes the configuration is as shown in Figure 11. The angle is measured positive counterclockwise. For this thesis only cruciform and x-stern configurations are considered. Cruciform configurations are modeled by modeling horizontal planes and both upper and lower vertical planes each with Φ set to zero. An x-stern is modeled by modeling only the upper and lower vertical planes, each with phi set to 45 degrees, GEORGE automatically models the other fin across the plane of symmetry.

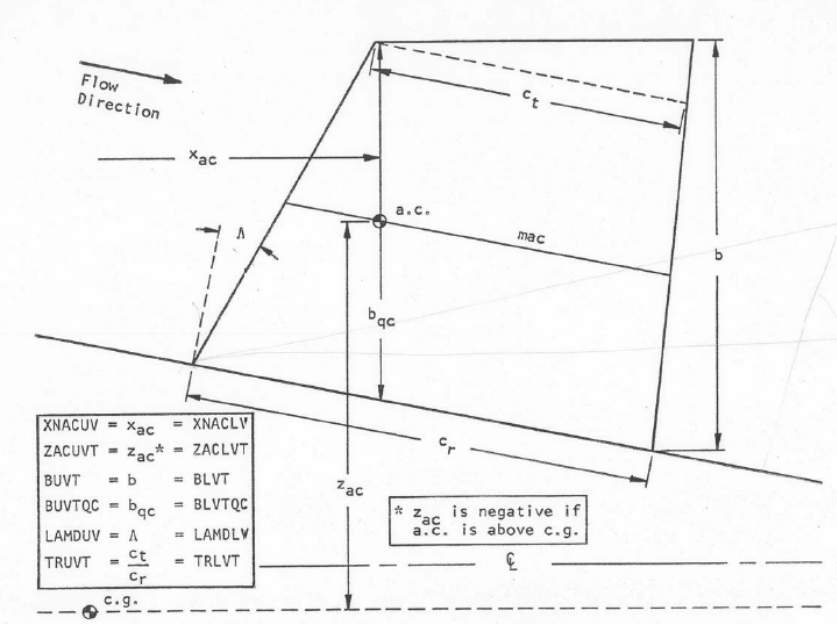

Figure 22. Vertical stern plane geometry, side view [10].

3.3.4.2 CEBAXI and LA_57

CEBAXI and LA_57 require that information for both the upper and lower rudders be input. The x-location, span, root chord, and tip chord of each plane is needed. The x-location is measured from the bow of the submarine and the span is measured from the centerline. In addition, the angle of each plane measured from the lower vertical is needed. For a cruciform stern configuration the upper and lower planes are at 180 and 0 degrees respectively. For an x-stern configuration the same input is needed however the planes are divided into two categories, the upper and lower starboard planes and upper and lower port planes. The upper and lower starboard planes are placed at angles of 135 and 45 degrees respectively and the upper and lower port planes are places at -135 and -45 degrees respectively. For an x-stern configuration the geometry for the upper port and starboard planes is equal to the geometry for the upper vertical

stern planes needed by GEORGE and the geometry for the lower port and starboard planes is equal to the geometry for the lower vertical stern plane needed by GEORGE.

3.3.5 General Procedure

This section details the process used to calculate the geometry of the controls surfaces needed by GEORGE and CEBAXI and LA_57. GEORGE requires more geometry to be input than the NSWCCD program, therefore the majority of this section refers to GEORGE input variables. It is indicated when an equation applies to both the input required by GEORGE and CEBAXI and LA_57. Table 9 summarizes the variables used in this section to calculate the geometry of the control surfaces.

Table 9. Basic definitions.

Basic Definitions	
L	overall length
D	diameter
c	mean chord
c_r	root chord
c_t	tip chord
b	span
b_{ac}	span at aerodynamic center
AR	aspect ratio, AR=b/c
A_p	projected area, Ap=bc
S	planform area, $S=AR/b^2$
t	taper ratio, t=ct/cr
X_{ac}	x-location of aerodynamic center measured from the nose
Z_{ac}	z-location of aerodynamic center measured from the centerline
Y_{ac}	y-location of aerodynamic center

Each design in the synthesis model and optimizer is given a unique set of control surfaces. The geometry of each control surface is dependent on the overall length and diameter of the design being considered. Given the overall length and diameter of the design, the control surface parameter, m, for each control surface is determined. Based on the data gained from the ten submarine designs measured to create the control surface database a plot for each control surface of the control surface parameter vs. length to diameter ratio was made. These plots are shown as Figures B1-B5 in Appendix B. In general as the length to diameter ratio increases so does the control surface parameter. It is assumed that the length to diameter ratio and control surface parameter are directly proportional and a linear trendline was fit to each set of data. This allows for the data to be easily extrapolated outside of the length to diameter range for which data was

collected. Once the control surface parameter is known the projected area for each design of a given length and diameter is calculated using Equation 48:

$$A_p = bc = \frac{LD}{m} \tag{48}$$

Given the projected area and the aspect ratio of the control surface the span can be calculated using Equation 49. The aspect ratio, AR, for each control surface is determined from the database. Like the control surface parameter the aspect ratio of each control surface for each design in the database was calculated and plotted against the length to diameter ratio to identify a trend in the data. Figures B6-B10 in Appendix B show the plots of the aspect ratio versus length to diameter ratio for each control surface. Based on this data linear trendlines were fit to each plot. Given this information the span of the control surface is calculated:

$$b = \sqrt{AR \cdot A_p} \tag{49}$$

The span for each control surface is used as an input for both GEORGE and the NSWCCD program. For CEBAXI and LA_57 the span of the stern planes is measured from the centerline therefore, the span for these control surfaces is calculated using Equation 49, adding the radius of the hull at the point of attachment. The radius at attachment is determined using Equation 73b. Once the span is known the mean chord can be calculated using Equation 50:

$$c = \frac{A_p}{b} \tag{50}$$

To determine the rest of the geometry needed by the stability programs it is necessary to assume a generic shape for each control surface. It is assumed that the plan view of each control surface is a trapezoid as shown in Figure 23. This assumption helps simplify the calculations needed to estimate the remaining parameters for each control surface. Based on the submarines used to create the database each control surface was in general a quadrilateral and most resembled a trapezoid. Keeping in mind that the goal of this procedure is to gather approximate data for each control surface it was determined this assumption would not alter the data in a way that would significantly alter the desired results.

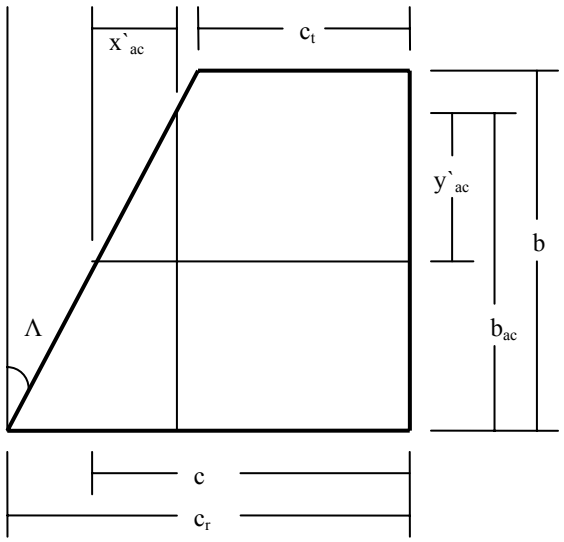

Figure 23. Generalized trapezoidal shape for control surfaces.

Based on this assumption the mean aerodynamic chord of each control surface in the database was calculated using the equation for the mean aerodynamic chord for a trapezoid (ref?):

$$\text{mac} = \frac{2}{3} \cdot c_r \cdot \frac{\left(1 + t + t^2\right)}{\left(1 + t\right)} \tag{51}$$

In addition the average chord was calculated for each control surface in the database.

$$c = \frac{c_r + c_t}{2} \tag{52}$$

The mean aerodynamic chord and average chord were then non-dimensionalized by the model length and compared as shown in Table 10.

Table 10. Calculated non-dimensional mean aerodynamic chord vs. measured non-dimensional mean chord.

Class		Skipjack	Permit	Sturgeon	Seawolf	LA	VA	GW	Ben Franklin	Lafayette	Ohio
Forward Planes	mac	0.041	0.036	0.033		0.036		0.022	0.022	0.022	0.024
	c	0.038	0.038	0.033		0.036		0.027	0.027	0.025	0.027
	error	9.328	3.846	0.000		0.962		21.875	21.875	12.500	14.706
Stern: Horizontal	mac	0.038	0.038	0.033	0.033	0.028	0.031	0.028	0.028	0.022	0.022
	c	0.051	0.049	0.033	0.033	0.030	0.031	0.033	0.031	0.028	0.025
	error	36.111	30.556	0.000	0.000	8.750	2.273	20.000	12.500	26.563	12.500
Stern: Vertical Top	mac	0.036	0.033	0.033	0.033	0.032	0.031	0.031	0.028	0.028	0.022
	c	0.044	0.043	0.043	0.042	0.032	0.040	0.041	0.030	0.035	0.029
	error	21.154	28.125	28.125	25.000	1.087	29.545	32.955	8.750	27.500	31.250
Stern: Vertical Bottom	mac	0.036	0.033	0.036	0.033	0.032	0.031	0.031	0.025	0.033	0.022
	c	0.044	0.043	0.048	0.042	0.038	0.040	0.041	0.028	0.038	0.029
	error	21.154	28.125	32.692	25.000	17.391	29.545	32.955	12.500	12.500	31.250

Data is not given for the forward planes for the Seawolf and Virginia Class submarines because these designs had bow planes attached to the body rather than the sail and were therefore, rectangular rather than trapezoidal. From this data it was determined that the average chord is a reasonable approximation of the mean aerodynamic chord. This approximation is necessary to simplify the method used to determine the root and tip chord of the control surfaces for each design.

Based on the measurements taken from the ten designs for the database the delta chord, defined as the absolute value of the difference between the measured root and tip chord, was calculated. These values were non-dimensionalized by the length of the model and then plotted for each control surface against the length to diameter ratio to determine any trends. These plots are shown in Figures B11-B15 in Appendix B. Linear trendlines are fit to the data and used to determine the delta chord value for each specific control surface for a given design. Figure B11, which shows the data for the forward plane only includes the designs in which the forward planes are attached to the sail. When the forward planes are attached to the body, the shape of the control surface is a rectangle as noted earlier, therefore, the root and tip chord are equal to the mean chord calculated using Equation 52. By assuming the mean aerodynamic chord is equal to the average chord the root and tip chord can be calculated from the delta chord as follows:

$$\begin{aligned} c_r &= \Delta\text{chord} + c \\ c_t &= \Delta\text{chord} - c \end{aligned} \tag{53}$$

The root chord and tip chord calculated using Equation 53 are used as an input for both GEORGE and CEBAXI and LA_57. From this information the taper ratio is determined,

$$t = \frac{c_r}{c_t} \tag{54}$$

The planform area is determined using the equation for the area of a trapezoid,

$$S = \frac{1}{2} b \cdot (c_r + c_t) \tag{55}$$

The sweep angle, defined as lambda in Figure 23, is determined by the equation,

$$\Lambda = \tan^{-1}\left(\frac{c_r - c_r}{b} \right) \tag{56}$$

Referring to Figure 23 the variable $x`_{ac}$ is the local x-distance from the leading edge of the control surface to its aerodynamic center. This distance can be determined using the low speed, thin airfoil approximation that the aerodynamic center is at quarter mean aerodynamic chord,

$$x'_{ac} = 0.25 \cdot c \tag{57}$$

The variable y'_{ac} is the local y distance from the aerodynamic center to where it intersects the perimeter of the control surface (refer to Figure 23). This distance is calculated as:

$$y'_{ac} = \frac{x'_{ac}}{\tan(\Lambda)} \tag{58}$$

Since it is assumed that the mean aerodynamic chord is equal to the mean chord then the span at the aerodynamic center is a function of the local y-distance and overall span:

$$b_{ac} = y'_{ac} + 0.5b \tag{59}$$

If the value of b_{ac} is greater than b, then is it assumed that the span at the aerodynamic center is equal to the overall span.

Information about the overall x and z location of the aerodynamic center for each control surface is also needed. The x location, defined as X_{ac}, is measured from the nose of the submarine and the z location, defined as Z_{ac} is measured from the centerline. The overall x-location of the aerodynamic center is a function of the local x-distance, x'_{ac} determined from Equation 57 and the distance from the nose of the submarine to the forward most point of the control surface. The database was used to determine the x-distance of each control surface measured from the nose of the submarine which is denoted as x. For each design in the database the distance x was measured and non-dimensionalized by the length. Table 11 shows the non-dimensional average location of each control surface measured from the nose of the vessel to the most forward point of the control surface. The distance x for each control surface varies whether or not sail or bow planes are present. For GEORGE only cases with sail planes are analyzed. CEBAXI and LA_57 can model either sail or bow planes.

Table 11. Non-Dimensional x-distance measured from vessel nose.

Non-Dimensional X-Distance measured from nose		
	Sail Planes	**Bow Planes**
Forward Plane	0.25	0.14
Horizontal Tail	0.92	0.90
Vertical Tail - Top	0.92	0.90
Vertical Tail - Bottom	0.92	0.90
Sail	0.24	0.24
Stern Plane x-location of 1/2c	0.95	0.93

Therefore, the equation used to determine the overall x-location of the aerodynamic center is:

$$X_{ac} = xL + x'_{ac} + (c_r - c) \tag{60}$$

CEBAXI and LA_57 only need to know the x-location of the control surfaces measured from the bow of the submarine which is simply the product of the non-dimensional x given in Table 11 and the length of the submarine. In addition, CEBAXI and LA_57 need to know the non-dimensional location of half chord of the stern planes which is also given in the last row of Table 11. These values were determined using data from the database created. The location is used in the CEBAXI program to generate the velocity profiles necessary for the boundary layer predictions.

The overall z-location of the aerodynamic center measured from the centerline for the fairwater and sail planes is:

$$Z_{ac} = 0.5 \cdot D + 0.5 \cdot b_{fairwater} \tag{61}$$

The z-location of the fairwater and sail planes is the same because it is assumed that the sail planes are placed on the fairwater at 50% of the fairwater span. There was no consensus from the designs used for the database as to where on the fairwater the sail planes are placed, therefore, 50% of the fairwater span was assumed. Typically, this location would be determined in part by the equipment that is placed in the fairwater, therefore it was determined that this generalization would not significantly affect the intended results of this study.

When sail planes are present and CEBAXI and LA_57 is being used then the height of the sail planes measured from the centerline is needed. This height is calculated using Equation 62:

$$Z_{sailplane} = \frac{D}{2} + 0.50 b_{fairwater} \tag{62}$$

Since the horizontal stern planes are always located on the centerline the overall z-location for the horizontal planes is always zero. The z-location of the vertical stern planes is dependent on the radius of the submarine at their location of attachment. The radius at this point is determined by the equation:

$$Z_{ac} = 0.5 \cdot D \cdot \left(1 - \left(\frac{x_a}{L_a} \right)^{n_a} \right) + 0.5 b_{vertical} \tag{63}$$

The span, b, in this equation is the span of the upper or lower vertical stern plane. L_a is the length of the aft portion of the submarine, n_a describes the fullness of the aft portion, and x_a is defined in Figure 24. A more detailed explanation of L_a and n_a is found in Section 3.3.

The y-location of the aerodynamic center is only required for the forward planes and horizontal stern planes. As shown in Figure 16 for the forward planes Y_{ac} is defined by:

$$Y_{ac} = \frac{t}{2} + 0.5b_{forward} \tag{64}$$

The span, b, is the span of the forward planes and t is the thickness of the fairwater which is determined from the thickness to chord ratio.

The y-location of the horizontal planes is determined in the same manner as the z-location for the vertical stern planes. It is a function of the radius of the submarine at attachment and the span of the control surface.

$$Y_{ac} = 0.5 \cdot D \cdot \left(1 - \left(\frac{x_a}{L_a} \right)^{n_a} \right) + 0.5b_{horizontal} \tag{65}$$

Finally, as shown in Figure 19 some ratios involving distances in reference to the placement of the forward planes on the fairwater are also needed by GEORGE. XOCHFW is defined in Figure 19 as

$$\frac{x'_{ac}}{c_{ac}} \tag{66}$$

The variable c_{ac} is the mean chord of the fairwater which is determined using Equation 52 and x'_{ac} is calculated as:

$$x'_{ac} = X_{ac,forward} - x_{sail} - (c_r - c)_{sail} \tag{67}$$

Where $X_{ac,forward}$ is the overall x-location of the forward planes determined in Equation 60, x_{sail} is the x-location of the forward most point of the sail measured from the nose (determined using Table 11), and c_r and c are properties of the fairwater. The variable ZOBHFW is defined in Figure 19 as:

$$\frac{z_{ac}}{b} \tag{68}$$

Z_{ac} in this equation is defined as the vertical distance from the base of the fairwater to the mean chord which is defined $0.5b_{fairwater}$ and b is the span of the fairwater.

These equations are implemented in a FORTRAN code (ControlSurfaces.f90) so the geometry of the control surfaces can be quickly determined for any given diameter, length to diameter ratio, plane configuration, and stern configuration.

3.4 Hull Offsets

In addition to the geometry of the control surfaces GEORGE and CEBAXI and LA_57 require the hull offsets to calculate the hydrodynamic coefficients. A traditional teardrop shape was assumed for the hullform. This idealized shape was chosen for its low submerged resistance and consists of an elliptical bow and parabolic stern as shown in Figure 24. The teardrop shape can be modified to include a section of parallel midbody as needed as also shown in Figure 24. The aft body is idealized as parabolic and L_a represents the length of the aft body while the nose is assumed to be elliptical and L_f represents its length. L_a and L_f are determined from the diameter as follows:

$$\begin{aligned} L_a &= 3.6D \\ L_f &= 2.4D \end{aligned} \tag{69}$$

The overall length, L, is determined from the diameter and length to diameter ratio,

$$L = D \cdot \frac{L}{D} \tag{70}$$

The length of the parallel midbody, L_{pmb} is a function of the overall length and length of the fore and aft bodies:

$$L_{pmb} = L - (L_a + L_f) \tag{71}$$

The hullform is defined by specifying 45 stations along the nose from the most forward point to the beginning of the parallel midbody section and by defining 45 stations along the stern from the end of the parallel midbody section to the aft most point of the vessel. Each station is defined by an x-distance measured from the bow and z-distance (radius) measured from the centerline. The x-location for the fore and aft bodies is determined as follows:

$$\begin{aligned} X_{f,i} &= \frac{L_f}{10} + X_{f,i-1} \\ X_{a,i} &= \frac{L_a}{10} + X_{a,i-1} \end{aligned} \tag{72a, 72b}$$

The index i varies from 1 to 39 for the forward body, $X_{f,40}$ is always equal to 0.5D. The index i for the aft body varies from 2 to 40 and $X_{a,1}$ is always equal to 0.5D. The radius for each station is determined using Equations 72a and 72b:

$$Z_{f,i} = \frac{D}{2}\left[1-\left(\frac{L_f - x_{f,i}}{L_f}\right)^{n_f}\right]^{\frac{1}{n_f}}$$

$$Z_{a,i} = \frac{D}{2}\left[1-\left(\frac{x_{a,i} - (L_f + L_{pmb})}{L_a}\right)^{n_a}\right] \qquad (73a, 73b)$$

In this equation n_f and n_a determine the fullness of the nose and stern respectively. These variables are used to indicate how quickly and at what slope the nose and stern taper to a point.

These equations are implemented in a FORTRAN code (HullOffsets.f90) to determine the offsets of any hullform defined by a diameter, length to diameter ratio, and the fullness exponents of the bow and stern.

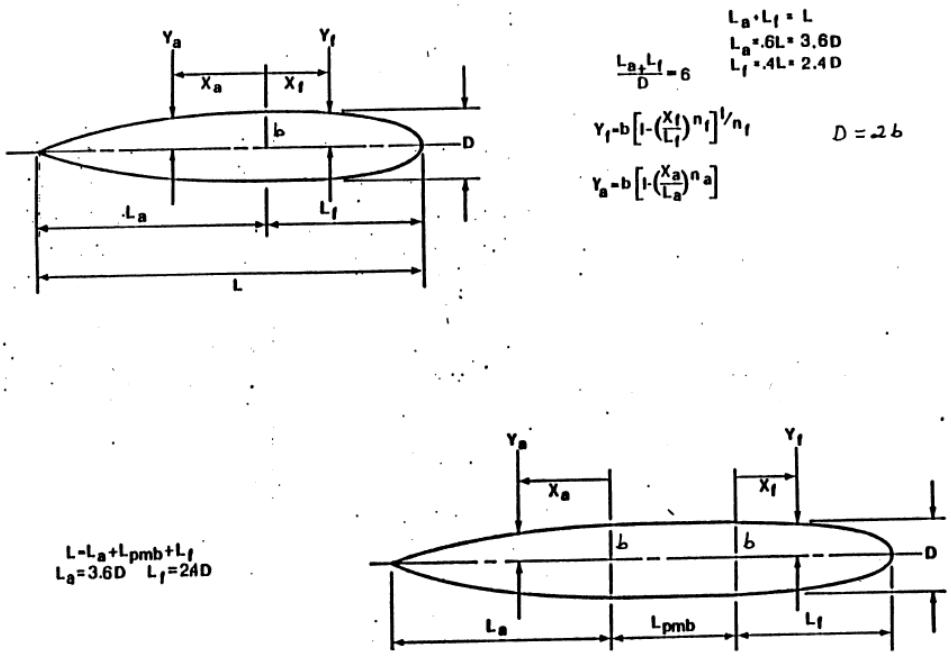

Figure 24. Teardrop and modified teardrop hullform [4].

CHAPTER 4 RESPONSE SURFACE MODEL (RSM) TOOLS

Response surface models are used to predict the behavior of response/output variables for a given set of input/design variables. Experimental data is used to develop a parametric equation to represent the response. This chapter summarizes the tools used to build the response surface models (RSMs). The first part of the chapter describes the tools used to automate the process of varying the inputs of GEORGE and CEBAXI and LA_57 (control surface geometry and hull offsets) to analyze their affect on the horizontal and vertical stability indices. ModelCenter is the main tool used however there are different plug-ins and tools utilized within the program which are described in more detail in the following sections. The second part of the chapter describes the process of integrating the stability programs and the control surfaces and hull offsets programs into the ModelCenter environment to perform the analysis.

4.1 Tools For Analysis

4.1.1 ModelCenter

ModelCenter is a visual environment for process integration developed by Phoenix Integration. It provides a means to link a number of design applications in one environment that allows for the sharing of input and output variables. It automates the process by providing tools for wrapping analysis programs, performing trade studies and optimizations, visualizing the design space, performing response surface modeling, developing parametric models of the design space, and archiving the results. This in turn reduces error, saves time, and produces more efficient designs [14].

Figure 25 shows an example of the ModelCenter environment. The server browser is located at the bottom and displays the components that can be added to the model which are added by clicking and dragging the component into the workspace. The workspace is represented by the area with the blue background. The component tree, displayed on the left, lists each component in the model, which are represented in the workspace by each box. Each component can be opened in the component tree to show the individual inputs and outputs associated with it.

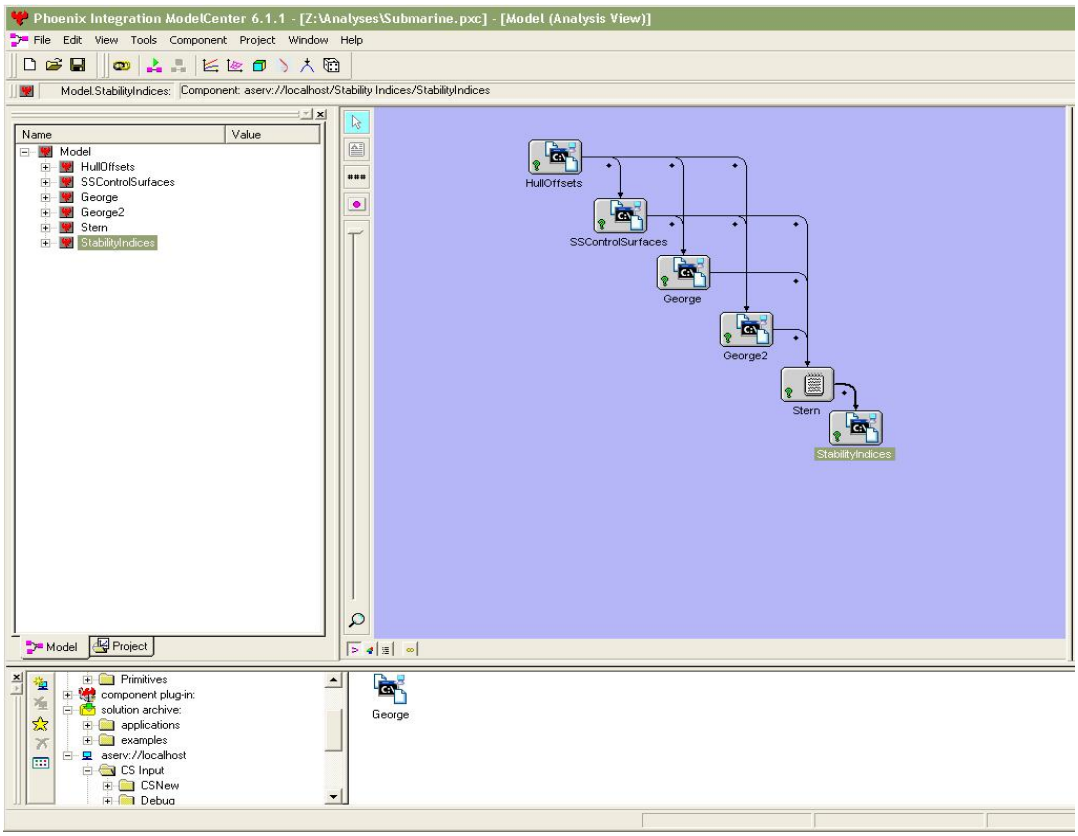

Figure 25. Example of ModelCenter environment.

4.1.2 Analysis Server

ModelCenter cannot be run without Analysis Server. Analysis server allows the user to wrap analysis software into usable components. Common programs such as FORTRAN codes, Excel spreadsheets, MATLAB m-files, and MATHCAD files can be wrapped using this tool. The purpose of wrapping a program is to convert program-specific input and output operations into a generic set of commands. The process of wrapping a program is discussed in more detail in Section 4.2.1. By wrapping a program, the process of manually creating individual input files necessary to run programs such as FORTRAN codes which require specific input files, is eliminated. This in turn speeds up the process of analyzing a variety of different input combinations and automates the process, leaving the user free to focus on the results.

4.1.3 Design of Experiments Toolkit

The design of experiments (DOE) tool simplifies the process of varying input/design variables to observe the corresponding affect on the output/response variables. A range is defined for each design variable and each point in the range defines a design point. The DOE tool selects

specific design points and documents the responses of the model at those chosen design points [14]. Figure 26 shows the DOE graphical interface in ModelCenter.

To perform a DOE the design variables and response variables need to be specified. This can be done by dragging them from the component tree into the DOE window. For each design variable a design range is defined by specifying high and low boundaries. The next step is to select a DOE algorithm to be used. The algorithm is selected based on the desired purpose of the experiment. Some algorithms are selected to test a design for robustness by determining the extent to which the designs in the specified design space are feasible. Other algorithms are used to define a design variable's effect on one another while others are selected to screen a large number of design variables to isolate those that have the greatest effect on the response variables. The DOE algorithms available are:

- Half Fractional Factorial
- Eighth Fractional Factorial
- Sixteenth Fractional Factorial
- Foldover
- Plackett-Burman
- Parameter Scan
- Full Factorial
- Latin-Hypercube
- Central Composite
- Face Centered Central Composite
- Box-Behnken

The half fractional factorial, eight fractional factorial, sixteenth fractional factorial, foldover, and Plackett-Burman designs are all screening experiments. Screening experiments are defined as experiments that are used to identify the most active variables and are most useful when a large number of variables are present.

The parameter scan and full factorial algorithms sample the entire design space. The parameter scan is limited to testing the high and low levels of each variable while the full factorial algorithm allows for more levels of each variable to be tested.

The Latin-Hypercube algorithm is the design used for analysis in this thesis. It is similar to the full factorial design in that it explores the entire design space but does so by taking a random sample of the entire design space. It does this by dividing the internal space into segments to achieve a more thorough investigation of the design space. The number of segments

and how many random combinations of variables and segments is determined by the specified number of designs. Once a DOE algorithm is selected the number of runs is specified which corresponds to the number of data sets to be collected [8].

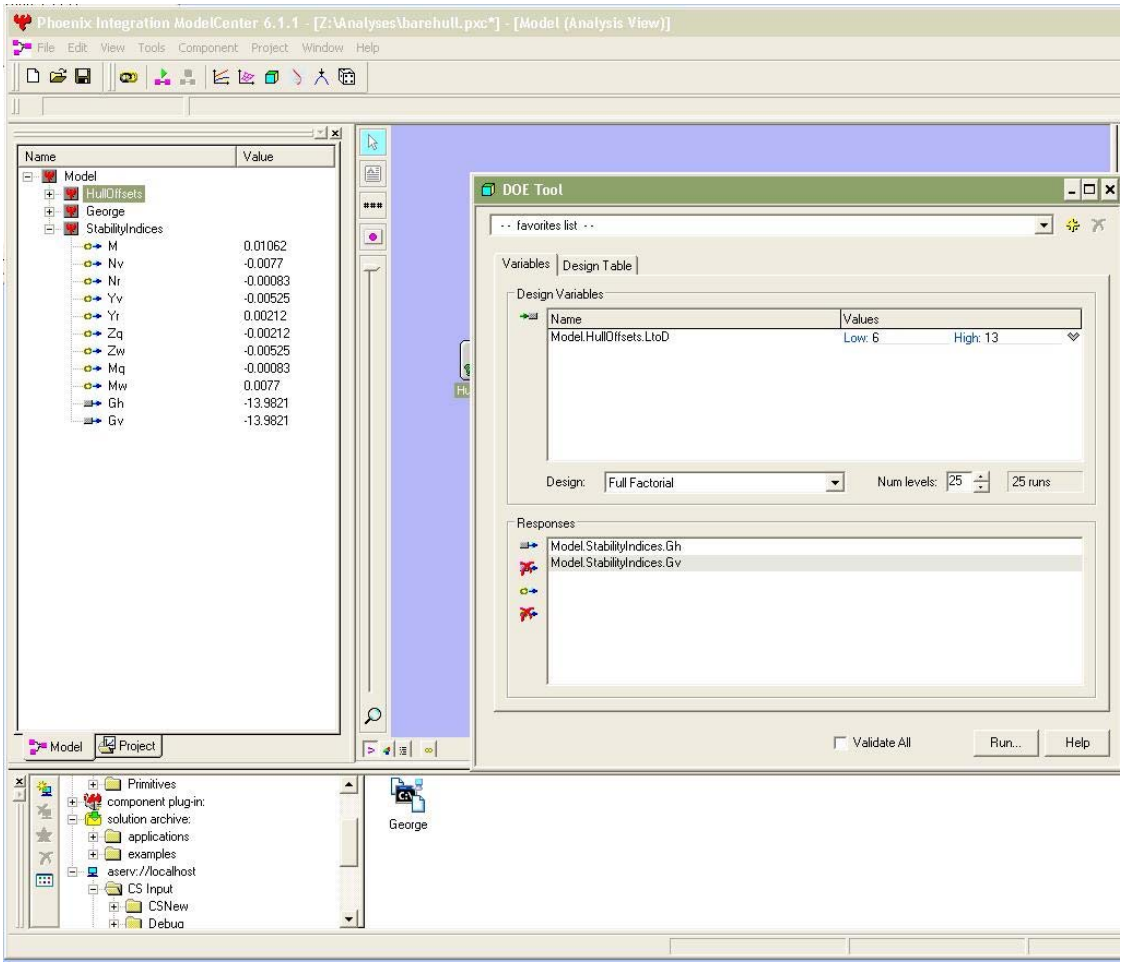

Figure 26. DOE Tool.

4.1.4 Response Surface Model (RSM) Toolkit

The RSM toolkit is used to create approximations of long running or complex models. The resulting RSM has a runtime that is much faster than the model it approximates making it more practical for use with optimization tools which can require thousands of iterations and evaluations of various functions [14].

The RSM toolkit uses the data generated by the DOE tool and is launched from the DOE toolbar once the DOE is complete. It allows the user to select which data sets collected by the DOE will be used to form the response surface. The response surface can then be modeled using several polynomial options:

- Stepwise Regression Quadratic
- Stepwise Regression Cubic
- Linear
- Linear plus Quadratic Interaction Terms
- Full Quadratic
- Linear plus Quadratic and Cubic Interaction Terms
- Full Cubic

After the RSM is generated statistical details of the response surface and graphs can be viewed to determine if the polynomial model chosen is a good fit. It is important to note however, that a statistical report that describes the resulting RSM as a good fit does not necessarily mean it is a good fit to the parent model. The resulting RSM is just an approximation of the actual response and the fit is dependent on the efficiency and sufficiency of the DOE. Therefore it is important that the appropriate DOE algorithm and sample size is chosen. The purpose of the RSM is to reduce computational time therefore large DOE sample sizes can be self-defeating and the DOE algorithm chosen should sufficiently represent the entire design space [8]. The user can create a number of different response surfaces and determine which gives the best fit. Once an appropriate RSM is chosen it can be returned to the ModelCenter workspace either as a module or to replace the parent model it was derived from.

4.1.5 Darwin Optimizer

Darwin is a genetic-algorithm-based trade study designed specifically for engineering optimization problems. Genetic algorithms are probability based and use processes analogous to natural selection to search for and determine the best designs. They can be used to solve design problems with both discrete and continuous design variables and any number of constraints. They can also be used to perform the Multi-Objective Genetic Optimization described in Section 1.2.4. Darwin allows the user to choose which design variables are used in the optimization and to specify the constraints. The use of the Darwin optimizer in this thesis will be described in more detail in Section 6.4.

4.2 Implementation of Dynamic Stability Modules in ModelCenter

This section describes the process of integrating the tools outlined in Chapter 3 into the ModelCenter environment. Both GEORGE and CEBAXI and LA_57 require input files that

specify the hull offsets of the submarine and the geometry of the control surfaces. Individual FORTRAN codes were written to determine the offsets (HullOffsets.f90) and control surface geometry (ControlSurfaces.f90) based on a given diameter and length to diameter ratio as described in Sections 3.4 and 3.3. An additional FORTRAN code (StabilityIndices.f90) was written to be used with GEORGE to calculate the stability indices derived in Chapter 2 based on the hydrodynamic coefficients output by GEORGE. These programs represent the individual components of the models that are created in ModelCenter. Two separate dynamic stability models are created; one using GEORGE and the one using CEBAXI and LA_57.

4.2.1 Creating a File Wrapper

ModelCenter requires each component to be "wrapped" using a file wrapper. A file wrapper is useful for programs that require input and output files. Typically, an input/output based program requires the user to manually modify the input file, run the executable, and extract pertinent data from the output file each time the program is run. A file wrapper automates this process by using a simple set of commands to modify an input file, run the executable, and search the output file each time the component is executed.

A wrapper consists of four sections: header, run command, input file, and output file. Figure 27 shows an example of a file wrapper. The header section documents the wrapper through a series of comment lines denoted by the symbol #. The run commands section communicates instructions to run the component. The command "generate inputFile" tells the component to create the input file necessary to run the executable. Run "HullOffsets.exe" tells ModelCenter which executable file to run. The command "parse outputFile" prompts ModelCenter to search the resulting output file for specific output variables. These output variables become part of the design space in ModelCenter and are made available to other components in the model.

The Input File section prompts an input template file to be opened and then generates a new input file by replacing specified variables with new values. The section begins with the command "RowFieldInputFile." This command defines the structure of the input file stating that each line is considered a row and each row is comprised of fields. The command "setdelimeters" specifies what separates the fields in a given row. The default setting is white space however commas and columns can also be used as delimiters. The variables that are replaced in the template file to create the new input file are determined by specifying the variable type (double,

integer, string, etc) and its location in the input file by specifying its row and field. Therefore the line:

```
variable: XNACSA        double      35    1
```

states that the variable XNACSA is type double and located in the input file on row 35, field 1.

The output file section is similar to the input file section. It contains instructions on how to retrieve values from an output file. The command fileToParse specifies the output file to be opened and searches it for specific outputs. Like the input file the structure of the output file is specified by the command "RowFieldOutputFile" and the command "setdelimiters" can be used to set what separates the individual fields. For components that have particularly large output files and only a few outputs are desired commands such as "MarkAsBeginning" can be used to mark a specific place in the output file to begin the search. Variables that are specified in a wrapper as an output are then available to all components in the model to be used as inputs. This allows for the different components of each model to be linked together.

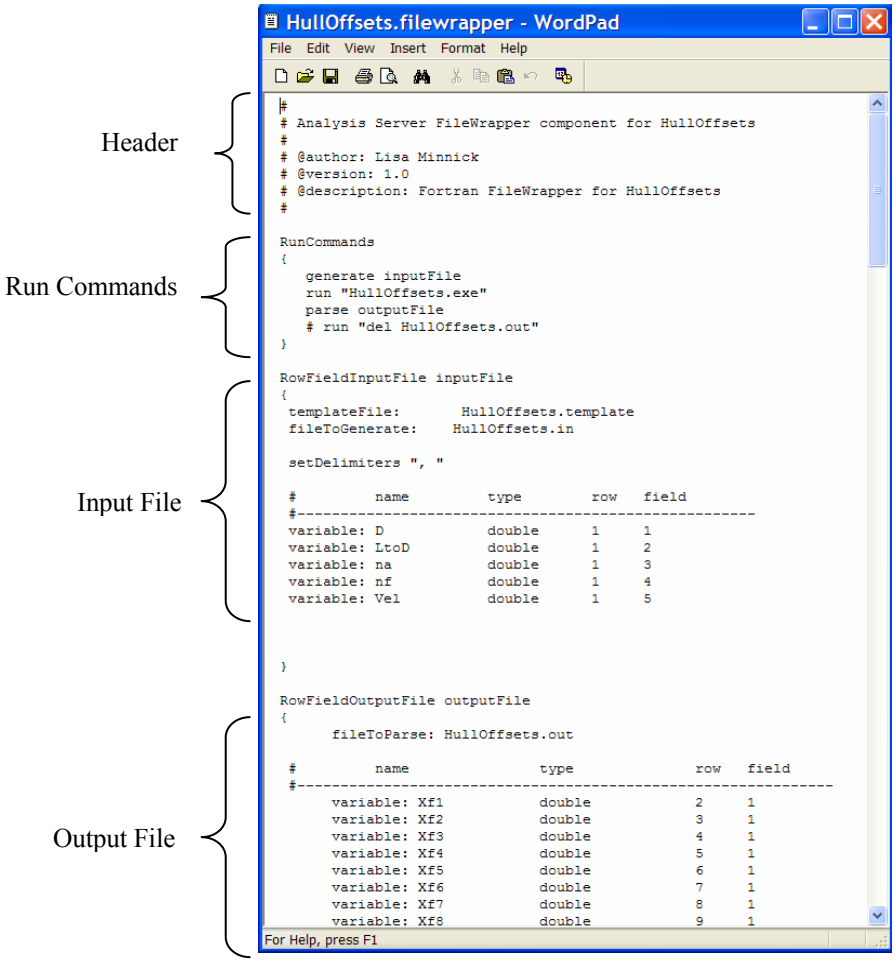

Figure 27. Example of file wrapper.

4.2.2 Link Editor

The link editor feature of ModelCenter provides a fast and easy way to link the outputs of one component as inputs to another. Figure 28 shows the link editor user interface. Variables are linked by opening each component in the component tree on the left and right of the interface and clicking and dragging the variable to be linked across the middle space to the other component. By doing so a link is created which is represented by the black lines shown in the Figure. A variable can be linked to more than one component.

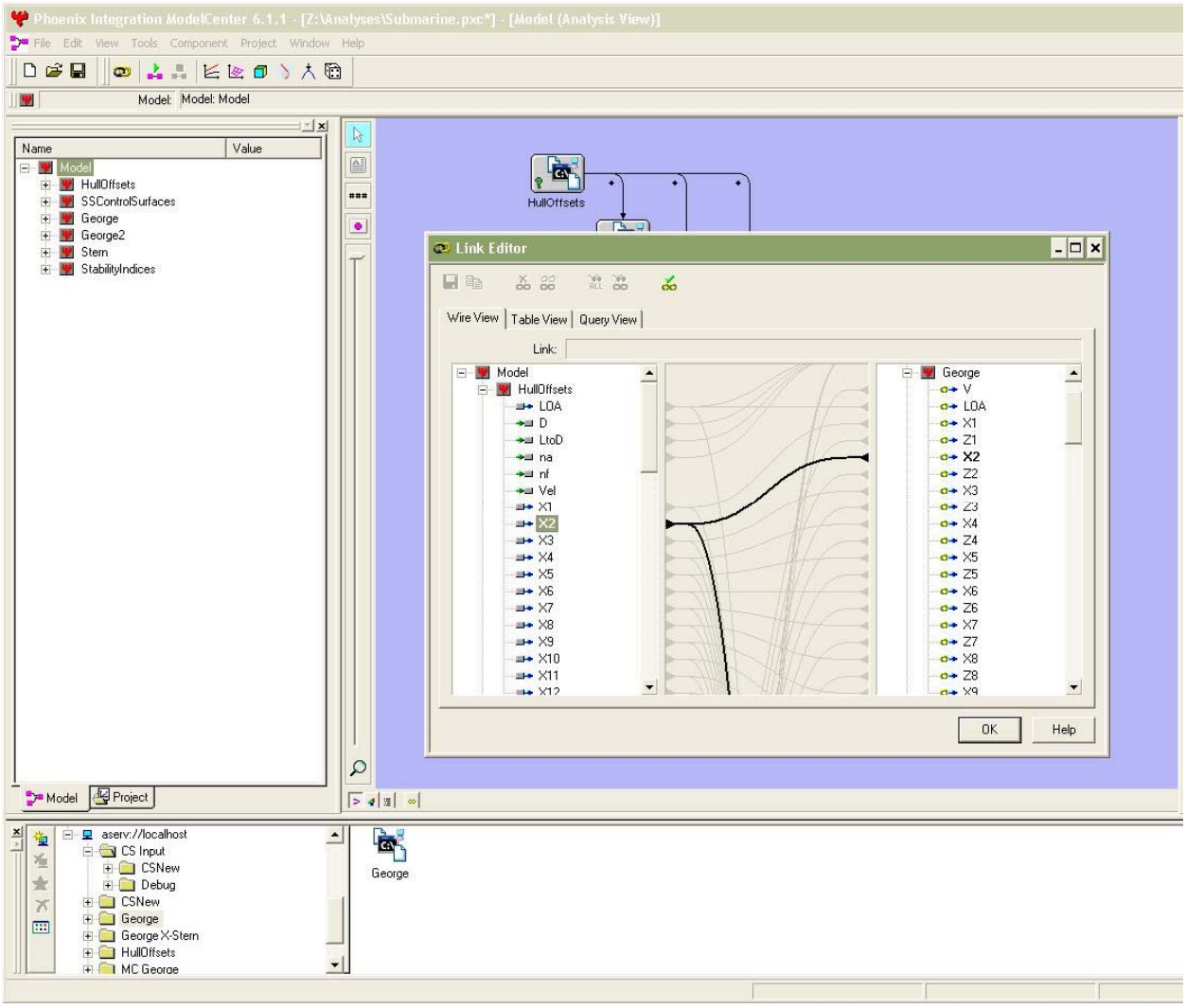

Figure 28. Example of Link Editor user interface.

4.2.3 Dynamic Stability Models

4.2.3.1 GEORGE Model

Figure 29 shows the dynamic stability model that was created in ModelCenter using GEORGE. It consists of six components: HullOffsets, SSControlSurfaces, George, George2, Stern, and StabilityIndices. The black lines show how the component inputs and outputs relate to one another. The HullOffsets component contains the HullOffsets.f90 Fortran code. Given a diameter and length to diameter ratio it outputs the x and z coordinates of the offsets, total submarine length, aft and fore body lengths, and length of the parallel midbody. These outputs are provided as part of the inputs for the SSControlSurfaces, George, and George2 components. The SSControlSurfaces component contains the ControlSurfaces.f90 Fortran code and outputs the geometry of the control surfaces. These outputs are provided as input for the George, George2, and Stern components.

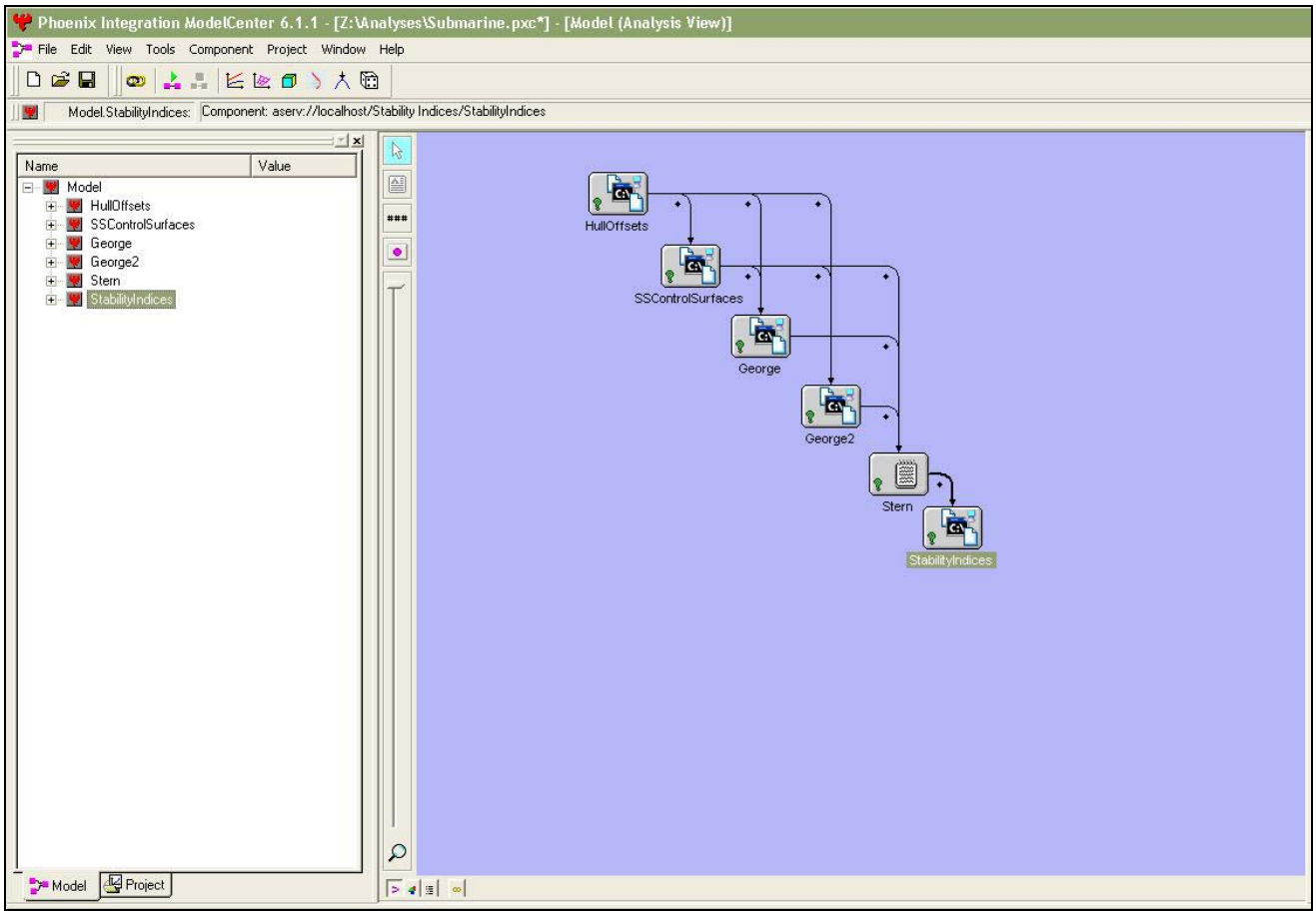

Figure 29. GEORGE Dynamic Stability Model.

There are two George components because each one represents a different stern configuration. The component George calculates the hydrodynamic coefficients assuming a cruciform stern configuration while George2 assumes an x-stern. When an x-stern is assumed only the vertical stern planes are modeled as described in section 3.2.4. There is a component for each stern configuration because the structure of the input file differs for each configuration. The stern configuration for the design is denoted by the variable stern which is specified as an input in the SSControlSurfaces component. If the variable stern has a value of 1 then an x-stern configuration is assumed, if variable stern is equal to zero then a cruciform stern is assumed. Both components, George and George2 are executed for each design and each output the hydrodynamic coefficients that are part of the stability indices. The coefficients output from the component George are marked by a subscript A and the coefficients output from George2 are marked with a subscript B. The component Stern determines which set of the hydrodynamic coefficients, A or B, are provided as inputs to the StabilityIndices component based on the value of the variable stern which is provided as an input.

StabilityIndices is the final component of the model. It inputs the hydrodynamic coefficients from the component Stern and calculates the value of the horizontal and vertical stability indices using Equations 25 and 47. These outputs represent the response variables that are analyzed using the DOE tool described in section 4.1.3.

4.2.3.2 CEBAXI and LA_57 Model

Figure 30 shows the CEBAXI and LA_57 stability model. It consists of three components: HullOffsets, SSControlSurfaces, and Stability. The HullOffsets and SSControlSurfaces components are the same components used in the George Dynamic Stability model. The component stability includes the CEBAXI and LA_57 programs that calculate the stability indices. The output of the HullOffsets component is part of the input to the SSControlSurfaces and Stability component. The output of the SSControlSurfaces component is provided as input for the Stability component.

The CEBAXI and LA_57 model can model bow planes or sail planes and an x-stern or cruciform stern. Therefore, in total there are four different configurations that can be analyzed: sail planes with an x-stern, sail planes with a cruciform stern, bow planes with an x-stern, and bow planes with a cruciform stern. This is done by setting the input variables STERN and BOWPLANES to either zero or one. If STERN is equal to zero then a cruciform stern is

assumed, if it is equal to one then an x-stern is modeled. If BOWPLANES is equal to zero then sail planes are modeled and if it is equal to one then bow planes are assumed.

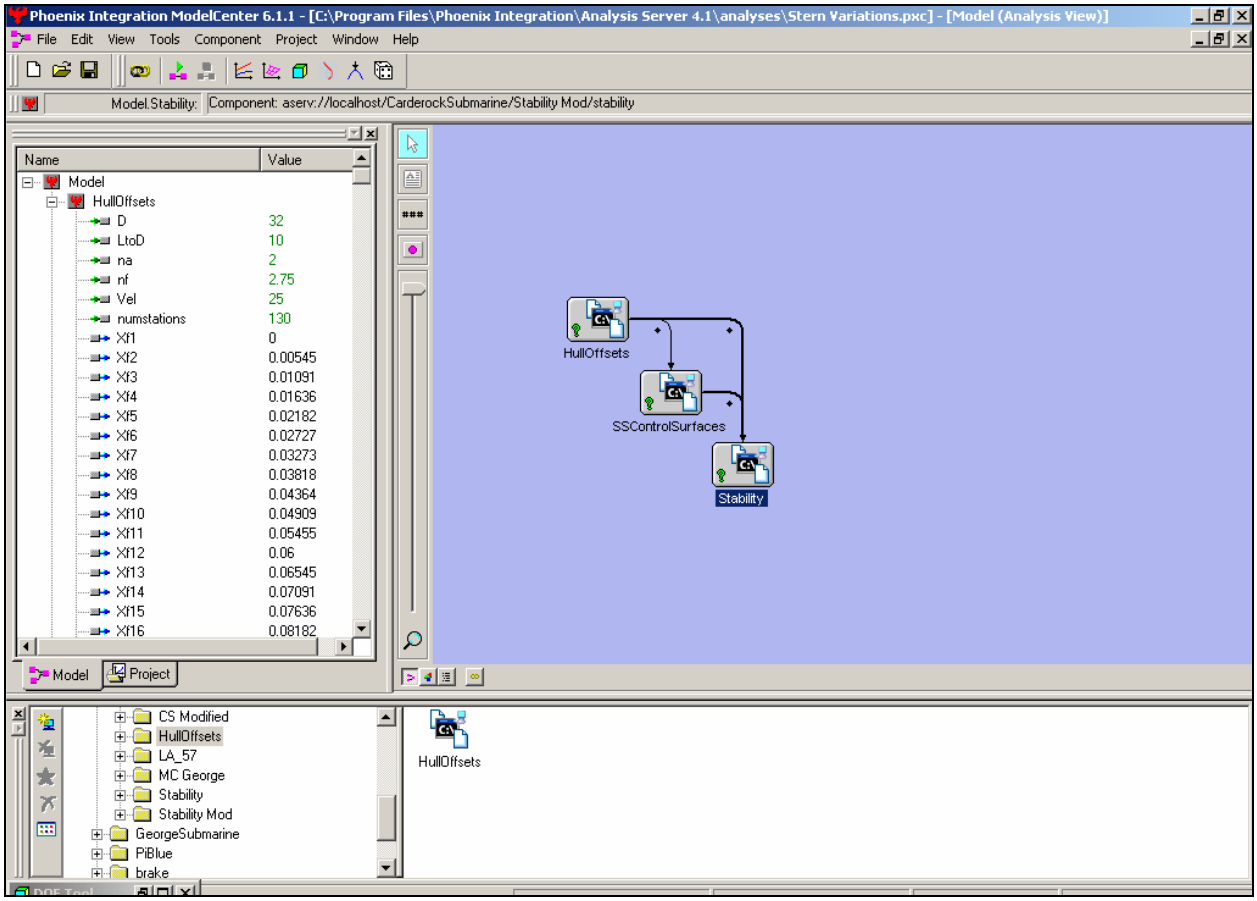

Figure 30. NSWCCD Dynamic Stability Model.

CHAPTER 5 DESIGN OF EXPERIMENTS RESULTS AND RESPONSE SURFACE MODELS

5.1 GEORGE Dynamic Stability Model

Two separate designs of experiments were performed using the GEORGE dynamic stability model, one for a cruciform stern configuration and one for an x-stern configuration. Both configurations had sail planes. Based on the DOE performed response surfaces were created for each configuration. The resulting plots from the GEORGE DOE performed and RSMs created are provided in Appendix C. For each DOE performed the Latin-Hypercube algorithm was chosen to ensure sufficient exploration of the entire design space and the number of runs was set to 200. Five input/design variables were examined: length to diameter ratio, diameter, aft body fullness factor, forward body fullness factor, and velocity. Table 12 shows the design variables and the low and high bounds used for the DOE. The horizontal and vertical stability indices, G_H and G_V, were the output/response variables examined. Once a DOE was complete the data collected was analyzed and any outlying data sets were discarded. Outliers were determined as data sets with values that were significantly outside of the general trend of the response variables. The modified data sets were then used to create corresponding response surfaces. The following sections detail the results of the DOE and RSMs.

Table 12. DOE variables and high and low boundaries for GEORGE stability model.

Design Variable	Low	High
L/D	6.5	13
D (ft)	22	32
na	2.5	3.5
nf	2	3
Velocity (knots)	10	25

5.1.1 Configuration 1: Cruciform Stern

Figure 31 and Figure 32 are plots of the main effects for the horizontal and vertical stability indices which demonstrate the sensitivity of the output variables to the input variables. A main effect is defined as the change in a response/output variable with respect to a design/input variable. It is determined by taking the average output value for a given input variable at its upper and lower bounds. The main effect is the difference between the two averages. The variable with the largest main effect has the most influence on the response

variable [14]. Therefore, Figure 31 and Figure 32 show that the length to diameter ratio, velocity and the forward body fullness factor variables have almost an equal influence on both stability indices.

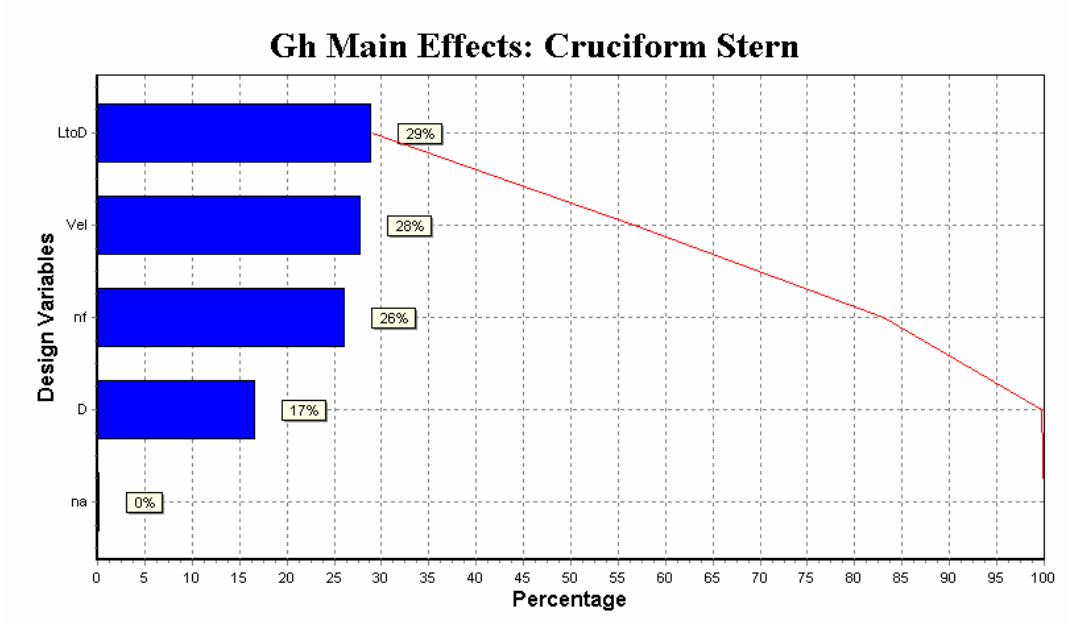

Figure 31. G_H main effects plot for GEORGE model with cruciform stern.

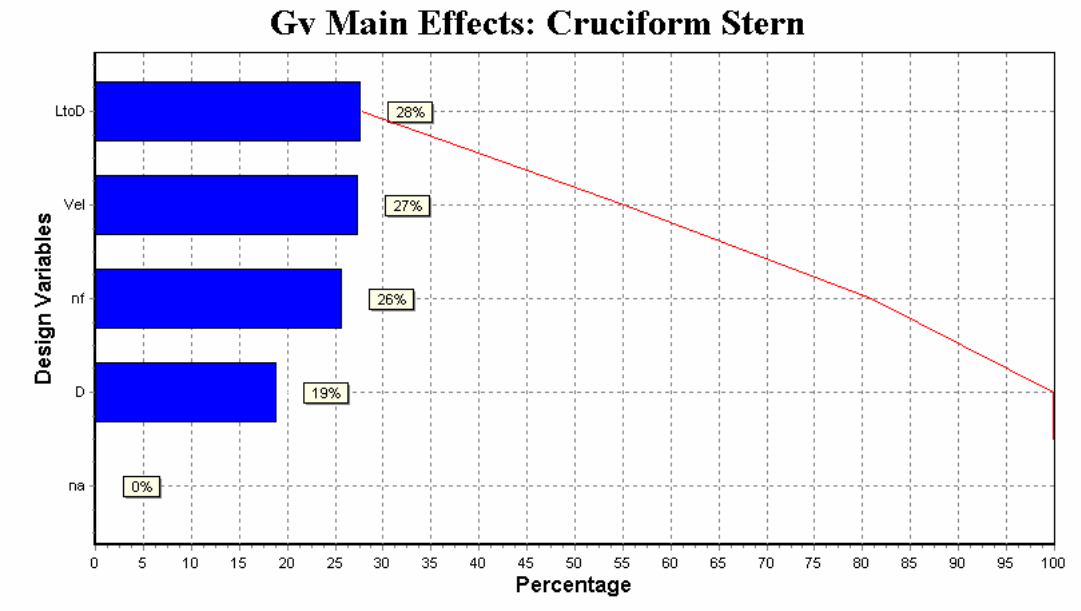

Figure 32. G_V main effects plot for GEORGE model with cruciform stern.

Figure 33 plots the stability indices as a function the length to diameter ratio. In general, as the length to diameter ratio increases the stability increases, however there is a discontinuity that occurs near a length to diameter ratio of 10 for G_H and 10.4 for G_v. At this length to diameter

ratio the stability indices increase dramatically over a small range of length to diameter ratios creating a sharp upward slope in the data. Designs below this length to diameter ratio are highly unstable while designs above this length to diameter ratio are highly stable.

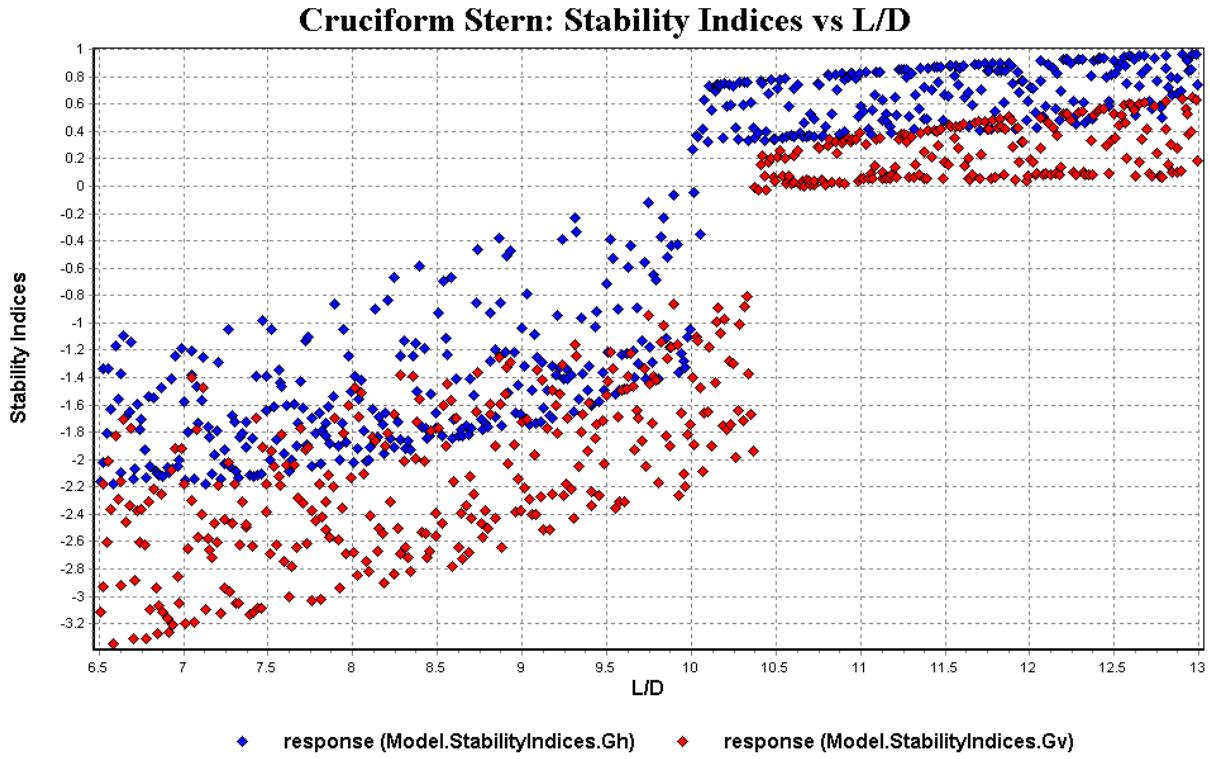

Figure 33. Stability indices vs.L/D for GEORGE model with cruciform stern

Figure 34 and Figure 35 are variable influence plots. The variable influence plots show both the main effects as well as the interaction effects of the design variables. Higher order effects involve more than two variables and are grouped together into one category. The other category includes variables with an importance less than 0.5% [14]. Therefore, Figure 34 and Figure 35 show that the length to diameter ratio has the greatest effect on the stability indices for this configuration and that the higher order terms also have a significant impact.

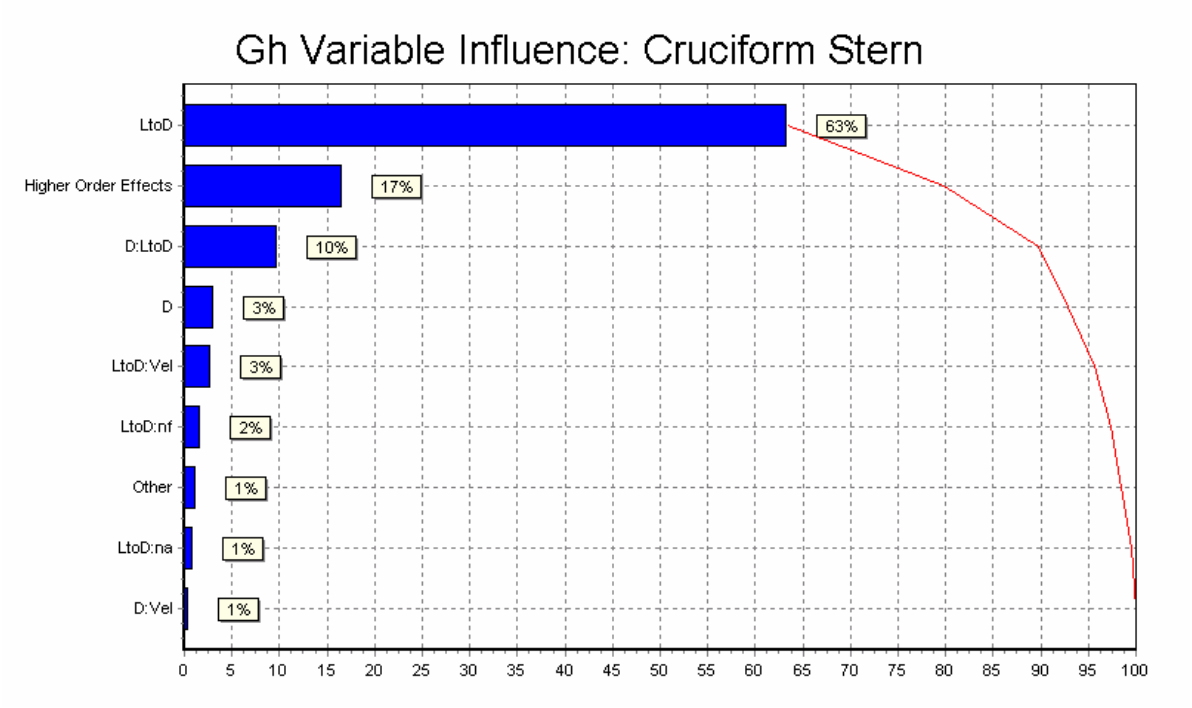

Figure 34. G_H variable influence for GEORGE model with a cruciform stern.

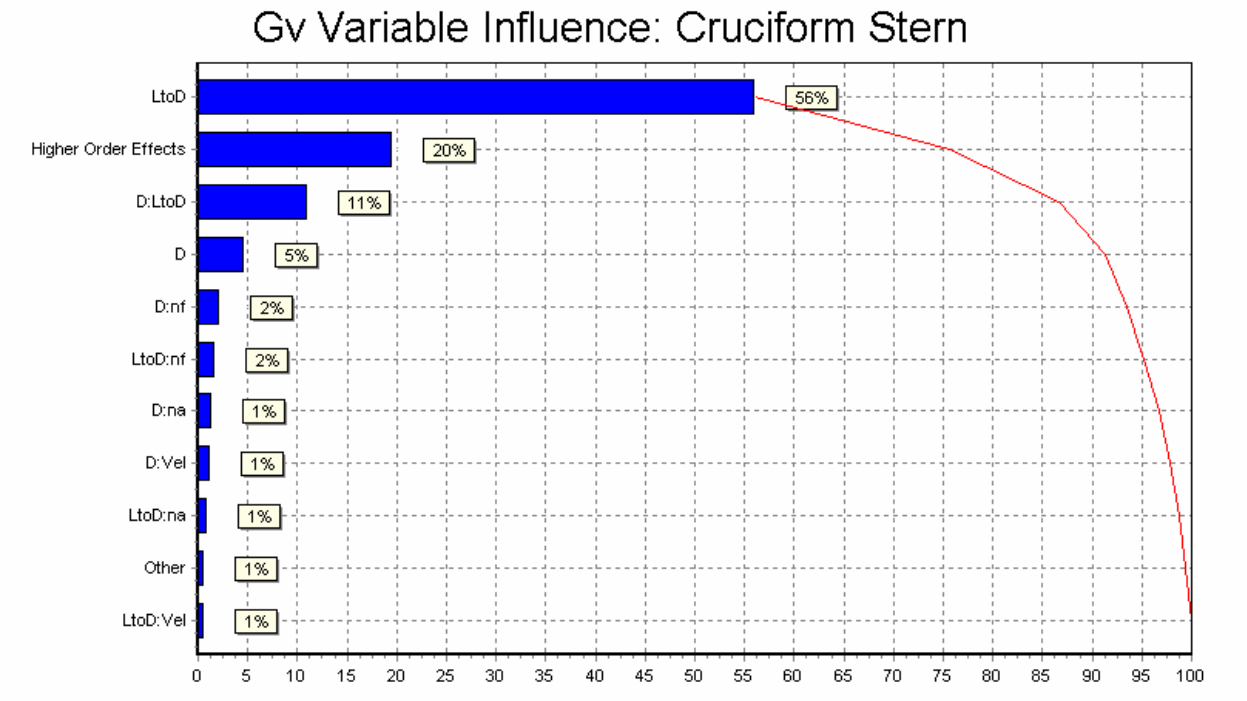

Figure 35. G_V variable influence for GEORGE model with a cruciform stern.

Based on this data response surfaces were created for each index. Since the higher order terms were shown to have an impact on the response variable a full cubic polynomial was used to create the response surfaces. Table 13 provides statistical details of the response surfaces that were created. The S value is the standard error of the response surface and estimates the standard deviation of the fit. The smaller the S value the better the fit. CoV is the Coefficient of Variation and is defined as the ratio of the Standard Error to the average value of the response variable (expressed as a percentage). Smaller CoV values indicate a better fit. R^2 is the Coefficient of Multiple Determination and is the ratio of the regression sum of squares to the total sum of squares of the fit (expressed as a percentage). It can be thought of as the percentage of the total variability in the data that is explained by the response surface approximation. R^2 varies between 0% and 100%, with values closer to 100% indicating a better fit. R^2_{adj} is the Adjusted Coefficient of Determination. R^2_{adj} should not differ substantially from R^2. If it does, this is an indication that the response surface model is overfitted, and not likely to do a good job at prediction [14].

Table 13. Summary of RSM statistical data for GEORGE model.

	Cruciform Stern	
	Gh	**Gv**
S	0.2934	0.3612
Cov (%)	0.29	0.36
R^2 (%)	95.3	94.05
R^2_{adj} (%)	93.31	91.78

5.1.2 Configuration 2: X-stern

Figure 36 and Figure 37 are the main effect plots for the x-stern configuration. They show that the forward body fullness factor has the most influence on both stability indices followed by the length to diameter ratio and velocity.

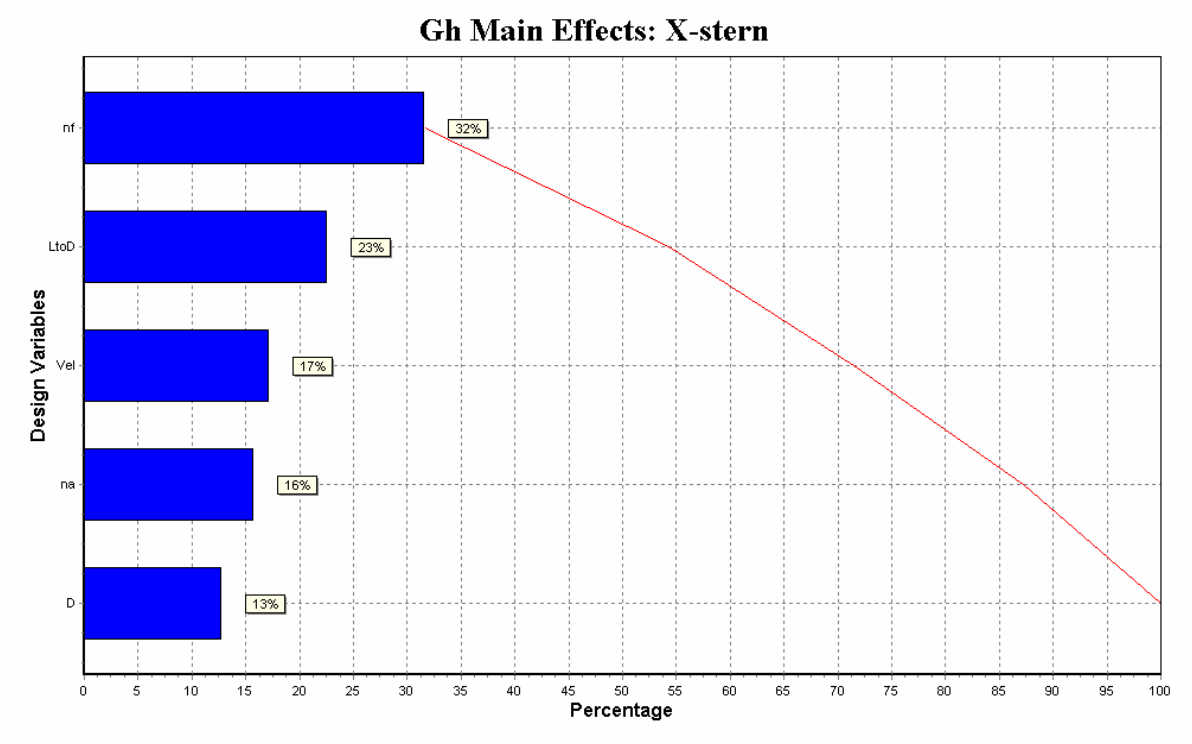

Figure 36. Gh main effects for GEORGE model with an x-stern.

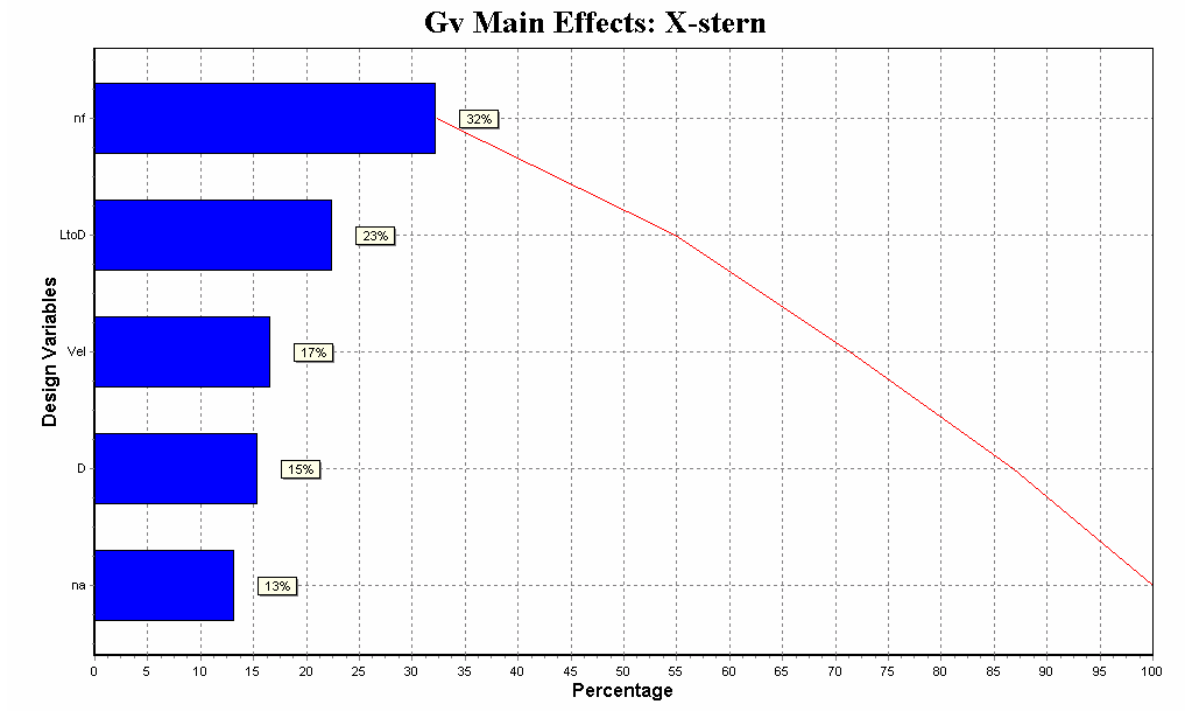

Figure 37. Gv main effects for GEORGE model with an x-stern.

Figure 38 shows the stability indices as a function of the length to diameter ratio. The stability indices increase with increasing length to diameter ratios. However, a discontinuity occurs at a length to diameter ratio of approximately 10 for both indices. At this length to diameter ratio the stability indices quickly increase over a small range of length to diameter ratios. Designs below a length to diameter ratio of 10 are unstable while designs with a length to diameter ratio greater than 10 are stable. The values of the stability indices tend to converge as the length to diameter ratio increases from 6.5 to 10 and begin to diverge as the length to diameter ratio increases from 10 to 13. In addition, the values of horizontal and vertical indices are closely coupled at higher length to diameter ratios.

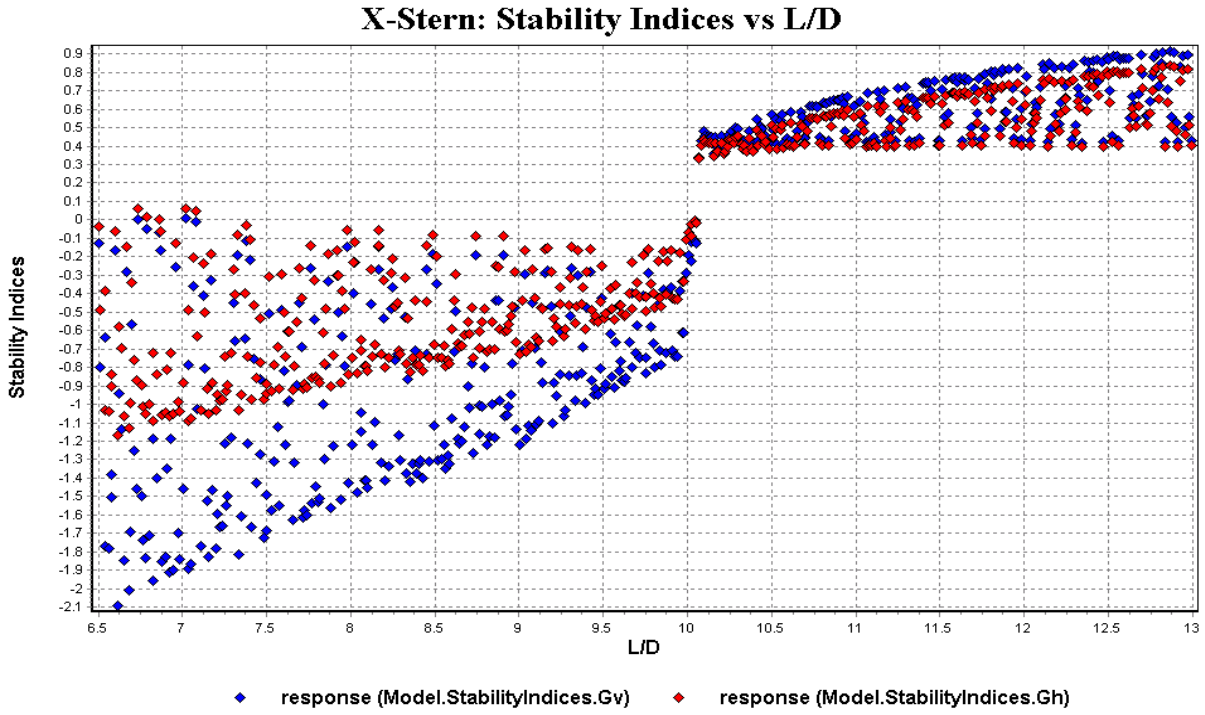

Figure 38. Stability indices vs. L/D for GEORGE model with an x-stern.

The variable influence plots shown in Figure 39 and Figure 40 indicate that the length to diameter ratio has the greatest effect on the indices and shows that the higher order terms are also important. Since the higher order terms are significant a full cubic polynomial was used to develop the response surfaces for both indices. Table 14 shows the statistical details of the response surfaces.

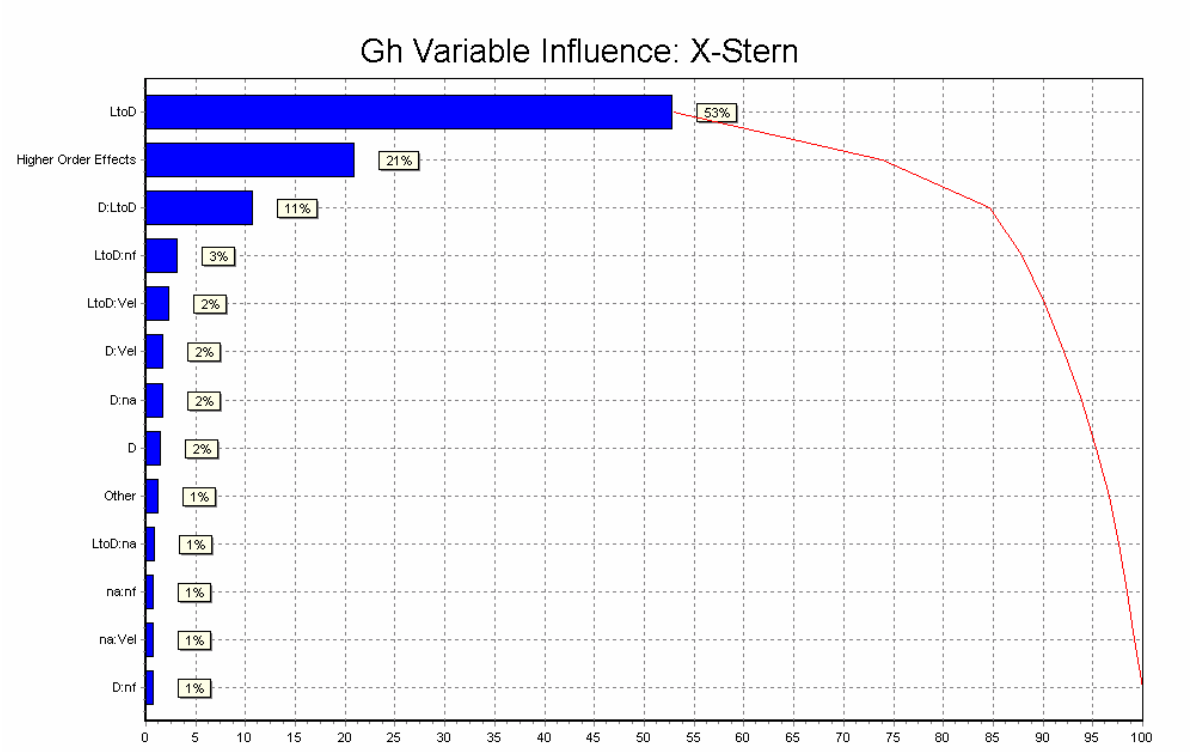

Figure 39. Gh variable influence for GEORGE model with an x-stern.

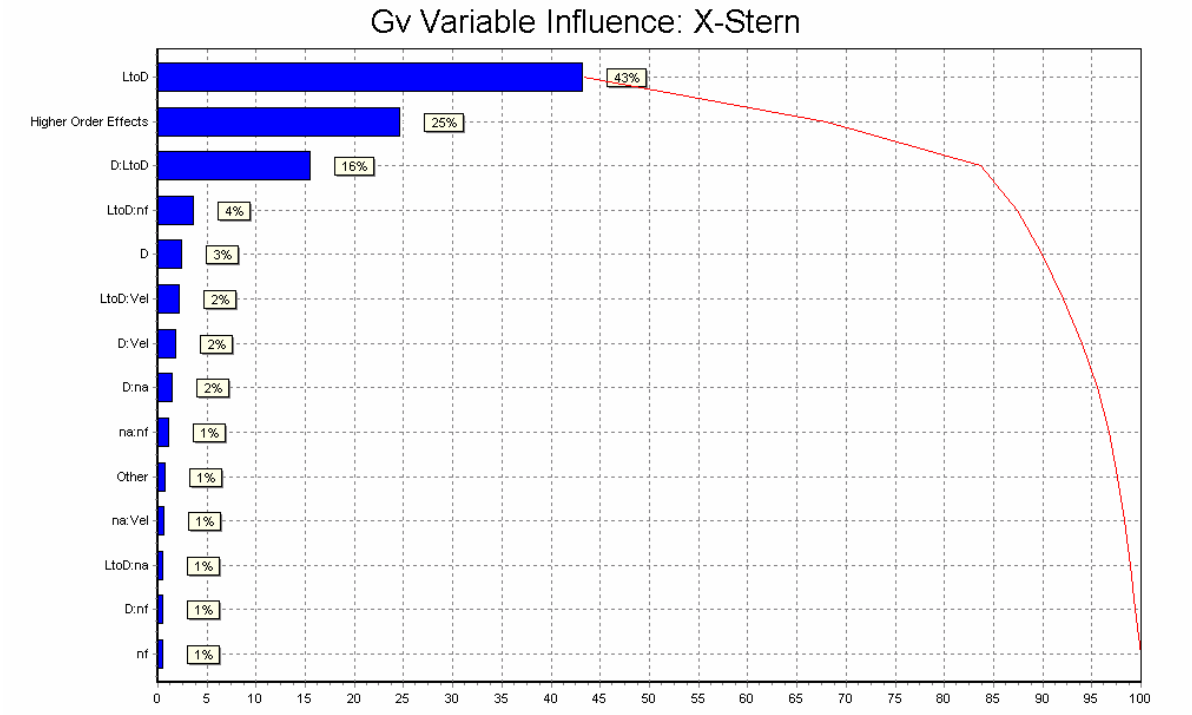

Figure 40. Gv variable influence for GEORGE model with an x-stern.

Table 14. Statistical summary for RSM results for GEORGE model with an x-stern.

	GEORGE: X-Stern	
	Gh	Gv
S	0.1421	0.2021
Cov (%)	0.14	0.2
R^2 (%)	95.84	95.93
R^2adj (%)	94.25	94.38

5.1.3 Summary and Discussion of Results

Both configurations have a discontinuity near a length to diameter ratio of 10. Designs below this length to diameter ratio are unstable while designs above this length to diameter ratio are stable. The presence of a discontinuity in the data was unexpected and difficult to explain. Since stability is dependent on the geometry of the hullform and control surfaces which have been modeled to vary linearly a discontinuity of this magnitude is unusual and indicates these results may be unreasonable.

To try and determine why this discontinuity exists the behavior of the individual stability derivatives was investigated as well as the behavior of the stability indices for the bare hull. Since both stern configurations had similar discontinuities only the cruciform stern configuration was analyzed in more detail to simplify the process. It is assumed that similar conclusions could be drawn by analyzing the x-stern configuration in more detail as well.

Figure 41 is a graph of the horizontal stability derivatives (N_v, N_r, Y_v, Y_r) versus length to diameter ratio. Similar to the data for the horizontal stability index shown in Figure 33, Figure 41 shows a discontinuity in the data at a length to diameter ratio of 10. This provides some insight to why the discontinuity for the stability index exists; the stability index is a function of the individual stability derivatives and there is a discontinuity in the individual stability derivatives at the same point where the discontinuity in the stability indices occur. In addition, the values of the numerator, $N'_v(Y'_r - m')$, and denominator, $Y'_v N'_r$, of the horizontal stability index as a function of length to diameter ratio were plotted and are shown in Figure 42. The point where the values intersect correspond to where the discontinuity occurs and stability is reached (G_H is greater than zero).

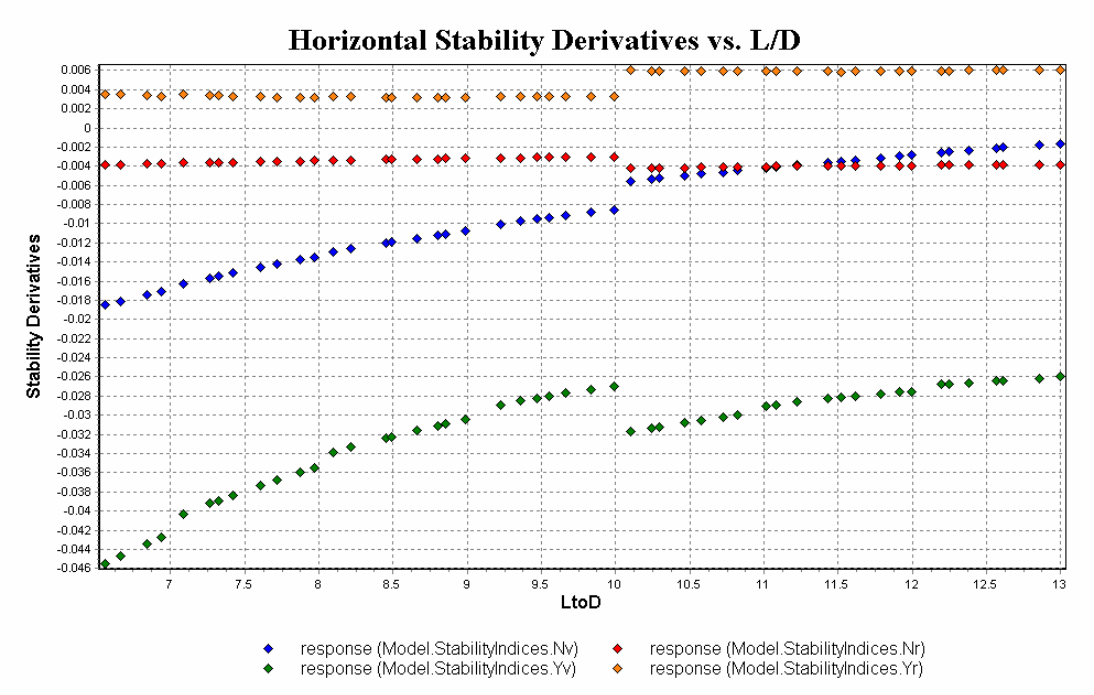

Figure 41. Horizontal plane stability derivatives vs. L/D.

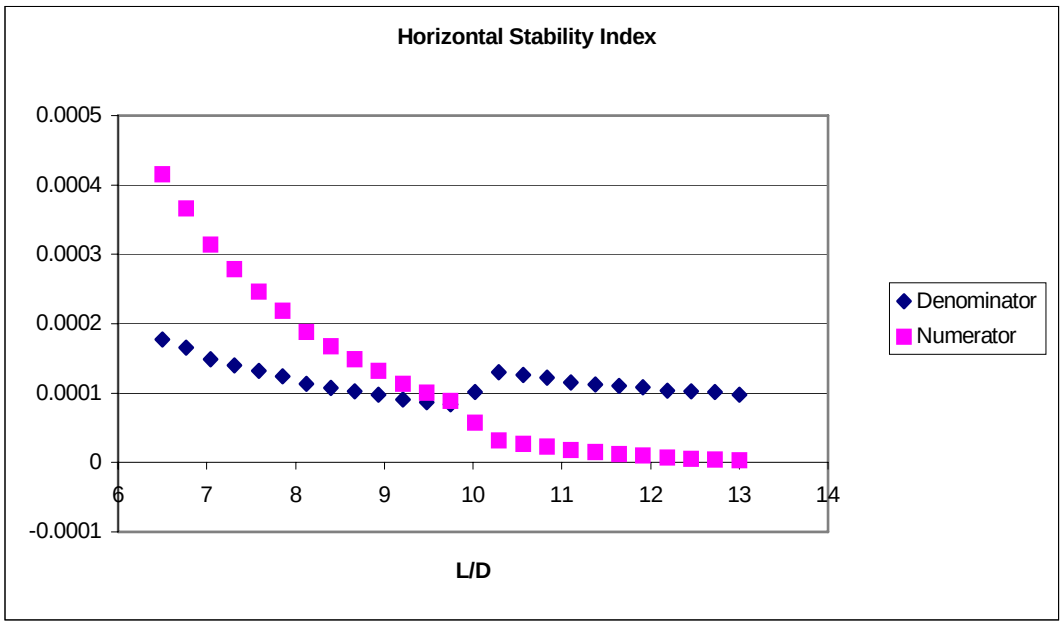

Figure 42. Values of denominator and numerator as a function of L/D.

Figure 43 is a graph of the vertical stability derivatives (Z_q, Z_w, M_q, M_w) versus length to diameter ratio. Similar to the data for the vertical stability index shown in Figure 33 there is a

discontinuity in the data at a length to diameter ratio of 10.25. The discontinuity in the individual stability derivatives corresponds to the discontinuity in the stability index. In addition, the values of the numerator, $M'_w (Z'_q + m')$, and denominator, $Z'_w M'_q$, of the vertical stability index as a function of length to diameter ratio were plotted and are shown in Figure 44. The point where the discontinuity in the numerator occurs corresponds to where the discontinuity for the vertical stability index occurs and stability is reached (G_V is greater than zero).

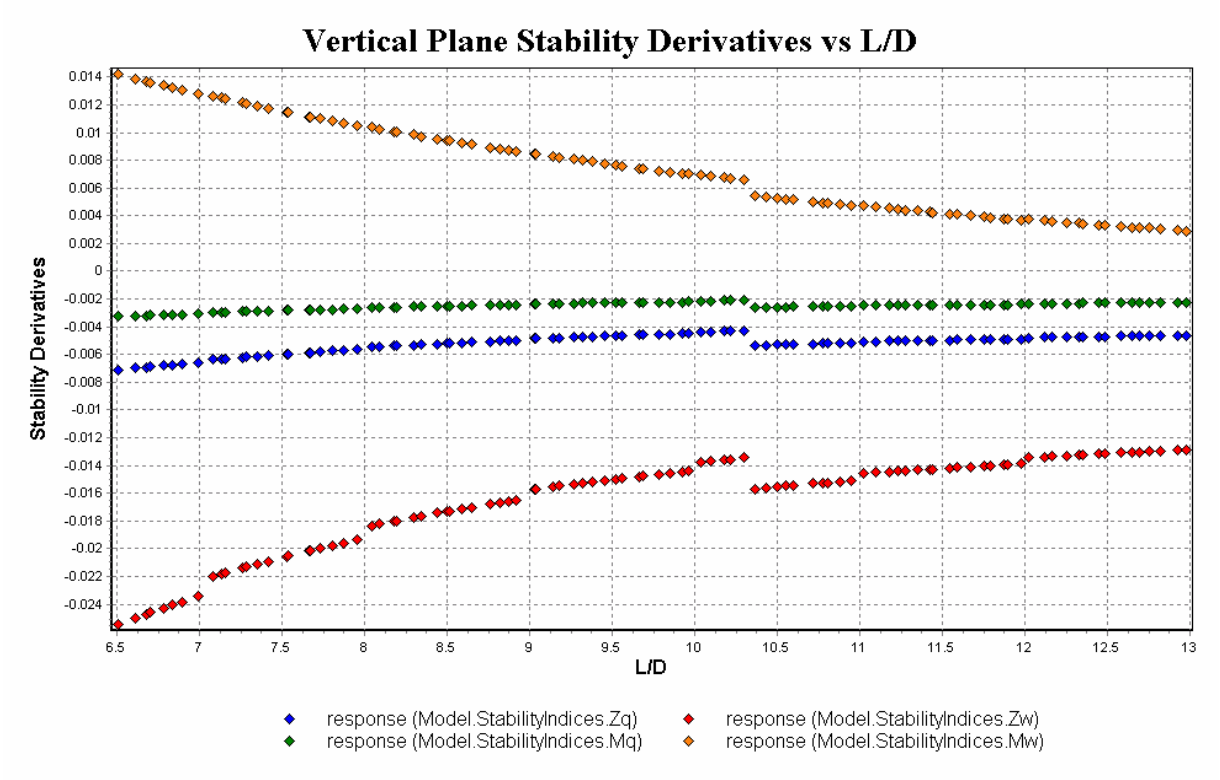

Figure 43. Vertical plane stability derivatives vs L/D.

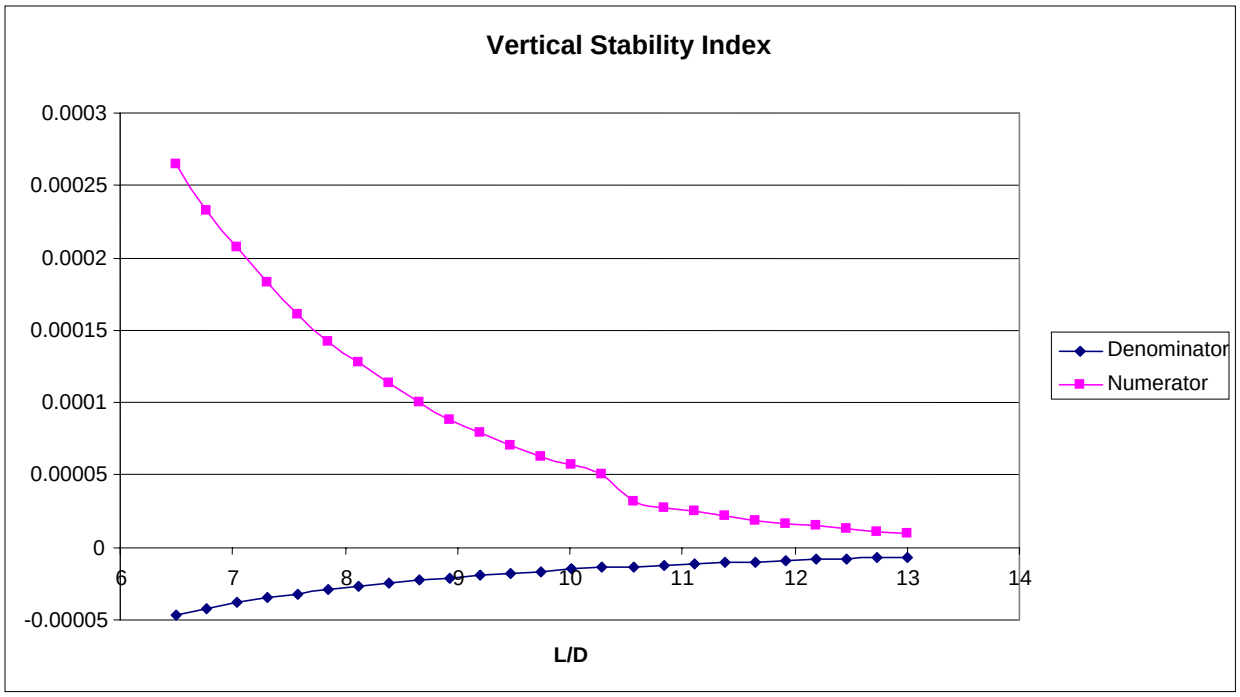

Figure 44. Denominator and numerator of vertical stability index vs L/D.

To further isolate the possible cause of the discontinuity the stability indices for the bare hull were also analyzed. This approach eliminates the control surface geometry as an input, making it dependent only on the hull offsets. Figure 45 is a plot of the stability indices versus the length to diameter ratio for the bare hull, i.e. no control surfaces. While there is not a large discontinuity there is a local maximum at a length to diameter ratio of about 9.75. There appears to be one trend in the data from length to diameter ratios of 6.5 to 9.75 and then a separate trend for length to diameter ratios greater than 9.75. This behavior is also unexpected. For a bare hull with no appendages a constant trend as the length to diameter ratio increases is expected. Eliminating the control surface geometry as an input and still finding an unusual trend in the data indicates that the initial cause of the discontinuity is not due to the control surfaces sizing method, instead it implies that the presence of the discontinuity may be due to the hull offsets. Therefore, the stability indices as a function of the length to diameter ratio for the bare hull using CEBAXI and LA_57 were also analyzed and the resulting plot is shown in Figure 46. There is one constant trend in the data as expected. Based on this information it was determined that it is likely that the cause of the discontinuity is not purely due to the hull offsets and control surface geometry methods derived in this thesis. The discontinuity may be a result of specific methods

utilized by GEORGE for specific calculations and there may be limitations to those methods that are unknown for the scope of this thesis.

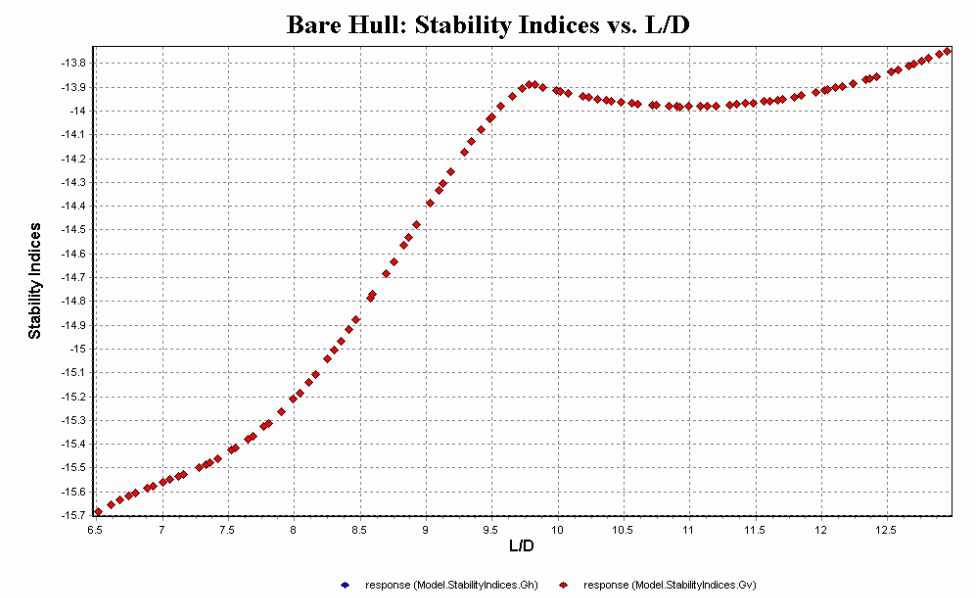

Figure 45. Stability indices vs. L/D for bare hull.

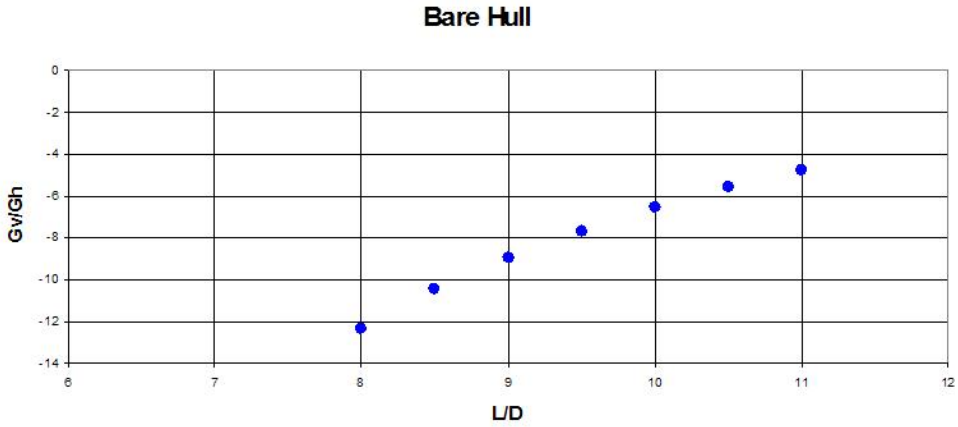

Figure 46. Stability indices vs L/D for bare hull data using CEBAXI and LA_57.

5.2 CEBAXI and LA_57 Dynamic Stability Model

Four separate design of experiments were performed using the CEBAXI and LA_57 model; one for each stern and forward plane configuration (sail planes with an x-stern, sail planes with a cruciform stern, bow planes with an x-stern, and bow planes with a cruciform

stern). The resulting plots for the DOE and RSM are provided in Appendix D. For each DOE the Latin-Hypercube algorithm was chosen to ensure sufficient exploration of the entire design space and the number of runs was set to 200. Four design variables were examined: length to diameter ratio, diameter, aft body fullness factor, and forward body fullness factor. Table 15 shows the specified range for each design variable. The horizontal and vertical stability indices, G_H and G_V, were the two response variables examined. The data sets created by the DOE were then analyzed and any outliers were deleted before further analysis was performed. An outlier was determined as a data set whose values were significantly outside of the apparent trend of the data. The modified data sets were then used to develop the corresponding RSM. The following sections detail the results of the four design of experiments that were performed and their resulting response surfaces.

Table 15. Design variables and high and low boundaries for CEBAXI and LA_57 stability model.

Design Variable	Low	High
L/D	6.5	13
D (ft)	22	32
na	2.5	3.5
nf	2	3

5.2.1 Configuration 1: Sail planes with an X-stern

Figure 47 and Figure 48 are plots of the main effects for the horizontal and vertical stability indices and demonstrate the sensitivity of the variables to one another. They show that the length to diameter ratio and diameter design variables have the greatest effect on the both of the stability indices for this configuration.

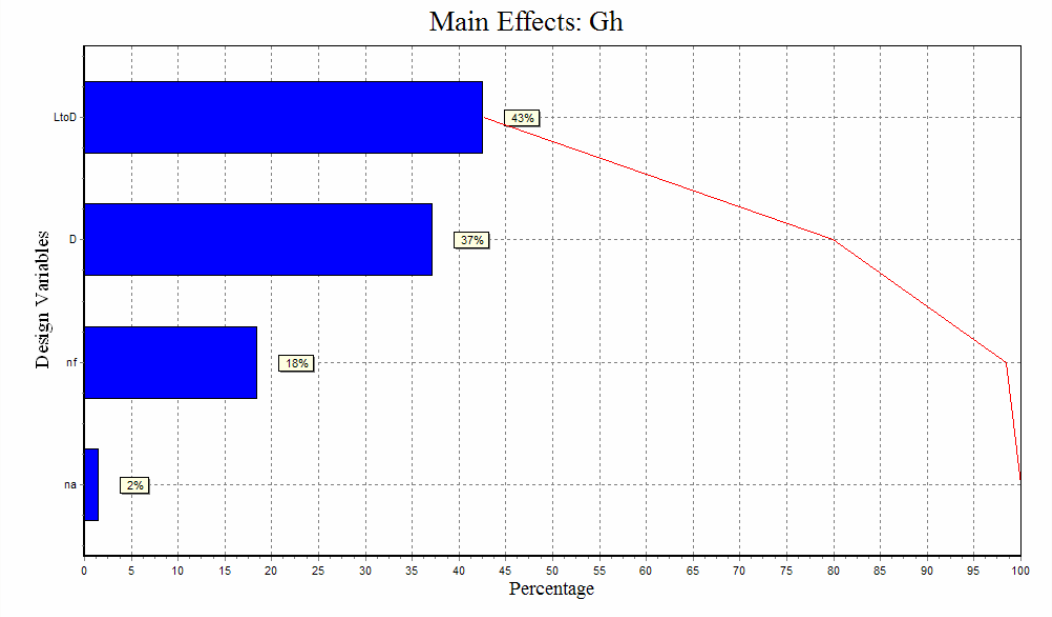

Figure 47. Gh main effects for CEBAXI and LA_57 configuration 1.

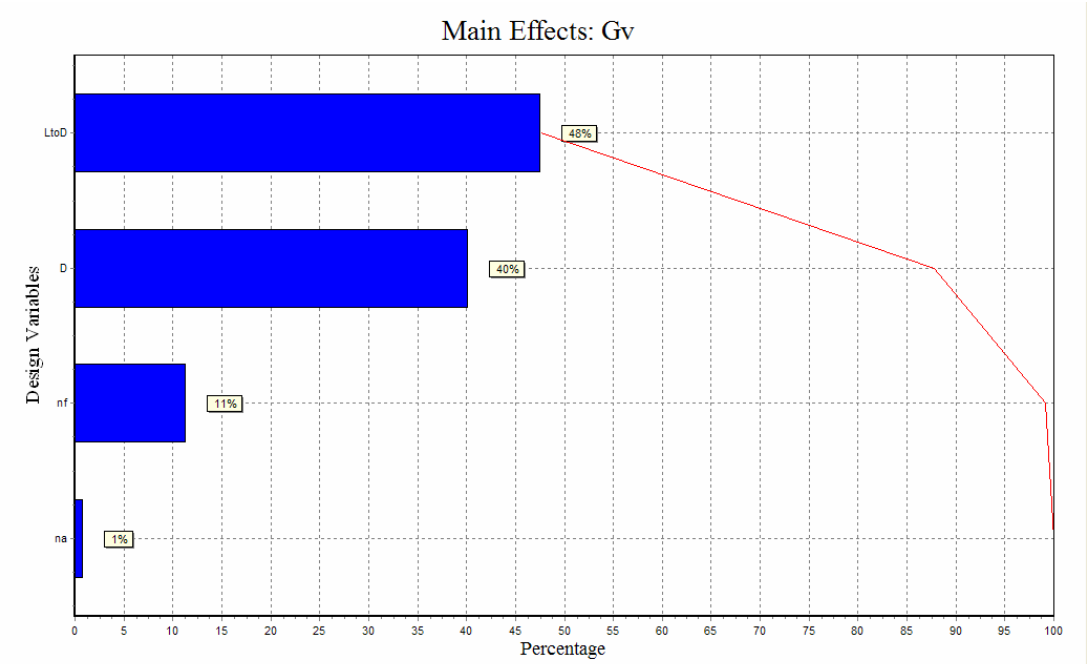

Figure 48. Gv main effects for CEBAXI and LA_57 configuration 1.

Figure 49 shows how the stability indices vary as a function of the length to diameter ratio. In general, the stability indices increase with increasing length to diameter ratios showing that long and slender submarines are more stable than short and fat submarines. Stable designs (indices greater than zero) do not occur until a length to diameter ratio of approximately 8.25. At

a length to diameter ratio near 11.5 stability in both the horizontal and vertical planes begins to plateau at values close to one indicating highly stable submarines.

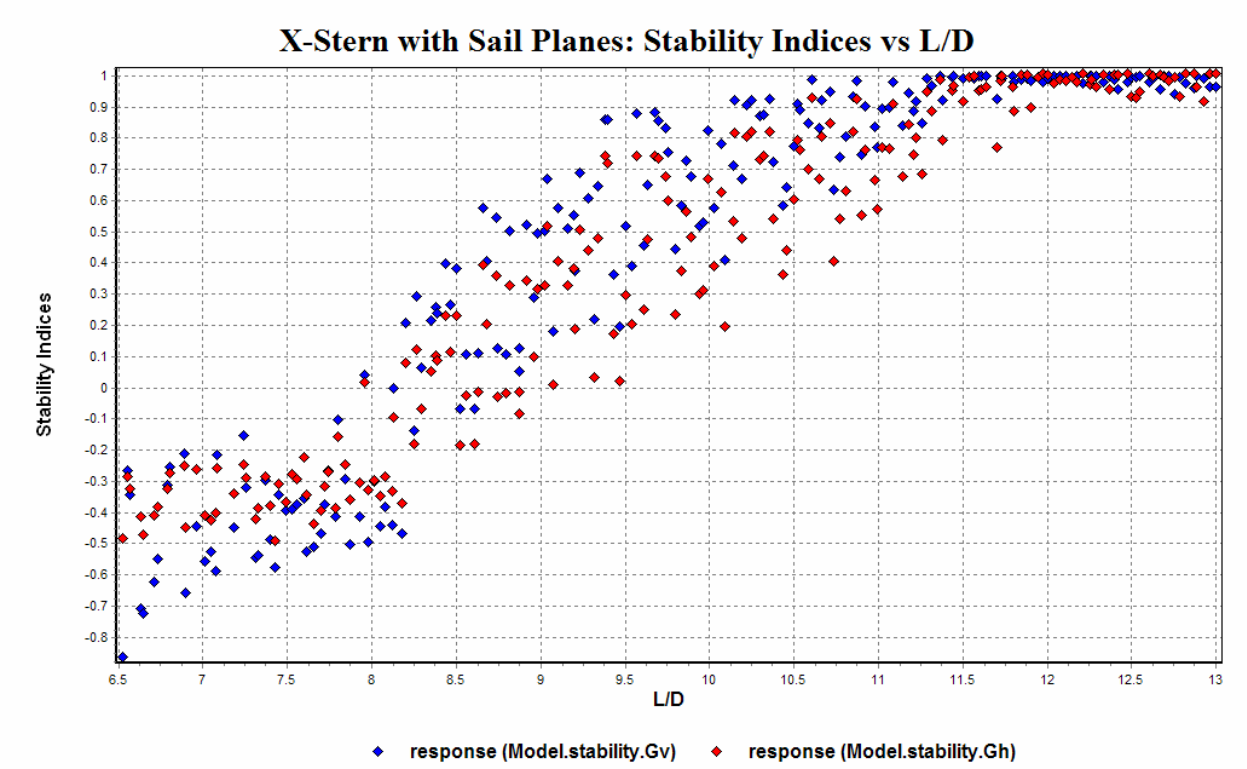

Figure 49. Stability indices vs L/D for configuration 1.

Figure 50 and Figure 51 are variable influence plots. The variable influence plots show both the main effects and interaction effects of the design variables. Higher order effects involve more than two variables and are grouped together into one category. The other category includes variables with an importance less than 0.5% for both stability indices the length to diameter ratio has the most influence. Therefore, Figure 50 and Figure 51 show that the length to diameter ratio has the most influence on both stability indices and the higher order effects are not of great importance.

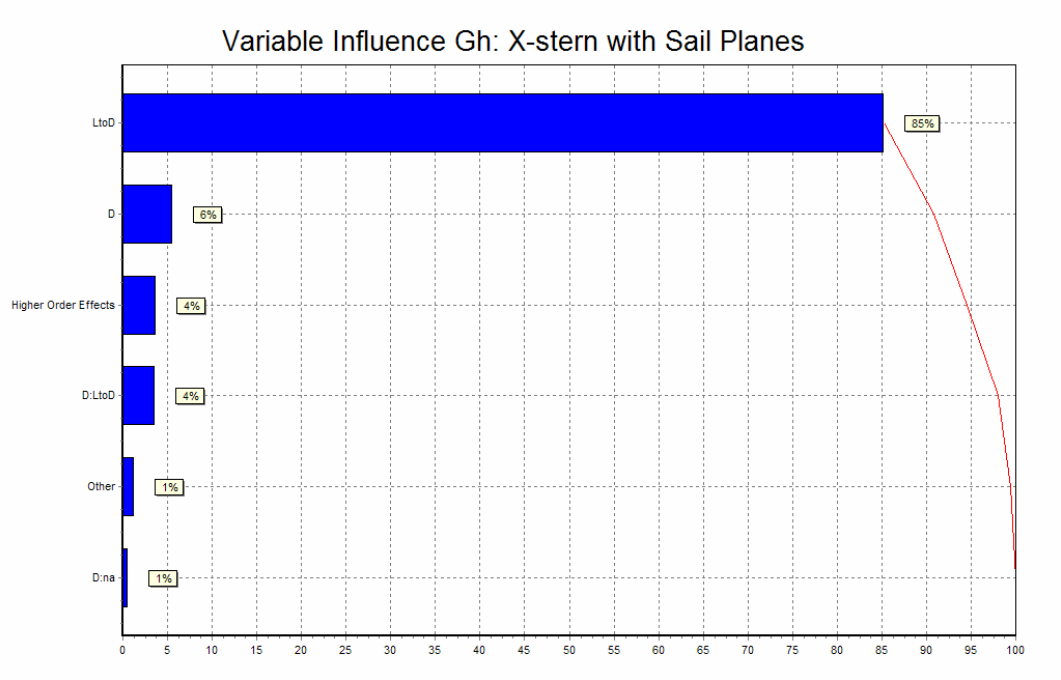

Figure 50. Gh variable influence for configuration 1.

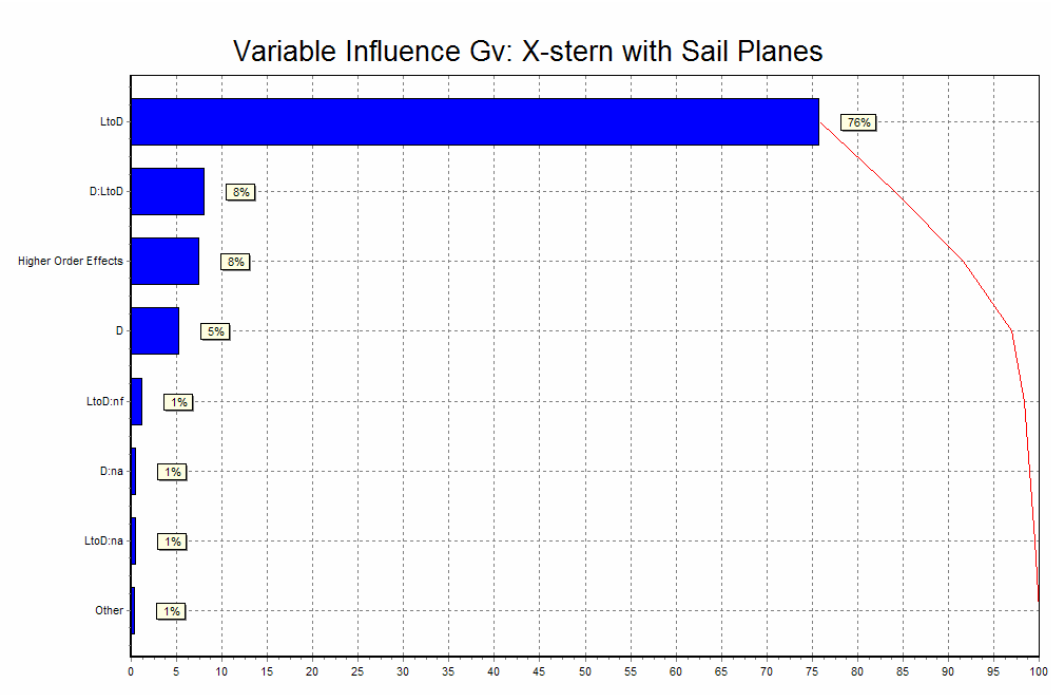

Figure 51. Gv variable influence for configuration 1.

Based on this information the response surface models were created using the full quadratic polynomial. Table 16 shows a summary of the statistical data for the response surfaces created.

Table 16. Statistical summary of RSM results for configuration 1.

X-stern with Sail Planes		
	Gh	Gv
S	0.1089	0.1348
Cov (%)	27.34	29.41
R^2 (%)	95.83	94.71
R^2_{adj} (%)	95.51	94.3

5.2.2 Configuration 2: X-stern with bow planes

Figure 52 and Figure 53 show that the length to diameter ratio and aft body fullness factor have the most influence on the stability indices and that diameter had less of an affect than in the X-stern configuration with sail planes (configuration 1).

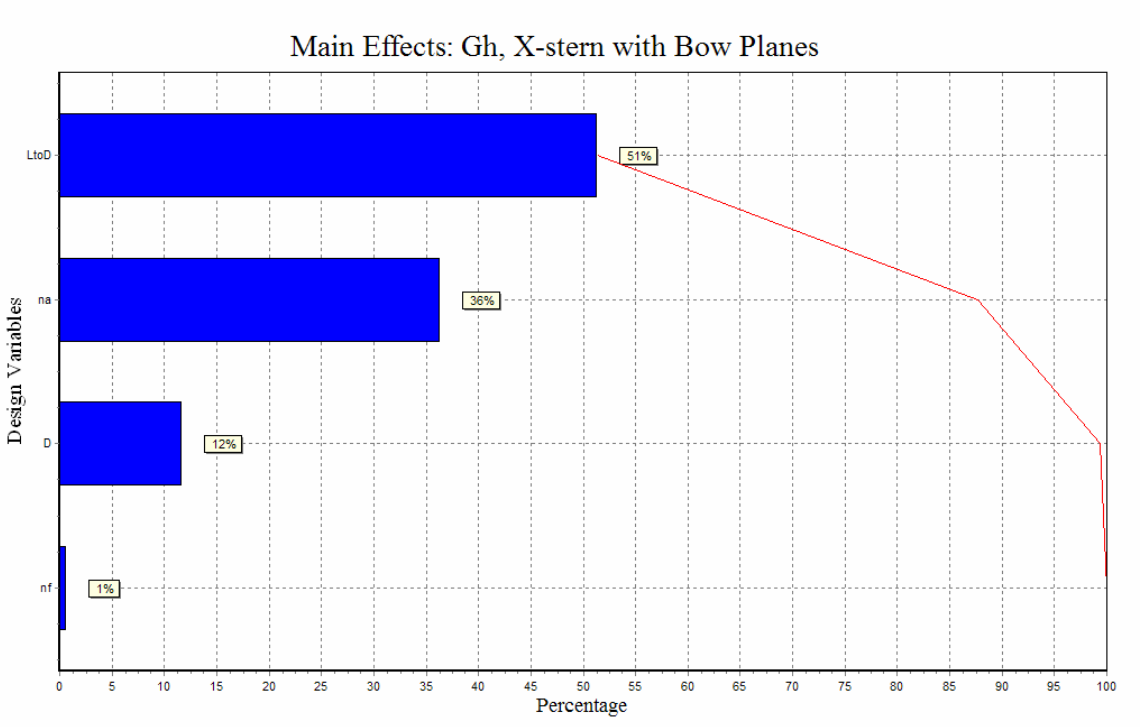

Figure 52. Gh main effects for configuration 2.

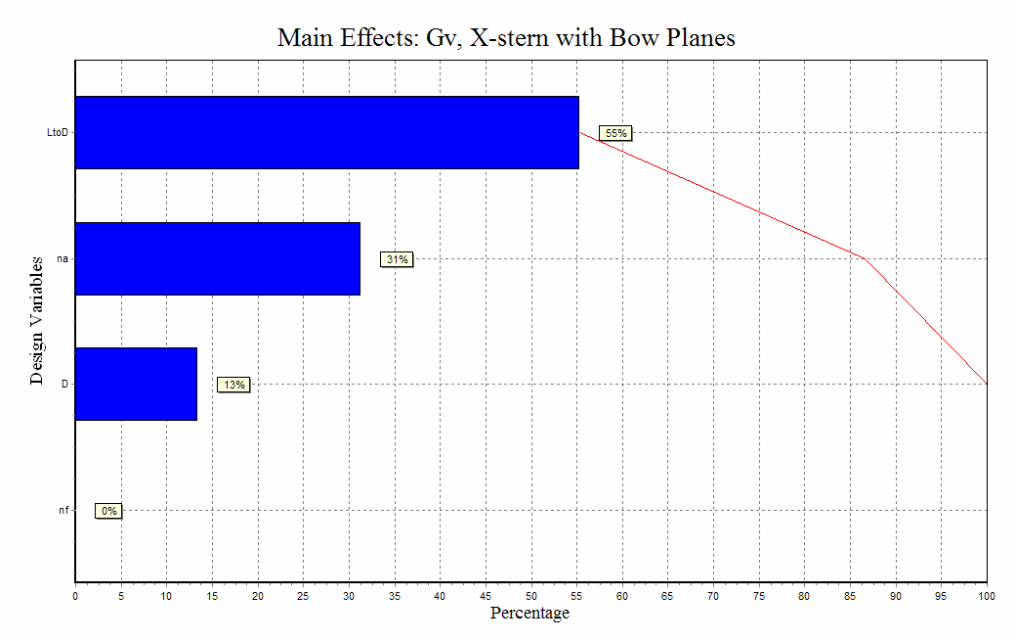

Figure 53. Gv main effects for configuration 2.

Figure 54 shows that as the length to diameter ratio and stability indices are directly proportional. Stable designs (indices greater than zero) are not seen until a length to diameter ratio of about 8.25. At a length to diameter ratio of approximately 11.5 the stability in both the horizontal and vertical planes begins to plateau and hover at values close to 1. In the middle range of length to diameter values (8.25 to 11.5) the span in values of G_H and G_v seems to be greater than in the X-stern configuration with sail planes (configuration 1).

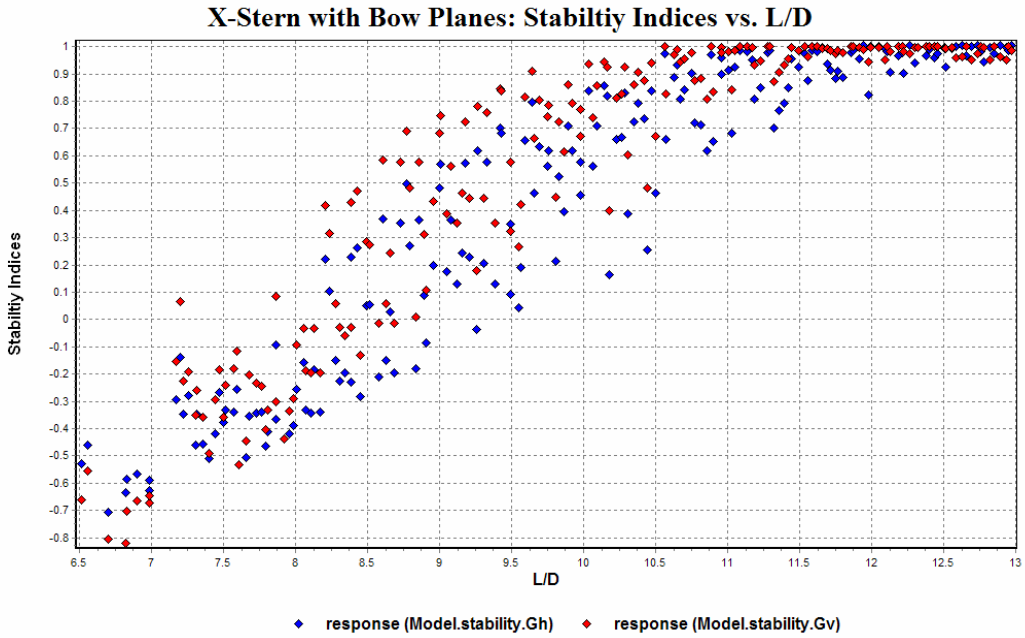

Figure 54. Stability indices vs L/D for configuration 2.

Figure 55 and Figure 56 show the main and interaction effects of the design variables. Length to diameter ratio is has the most influence on the stability indices and the higher order term effects are minimal. Therefore, a full quadratic polynomial response surface was fit to the data collected and the statistical details are shown in Table 17.

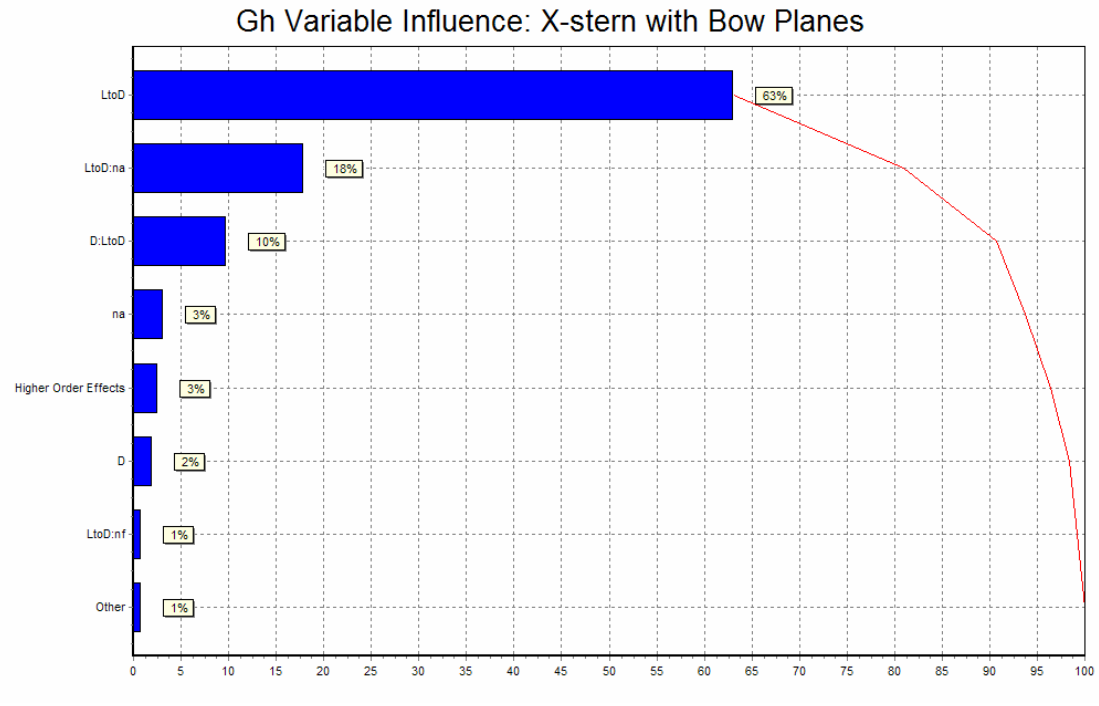

Figure 55. Gh variable influence for configuration 2.

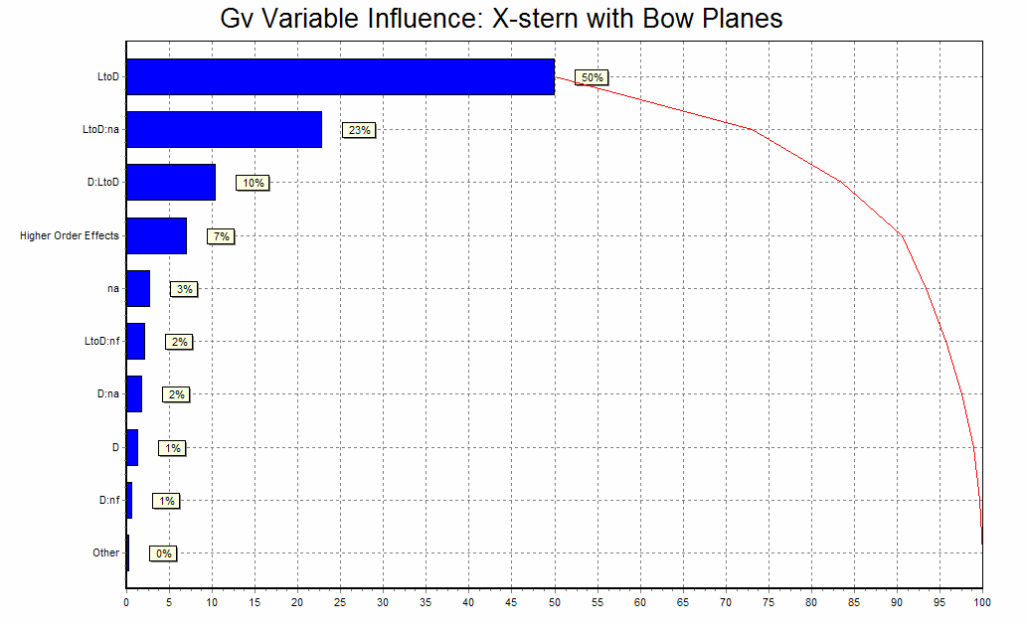

Figure 56. Gv variable influence for configuration 2.

Table 17. Statistical summary of RSM results for configuration 2.

X-stern with Bow Planes		
	Gh	Gv
S	0.1232	0.1199
Cov (%)	29.2	22.78
R^2 (%)	95.21	95.3
R^2_{adj} (%)	94.83	94.92

5.2.3 Configuration 3: Cruciform Stern with Sail Planes

Figure 57 and Figure 58 show that the length to diameter ratio and forward body fullness factor have the greatest effect on the stability indices.

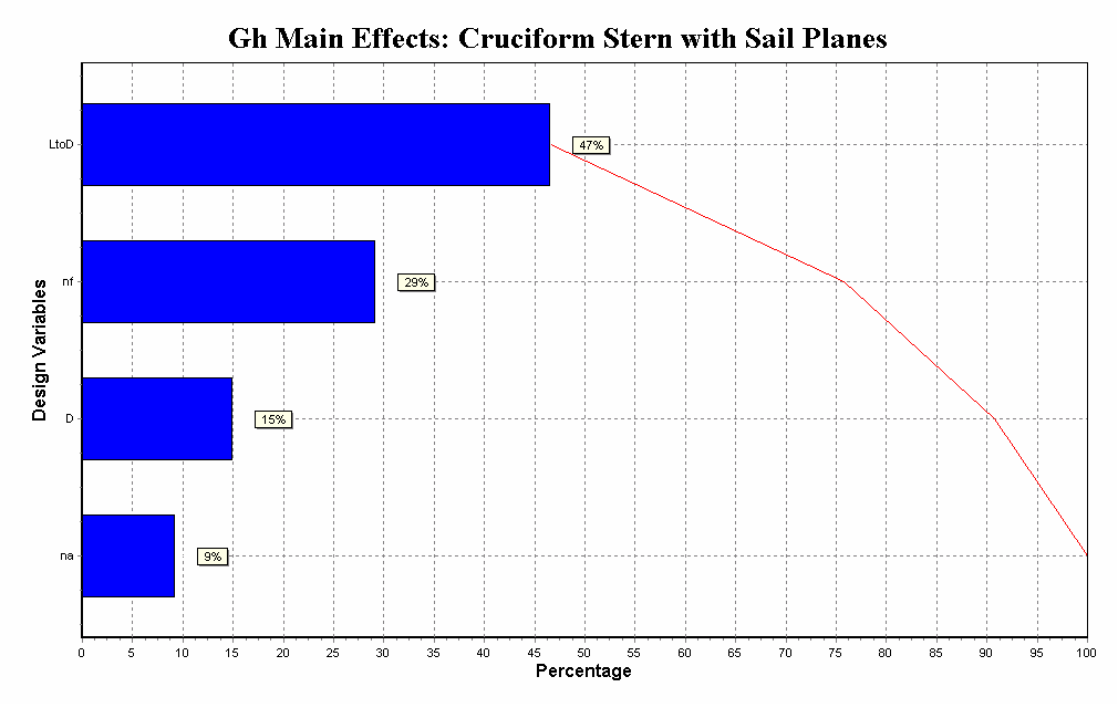

Figure 57. Gh main effects for configuration 3.

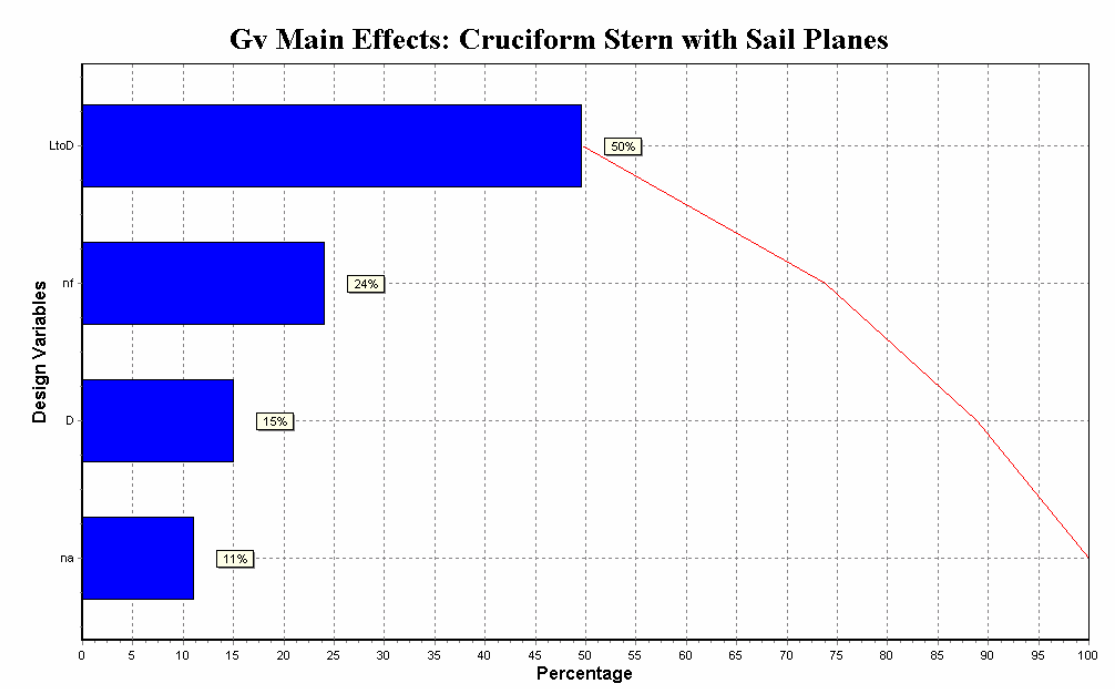

Figure 58. Gv main effects for configuration 3.

Figure 59 is a plot of the stability indices versus the length to diameter ratio. As the length to diameter ratio increases the stability indices increase. Designs with a length to diameter ratio approximately equal to or greater than 8 have stability in both the horizontal and vertical planes. For the designs with a length to diameter ratio less than 8 some have stability in the vertical plane, but none have horizontal plane stability. At a length to diameter ratio of 11.5 and greater stability in both planes plateaus to values close to one, indicating designs that are highly stable, but have limited maneuverability.

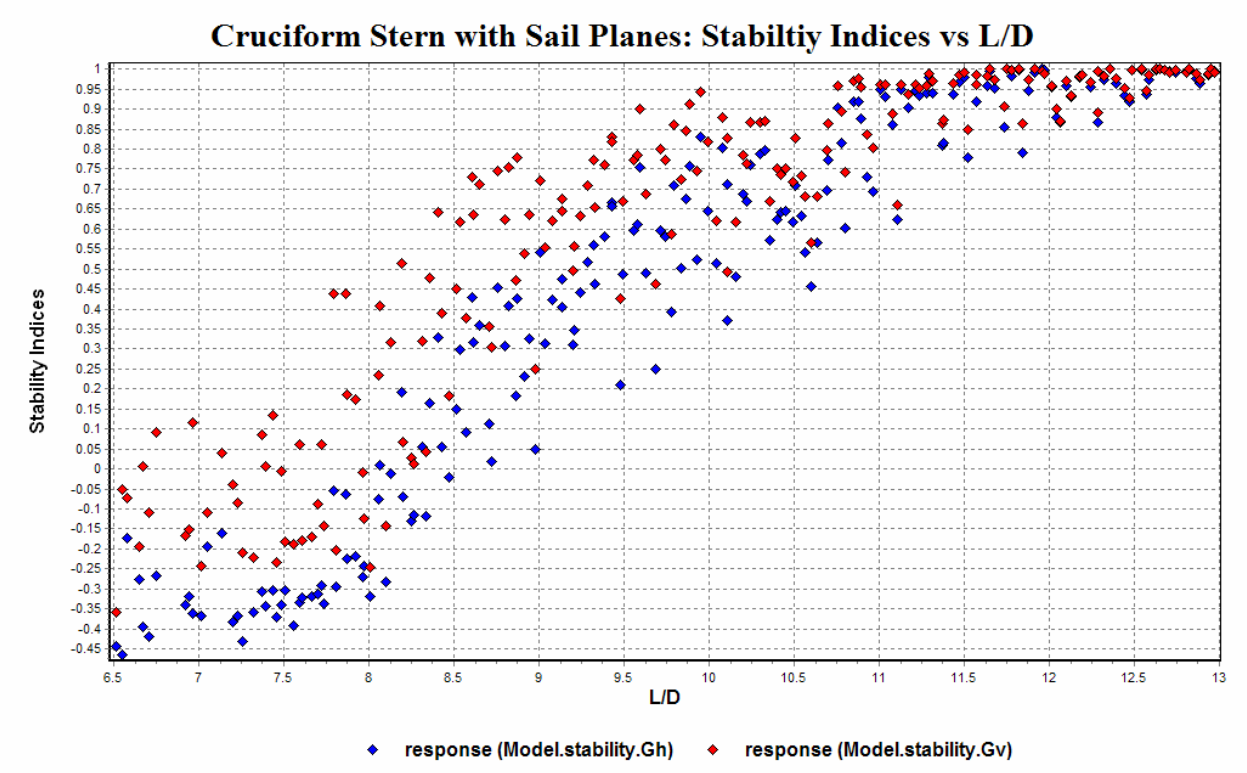

Figure 59. Stability indices vs. L/D for configuration 3.

Figure 60 and Figure 61 display the main and interaction effects for this configuration. The length to diameter ratio is the dominating effect and the higher order terms have little influence on the stability indices. Therefore, a full quadratic response surface was created. The statistical details of the horizontal and vertical stability indices response surfaces are shown in Table 18.

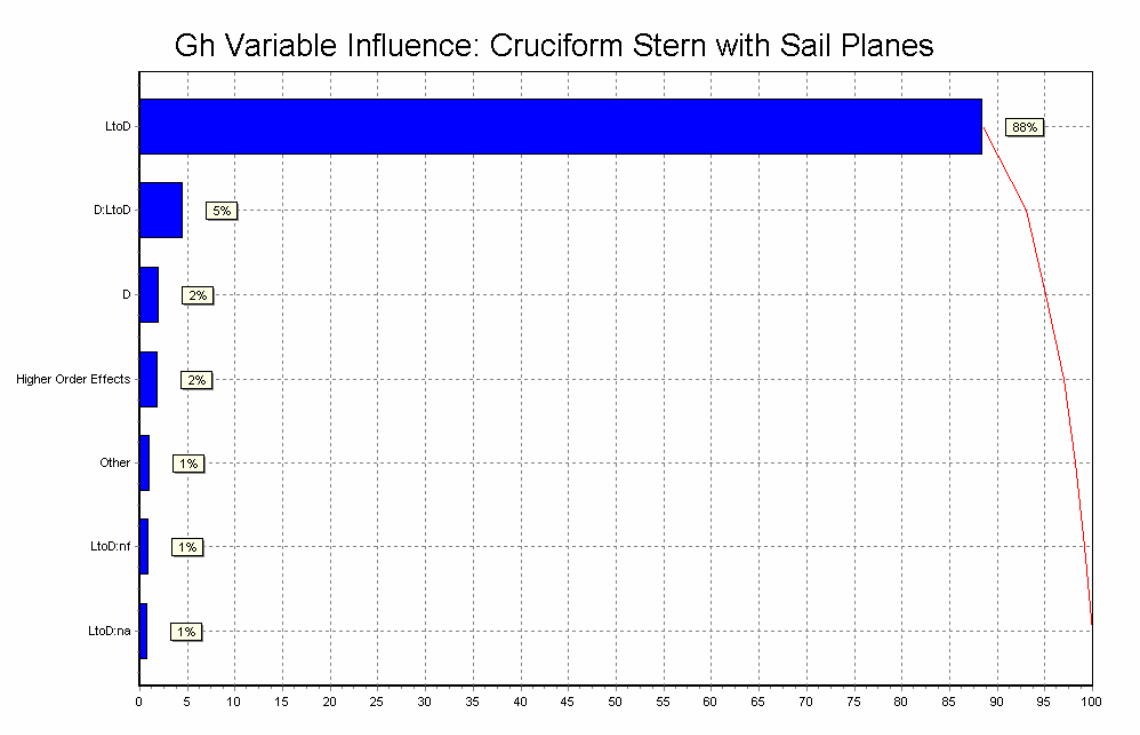

Figure 60. Gh variable influence for configuration 3.

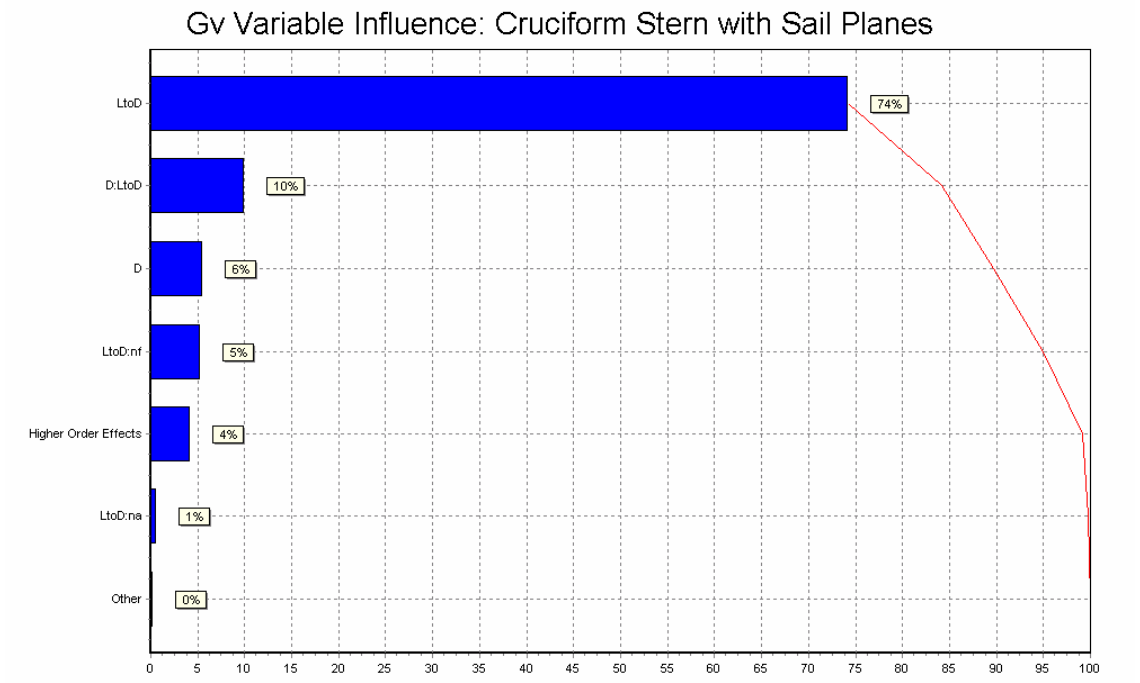

Figure 61. Gv variable influence for configuration 3.

Table 18. Statistical summary of RSM results for configuration 3.

Cruciform Stern with Sail Planes		
	Gh	Gv
S	0.1025	0.0877
Cov (%)	22.25	14.51
R^2 (%)	95.9	95.65
R^2adj (%)	95.57	95.3

5.2.4 Configuration 4: Cruciform Stern with Bow Planes

A summary of the main effects for each stability index is shown in Figure 62 and Figure 63. The length to diameter ratio has the greatest influence on both the horizontal and vertical stability indices.

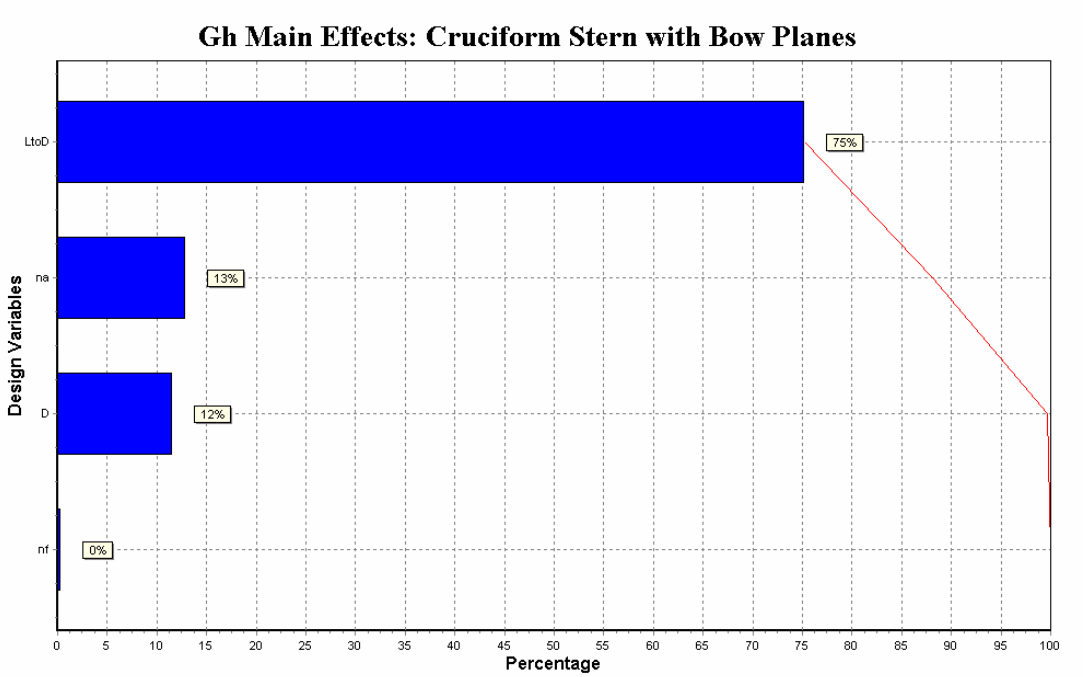

Figure 62. Gh main effects for configuration 4.

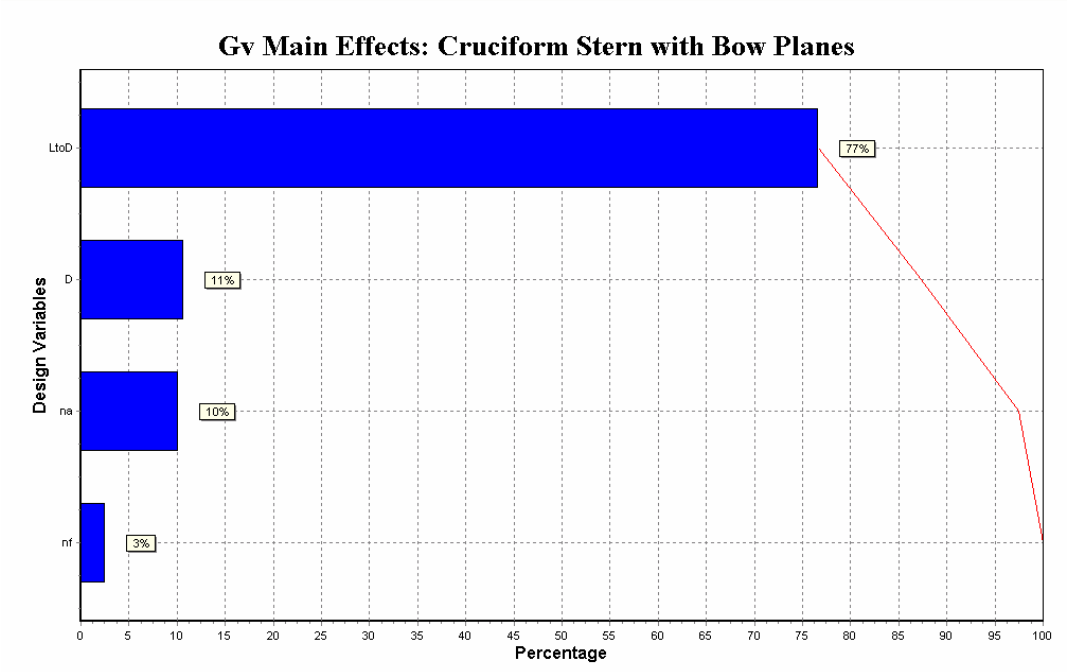

Figure 63. Gv main effects for configuration 4.

Figure 64 plots the stability indices as a function of the length to diameter ratio. The stability indices are directly related to the length to diameter ratio. Designs that have a length to diameter ratio approximately equal to or greater than 8 are stable. For designs with a length to diameter ratio less than 8 some achieve vertical stability, but none are horizontally stable.

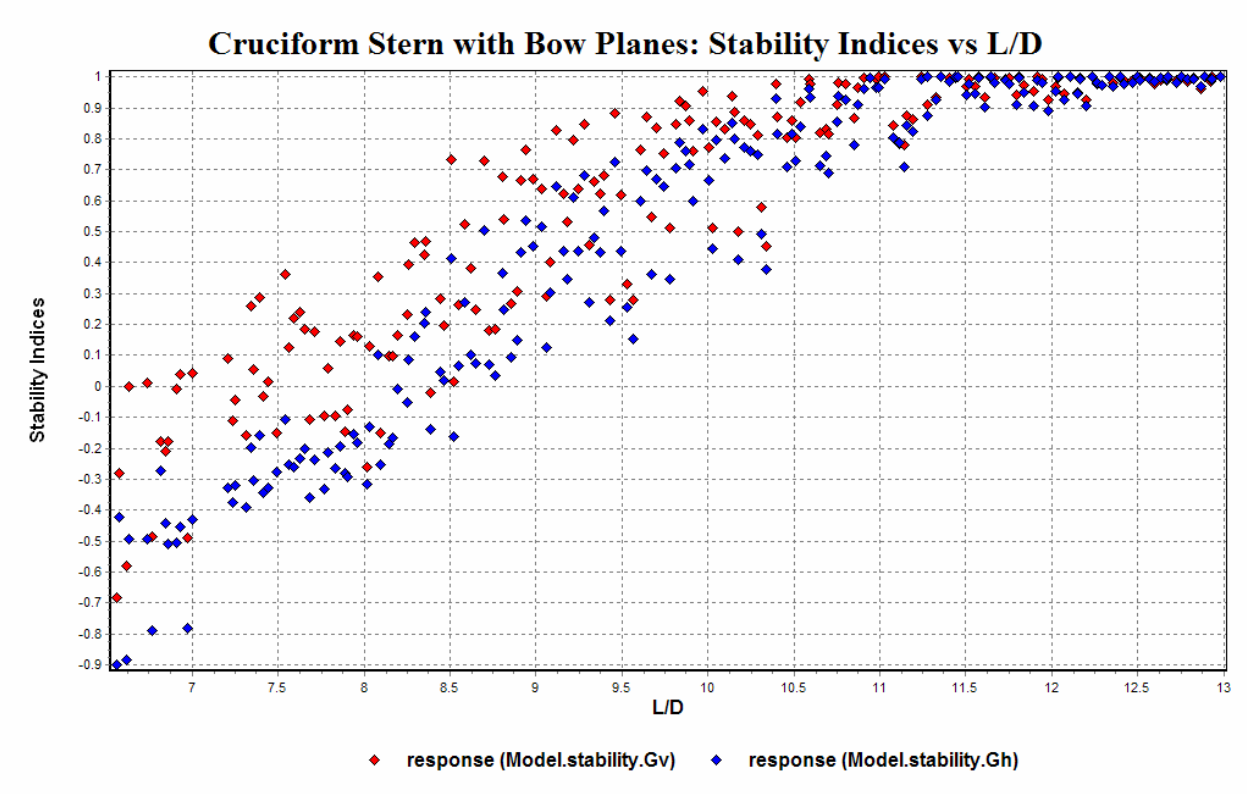

Figure 64. Stability indices vs L/D for configuration 4.

Figure 65 and Figure 66 show the main and interaction effects for the horizontal and vertical stability indices respectively. The length to diameter ratio is the dominating variable and the higher order terms have little effect. Therefore, a full quadratic polynomial was used to create the horizontal and vertical response surfaces. The statistical details of these response surfaces are provided in Table 19.

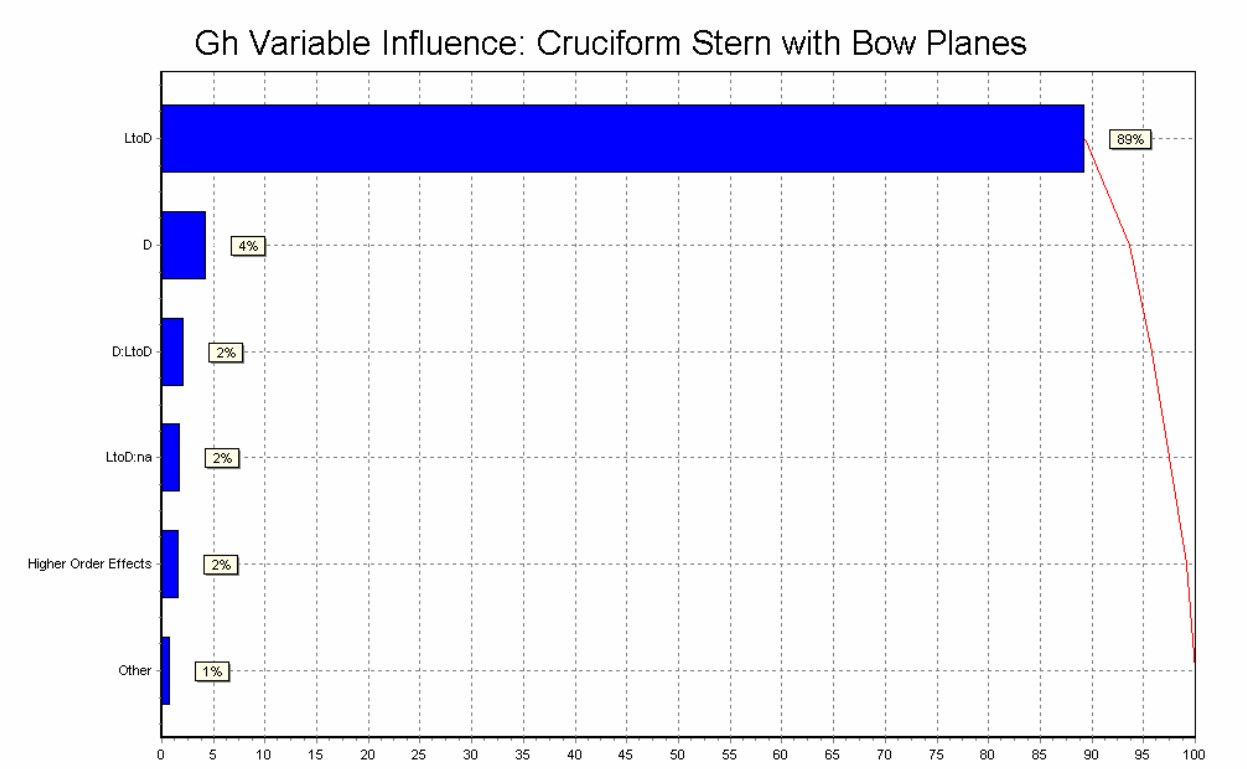

Figure 65. Gh variable influence for configuration 4.

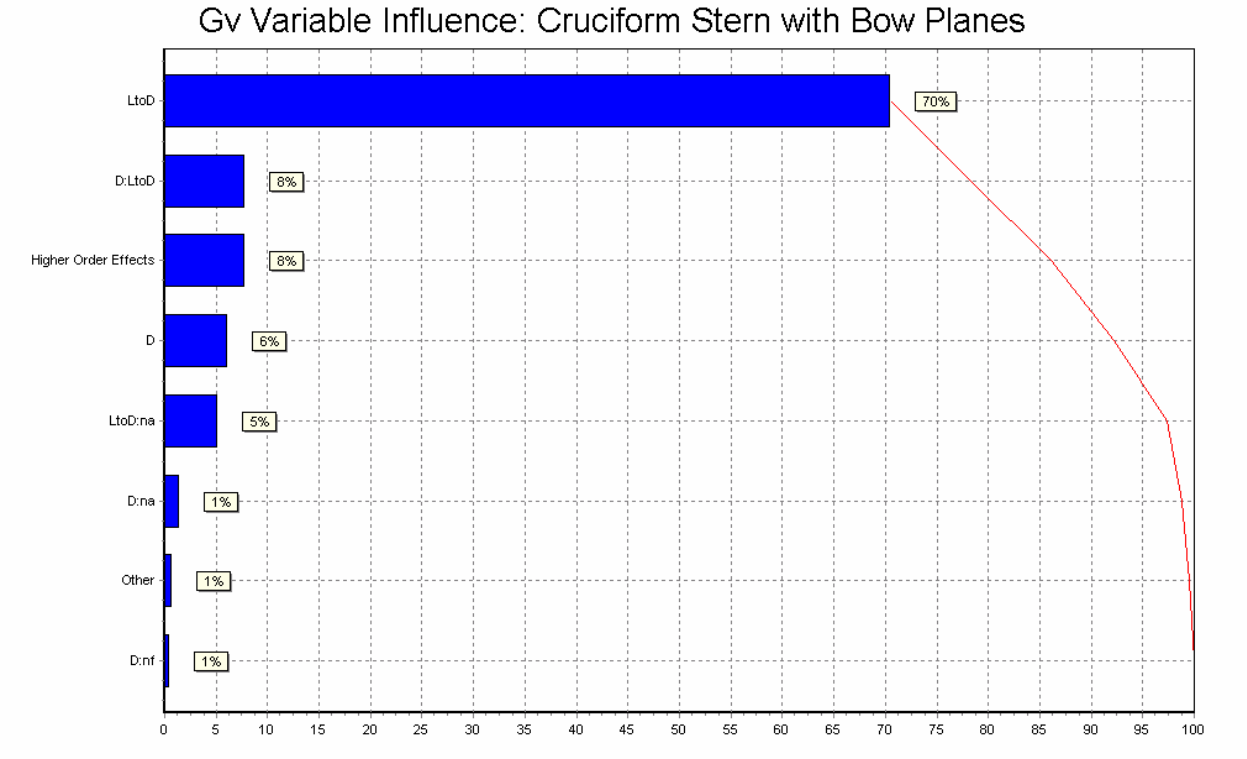

Figure 66. Gv variable influence for configuration 4.

Table 19. Statistical summary of RSM results for configuration 4.

Cruciform Stern with Bow Planes		
	Gh	Gv
S	0.086	0.0727
Cov (%)	17.65	11.68
R^2 (%)	97.27	96.84
R^2_{adj} (%)	97.04	96.59

5.2.5 Summary

A design of experiments was performed for each forward plane and stern plane configuration and based on the data collected corresponding response surfaces were created. For all four configurations the length to diameter ratio had the greatest impact on the stability indices. For x-stern configuration stability in both the horizontal and vertical planes was not reached until a length to diameter ratio of approximately 8.25. For cruciform stern configurations stability was achieved in both planes at a length to diameter ratios of approximately 8 or greater. Stability for both planes began to plateau at values close to one for length to diameter ratios of 11.5 and greater for all configurations. The difference between the values for the horizontal and vertical stability indices for a given design is greater for designs with a cruciform stern. Therefore, based on the criteria set in Chapter 2 to guarantee a good tradeoff of stability and maneuverability for the individual indices (G_H should vary from 0.15 to 0.30 and G_v should vary form 0.5 to 0.7) the data collected shows that a cruciform stern would be the most effective towards meeting this criteria.

In all configurations, there were fewer designs evaluated at the lowest range of length to diameter ratios, specifically from length to diameter ratios in the range of 6.5 to 8. This is because this range had a high number of data sets that were outliers and deleted before analysis was performed. This concentration of outliers is suspected to be due to two different factors. One factor is that the CEBAXI program designed to make boundary layer approximation necessary to run LA_57 is sensitive to the placement of the stern planes on the aft end of the hull. If the stern planes are placed at a point on the hull where the radius is too large then the program has difficulty creating the stern velocity profiles. This causes the program to either stop its execution without producing any data or to produce velocity profiles that may be poor approximations. The other factor to consider is that the control surface database was created using designs that had a range of length to diameter ratios from 8 to 13. Designs with a ratio less than 8 were not included because it was difficult to find these designs. A linear trendline was used to fit the control surface

data so that it could be easily extrapolated to included designs with a lower length to diameter ratio. The fact that the data collected at these lower ratios may indicate that this linear assumption at low length to diameter ratios is not an appropriate assumption. This would also explain why there were no designs below a length to diameter ratio of 8 that were stable. It is known that shorter, fat submarines are inherently more unstable than long, slender submarines. Therefore, the designs with a smaller length to diameter ratio need larger control surfaces to increase stability. The assumption of a linear trendline would again not be accurate.

5.3 GEORGE and CEBAXI and LA_57 Comparison

The results obtained from CEBAXI and LA_57 model differed from the results of the GEORGE model. CEBAXI and LA_57 model did not show significant discontinuities in the data like those shown in the GEORGE model. CEBAXI and LA_57 model did have difficultly predicting the stability indices at the upper and lower bounds of the ranges explored but this is most likely a consequence of the data used to create the control surface database as discussed in Section 5.2.5. Based on these conclusions it was determined that CEBAXI and LA_57 model provided the most reasonable data.

CHAPTER 6 CONVENTIONAL GUIDED MISSILE SUBMARINE (SSG(X)) DESIGN CASE STUDY

This chapter describes a case study based on the concept exploration of a submarine from Virginia Tech's 2006 Senior Design course. Section 1.2 describes the general multi-objective optimization process used in this course. This chapter describes the SSG(X) required missions and the OMOE (Overall Measure of Effectiveness) metrics used to assess the design. The response surfaces created in Chapter 5 are included as part of the OMOE evaluation for the design. The details of the submarine synthesis model are described and an optimization is set up, run, and the results discussed.

6.1 SSG(X) Mission Definition and OMOE Development

SSG(X) is a conventional guided missile submarine developed to perform two main missions:

1. Time sensitive and covert missile and torpedo launch.
2. Covert Intelligence, Surveillance, and Reconnaissance (ISR) operations.

In addition, the SSG(X) should be designed for minimum cost. The lead-ship acquisition cost should be less than $1B and the follow-ship acquisition cost should be no more than $700M. The platform must be highly producible to minimize time from concept to delivery. It should also be flexible enough to support variants. The platform must operate within current logistics support capabilities and it must consider inter-service and C^4/I. The design should focus on survivability in a high-threat environment and operation in all warfare areas. The platform should be non-nuclear since the SSG(X) will operate in enemy littoral regions. A typical mission scenario for each mission is described in Table 20 and Table 21.

Table 20. ISR Mission Scenario [1].

Day	Mission scenario
1-15	Depart from CONUS on snorkel to area of hostilities
15-16	Proceed independently to within 10 nautical miles (nm) of enemy mainland
16-20	Conduct ISR
16	Avoid/neutralize enemy submarine attack
17	Conduct mine counter warfare. Launch counter mine AUVs that will detect and neutralize threat.
20-30	Continue ISR
28	Engage enemy patrol craft using Harpoon cruise missile
30	Return to sea base for rearming and refueling

Table 21. Missile Mission Scenario [1].

Day	Mission scenario
1-15	Depart from home base submerged. Transit at snorkel depth, having batteries charged upon arrival.
15	Launch strike missiles against land target. Launch anti-air defense against an enemy ASW helicopter.
16	Kill incoming cruise missile salvo against CBG in cooperation with DDG.
17	Avoid/neutralize enemy submarine attack
18	Receive re-targeting information and perform cruise missile strike against updated targets.
19-20	Conduct mine counter warfare. Launch counter mine AUVs that will detect and neutralize threat.
15-30	Conduct EM, visual and radio reconnaissance
20	Replenish fuel and stores at sea base
25	Cooperatively, with Aegis unit, detect, engage, and kill incoming cruise missile salvo on CBG unit
26	Engage and destroy enemy surface ships using Harpoon cruise missiles
30	Return to sea base for rearming and refueling

Required Operational Capabilities (ROCs) are identified to perform each mission and measures of performance (MOPs) are defined to specify those capabilities that will vary in the designs as a function of the submarine Design Variables (DVs). Each MOP is assigned a threshold and goal value. ROCs and applicable restraints to all designs are specified in Table 22.

Table 22 - ROC/MOP/DV Summary [1].

ROCs	Description	Applicable Systems and Technology	MOP	Related DV	Goal	Threshold
AAW 1.2	Support area anti-air defense	VLS; Sea Sentry; BPS-16 Radar; BPS-15 Radar; BSY-1; BSY-2; SUBTICS	AAW C4I/SPW	SAIL VLS SONARSYS	SAIL=1 VLS=1 SONARSYS=1	SAIL=4 VLS=3 SONARSYS=4
AAW 2	Provide anti-air defense in cooperation with other forces	VLS; Sea Sentry; BPS-16 Radar; BPS-15 Radar; BSY-1; BSY-2; SUBTICS; AN/BRAi-34	AAW C4I/SPW	SAIL VLS SONARSYS	SAIL=1 VLS=1 SONARSYS=1	SAIL=4 VLS=3 SONARSYS=4
AAW 9	Engage airborne threats using surface-to-air armament	VLS; Sea Sentry; BPS-16 Radar; BPS-15 Radar; BSY-1; BSY-2; SUBTICS	AAW C4I/SPW	SAIL VLS SONARSYS	SAIL=1 VLS=1 SONARSYS=1	SAIL=4 VLS=3 SONARSYS=4
AMW 6	Conduct airborne autonomous vehicle (AAV) operations	Sea Sentry; BPS-16 Radar; BPS-15 Radar; BSY-1; BSY-2; SUBTICS	AAW C4I/SPW	SAIL SONARSYS	SAIL=1 SONARSYS=1	SAIL=3 SONARSYS=4
ASU 1	Engage surface threats with anti-surface armaments	Full 6 or 4 21" tubes; Sea Sentry; BPS-16 Radar; BPS-15 Radar; BQQ-10 Sonar; BQQ-5 Sonar; BQQ-6 Sonar; Thales Suite Sonar; BSY-1; BSY-2; SUBTICS	ASuW	TORP SONARSYS SAIL VLS	TORP=1 SONARSYS=1 SAIL=1 VLS =1	TORP=9 SONARSYS=4 SAIL=4 VLS =3
ASU 1.1	Engage surface ships at long range	Full 6 or 4 21" tubes; Sea Sentry; BPS-16	ASuW	TORP SONARSYS	TORP=1 SONARSYS=1	TORP=9 SONARSYS=4

ROCs	Description	Applicable Systems and Technology	MOP	Related DV	Goal	Threshold
		Radar; BPS-15 Radar; BQQ-10 Sonar; BQQ-5 Sonar; BQQ-6 Sonar; Thales Suite Sonar; BSY-1; BSY-2; SUBTICS		SAIL VLS	SAIL=1 VLS =1	SAIL=4 VLS =3
ASU 1.2	Engage surface ships at medium range	Full 6 or 4 21" tubes; Sea Sentry; BPS-16 Radar; BPS-15 Radar; BQQ-10 Sonar; BQQ-5 Sonar; BQQ-6 Sonar; Thales Suite Sonar; BSY-1; BSY-2; SUBTICS	ASuW	TORP SONARSYS SAIL VLS	TORP=1 SONARSYS=1 SAIL=1 VLS =1	TORP=9 SONARSYS=4 SAIL=4 VLS =3
ASU 2	Engage surface ships in cooperation with other forces	Full 6 or 4 21" tubes; Sea Sentry; BPS-16 Radar; BPS-15 Radar; BQQ-10 Sonar; BQQ-5 Sonar; BQQ-6 Sonar; Thales Suite Sonar; BSY-1; BSY-2; SUBTICS	ASuW C4I/SPW	TORP SONARSYS SAIL VLS	TORP=1 SONARSYS=1 SAIL=1 VLS =1	TORP=9 SONARSYS=4 SAIL=4 VLS =3
ASU 4.2	Detect and track a surface target using sonar	Full 6 or 4 21" tubes; Sea Sentry; BPS-16 Radar; BPS-15 Radar; BQQ-10 Sonar; BQQ-5 Sonar; BQQ-6 Sonar; Thales Suite Sonar; BSY-1; BSY-2; SUBTICS	ASuW	TORP SONARSYS SAIL VLS	TORP=1 SONARSYS=1 SAIL=1 VLS =1	TORP=9 SONARSYS=4 SAIL=4 VLS =3
ASU 6	Disengage, evade and avoid surface attack	Full 6 or 4 21" tubes; Sea Sentry; BPS-16 Radar; BPS-15 Radar; BQQ-10 Sonar; BQQ-5 Sonar; BQQ-6 Sonar; Thales Suite Sonar; BSY-1; BSY-2; SUBTICS ;Shrike ESM; WLY-1 system; AN/BLQ-10 (ESM); WLR-8(V)2 ESM; AN/BRD-7/BLD-1	ASuW	TORP SONARSYS SAIL VLS ESM	TORP=1 SONARSYS=1 SAIL=1 VLS =1 ESM = 1	TORP=9 SONARSYS=4 SAIL=4 VLS =3 ESM = 2
ASW 1	Engage submarines	Full 4-6x21" tubes w/ Reloads, Encapsulated Torpedoes; Sea Sentry; LWWAA, WAA, BQQ-10 Sonar, BQQ-5, BQQ-6, BQR-19 Navigation, BQR-13 Active, Chin-Array, TB-16, TB-29A, Thales Sonar Suite; BSY-1, BSY-2, SUBTICS	ASW	TORP VLS SONARSYS	TORP =1 VLS =1 SONARSYS =1	TORP =9 VLS =3 SONARSYS=4
ASW 1.2	Engage submarines at medium range	Full 4-6x21" tubes w/ Reloads, Encapsulated Torpedoes; Sea Sentry; LWWAA, WAA, BQQ-10 Sonar, BQQ-5, BQQ-6, BQR-19 Navigation, BQR-13 Active, Chin-Array, TB-16, TB-29A,	ASW	TORP VLS SONARSYS	TORP =1 VLS =1 SONARSYS =1	TORP =9 VLS =3 SONARSYS=4

ROCs	Description	Applicable Systems and Technology	MOP	Related DV	Goal	Threshold
		Thales Sonar Suite; BSY-1, BSY-2, SUBTICS				
ASW 1.3	Engage submarines at close range	Full 4-6x21" tubes w/ Reloads, Encapsulated Torpedoes; Sea Sentry; SPAT; LWWAA, WAA, BQQ-10 Sonar, BQQ-5, BQQ-6, BQR-19 Navigation, BQR-13 Active, Chin-Array, TB-16, TB-29A, Thales Sonar Suite; BSY-1, BSY-2, SUBTICS	ASW	TORP VLS SONARSYS	TORP =1 VLS =1 SONARSYS =1	TORP =9 VLS =3 SONARSYS=4
ASW 2	Engage submarines in cooperation with other forces	Full 4-6x21" tubes w/ Reloads, Encapsulated Torpedoes; Sea Sentry; SPAT; LWWAA, WAA, BQQ-10 Sonar, BQQ-5, BQQ-6, BQR-19 Navigation, BQR-13 Active, Chin-Array, TB-16, TB-29A, Thales Sonar Suite; BSY-1, BSY-2, SUBTICS; AN/BRAi-34	ASW C4I/SPW	TORP VLS SONARSYS	TORP =1 VLS =1 SONARSYS =1	TORP =9 VLS =3 SONARSYS=4
ASW 7	Attack submarines with antisubmarine armament	Full 4-6x21" tubes w/ Reloads, Encapsulated Torpedoes; Sea Sentry; SPAT; LWWAA, WAA, BQQ-10 Sonar, BQQ-5, BQQ-6, BQR-19 Navigation, BQR-13 Active, Chin-Array, TB-16, TB-29A, Thales Sonar Suite; BSY-1, BSY-2, SUBTICS, MK 60 Mine Launcher	ASW MIW	TORP VLS SONARSYS	TORP =1 VLS =1 SONARSYS =1	TORP =9 VLS =3 SONARSYS=4
ASW 7.6	Engage submarines with torpedoes	Full 4-6x21" tubes w/ Reloads, Encapsulated Torpedoes; Sea Sentry; SPAT; LWWAA, WAA, BQQ-10 Sonar, BQQ-5, BQQ-6, BQR-19 Navigation, BQR-13 Active, Chin-Array, TB-16, TB-29A, Thales Sonar Suite; BSY-1, BSY-2, SUBTICS	ASW	TORP VLS SONARSYS	TORP =1 VLS =1 SONARSYS =1	TORP =9 VLS =3 SONARSYS=4
ASW 8	Disengage, evade, avoid and deceive submarines	Full 4-6x21" tubes w/ Reloads, Encapsulated Torpedoes; Sea Sentry; SPAT; LWWAA, WAA, BQQ-10 Sonar, BQQ-5, BQQ-6, BQR-19 Navigation, BQR-13 Active, Chin-Array, TB-16, TB-29A, Thales Sonar Suite; BSY-1, BSY-2, SUBTICS; 3"-6.75" Countermeasure	ASW ESM IR Acoustic	TORP VLS SONARSYS PSYStype PROPtype	TORP =1 VLS =1 SONARSYS =1 PSYStype =6 PROPtype =1	TORP =9 VLS =3 SONARSYS =4 PSYStype =4 PROPtype =2

ROCs	Description	Applicable Systems and Technology	MOP	Related DV	Goal	Threshold
		Launcher w/ Reloads;				
CCC 3	Provide own unit Command and Control	BSY-1, BSY-2, SUBTICS	C4I/SPW	SONARSYS	SONARSYS =1	SONARSYS =4
CCC 4	Maintain data link capability	BSY-1, BSY-2, SUBTICS	C4I/SPW	SONARSYS	SONARSYS =1	SONARSYS =4
CCC 6	Provide communications for own unit	BSY-1, BSY-2, SUBTICS	C4I/SPW	SONARSYS	SONARSYS =1	SONARSYS =4
CCC 9	Relay communications	BSY-1, BSY-2, SUBTICS; BPS-16 Radar; AN/BRAi-34; EHF/SHF HDR Multiband; IEM; OE-315 HSBCA	C4I/SPW	SONARSYS	SONARSYS =1	SONARSYS =4
CCC 21	Perform cooperative engagement	BSY-1, BSY-2, SUBTICS; BPS-16 Radar; AN/BRAi-34; EHF/SHF HDR Multiband; IEM; OE-315 HSBCA	C4I/SPW	SONARSYS	SONARSYS =1	SONARSYS =4
FSO 3	Provide support services to other units	All Designs	N/A			
FSO 5	Conduct towing/search/salvage rescue operations	All Designs	N/A			
FSO 6	Conduct SAR operations	All Designs	N/A			
FSO 7	Provide explosive ordnance disposal services	All Designs	N/A			
FSO 9	Provide routine health care	All Designs	N/A			
FSO 10	Provide first aid assistance	All Designs	N/A			
INT 1	Support/conduct intelligence collection	Sea Sentry; Full 4-6x21" tubes w/ Reloads; BSY-1, BSY-2, SUBTICS; 4-man lock out	C4I/SPW	TORP SAIL SONARSYS SPW	TORP =1 SAIL =1 SONARSYS =1 SPW =1	TORP =9 SAIL =4 SONARSYS=4 SPW =2
INT 3	Conduct surveillance and reconnaissance	Sea Sentry; Full 4-6x21" tubes w/ Reloads; BSY-1, BSY-2, SUBTICS; 4-man lock out	C4I/SPW	TORP SAIL SONARSYS SPW	TORP =1 SAIL =1 SONARSYS =1 SPW =1	TORP =9 SAIL =4 SONARSYS=4 SPW =2
INT 9	Disseminate surveillance and reconnaissance information	Sea Sentry; Full 4-6x21" tubes w/ Reloads; BSY-1, BSY-2, SUBTICS; 4-man lock out	C4I/SPW	TORP SAIL SONARSYS SPW	TORP =1 SAIL =1 SONARSYS =1 SPW =1	TORP =9 SAIL =4 SONARSYS=4 SPW =2
MIW 3	Conduct mine neutralization/ destruction	Full 4-6x21" tubes w/Reloads; BSY-1, BSY-2, SUBTICS;	MIW	TORP SONARSYS	TORP =1 SONARSYS =1	TORP =9 SONARSYS=4
MIW 3.1	Deploy AUVs and UUVs for mine detection and neutralization	Full 4-6x21" tubes w/Reloads; Sea Sentry; UUV's; BSY-1, BSY-2, SUBTICS;	MIW	TORP SONARSYS	TORP =1 SONARSYS =1	TORP =9 SONARSYS=4
MIW 4	Conduct mine avoidance	Full 4-6x21" tubes w/Reloads; BSY-1, BSY-2, SUBTICS;	MIW	TORP SONARSYS	TORP =1 SONARSYS =1	TORP =9 SONARSYS=4
MIW 6	Conduct magnetic silencing (Ndegaussing, deperming)	Ndegaussing	Magnetic Signature		NDEGAUS=1	NDEGAUS =0
MIW 6.7	Maintain magnetic signature limits	Ndegaussing	Magnetic Signature		NDEGAUS =1	NDEGAUS =0

ROCs	Description	Applicable Systems and Technology	MOP	Related DV	Goal	Threshold
MOB 1	Steam to design capacity in most fuel efficient manner	Hull, Propulsion	Speed Sprint, End; End Range Snorkel, AIP, Sprint	Hullform, PSYStype, PROPtype	Esnork =4000 nm Eaip =30 days Vs=22 knt Es=2hr	Esnork=3000 nm Eaip=20 days Vs=15 knt Es=1hr
MOB 3	Prevent and control damage	All Designs	N/A			
MOB 7	Perform seamanship, airmanship and navigation tasks (navigate, anchor, mooring, scuttle, life boat/raft capacity, tow/be-towed)	All Designs	N/A			
MOB 10	Replenish at sea	All Designs	N/A			
MOB 12	Maintain health and well being of crew	All Designs	N/A			
MOB 13	Operate and sustain self as a forward deployed unit for an extended period of time during peace and war without shore-based support	All Designs	N/A	Ts	45days	25days
MOB 16	Operate in day and night environments	All Designs	N/A			
MOB 17	Operate in heavy weather	Hullform	STABI	Depth	1000 ft	500 ft
MOB 18	Operate in full compliance of existing US and international pollution control laws and regulations	All Designs	N/A			
MOB 19	Operate submerged using AIP and batteries	Propulsion, Batteries	End AIP	PSYStype, BAT, BATC, WFAIP	Ebat =9000kwhr WFaip=200lt	Ebat =2500kwhr WFaip=100lt
MOB 20	Operate and transit on snorkel	Propulsion; Snorkel	End Snorkel and Speed	SAIL, PSYStype, WFS	SAIL=1 WFsnork=200lt	SAIL=2 WFsnork=100lt
NCO 3	Provide upkeep and maintenance of own unit	All Designs	N/A			
SEW 2	Conduct sensor and ECM operations	Shrike ESM; WLY-1; AN/BLQ-10 (ESM); WLR-8(v)2 interceptors; AN/BRD-7/BLD-1	AAW, ASuW, MIW, ASW,	ESM	ESM =1	ESM =2
SEW 5	Conduct coordinated SEW operations with other units	Shrike ESM; WLY-1; AN/BLQ-10 (ESM); WLR-8(v)2 interceptors, AN/BRD-7/BLD-1; EHF/SHF HDR Multi-band; AN/BRAi-34; OE-315 HSBCA	AAW, ASuW, MIW, ASW, C4I/SPW	ESM SAIL	ESM =1 SAIL=1	ESM =2 SAIL=2
STW 3	Support/conduct multiple cruise missile strikes	VLS, BSY-1, BSY-2, SUBTICS	STK	VLS, SONARSYS	VLS =1 SONARSYS =1	VLS =3 SONARSYS=4

An OMOE hierarchy, shown in Figure 67, is developed based on the defined MOPs, summarized in Table 23. AHP and pair-wise comparison are used to calculate MOP weights and Multi-Attribute Value Theory (MAVT) is used to develop individual MOP value functions. Expert and customer opinion are required to calculate AHP weights using pair-wise comparison questionnaires. VOPs (Values of Performance) are calculated for each MOP using VOP functions, usually S-curves. A VOP of 0 corresponds to the MOP threshold value, while a VOP of 1.0 corresponds to the MOP goal value .The result is the weighted overall effectiveness function (OMOE) as described in Section 1.2.1 to be used as an objective in the multi-objective optimization.

Table 23. MOP Table [1].

MOP #	MOP	Metric	Goal	Threshold
1	AAW	VLS Option SONARSYS Option SAIL Option ESM Option	VLS =1 SONARSYS =1 SAIL =1 ESM =1	VLS =3 SONARSYS=4 SAIL =4 ESM =2
2	ASW	TORP Option VLS Option SONARSYS Option SAIL Option ESM Option	TORP =1 VLS =1 SONARSYS =1 SAIL =1 ESM =1	TORP =9 VLS =3 SONARSYS=4 SAIL =4 ESM =2
3	ASuW	SONARSYS Option SAIL Option TORP Option ESM Option VLS Option	SONARSYS =1 SAIL =1 TORP =1 ESM =1 VLS =1	SONARSYS=4 SAIL =4 TORP =9 ESM =2 VLS =3
4	C4I/SPW	SONARSYS Option SAIL Option TOR Option SPW Option	SONARSYS =1 SAIL =1 TOR =1 SPW =1	SONARSYS=4 SAIL =4 TOR =9 SPW =2
5	STK	SONARSYS Option SAIL Option VLS Option	SONARSYS =1 SAIL =1 VLS =1	SONARSYS=4 SAIL =4 VLS =3
6	MIW	SONARSYS Option SAIL Option TORP Option	SONARSYS =1 SAIL =1 TORP =1	SONARSYS=4 SAIL =4 TORP =9
7	Vs (Sprint Speed)	Knots	22knts	15knts
8	Es (Sprint Duration)	Hr	2hr	1hr
9	Esnork (@ 12 knts)	nm	4000nm	3000nm
10	Eaip (AIP Duration @ 5 knts)	Days	30days	20days
11	Depth	Feet	1000ft	500ft
12	STABI	Index	4	1
13	Hull Vulnerability	Depth (ft)	1000	500
14	Acoustic Signature	PSYStype PROPtype	PSYStype =5 PROPtype =1	PSYStype =3 PROPtype =2
15	IR Signature	PROPtype	PROPtype =1	PROPtype =2
16	Magnetic Signature	DEGAUS	Ndegaus =1	Ndegaus =0

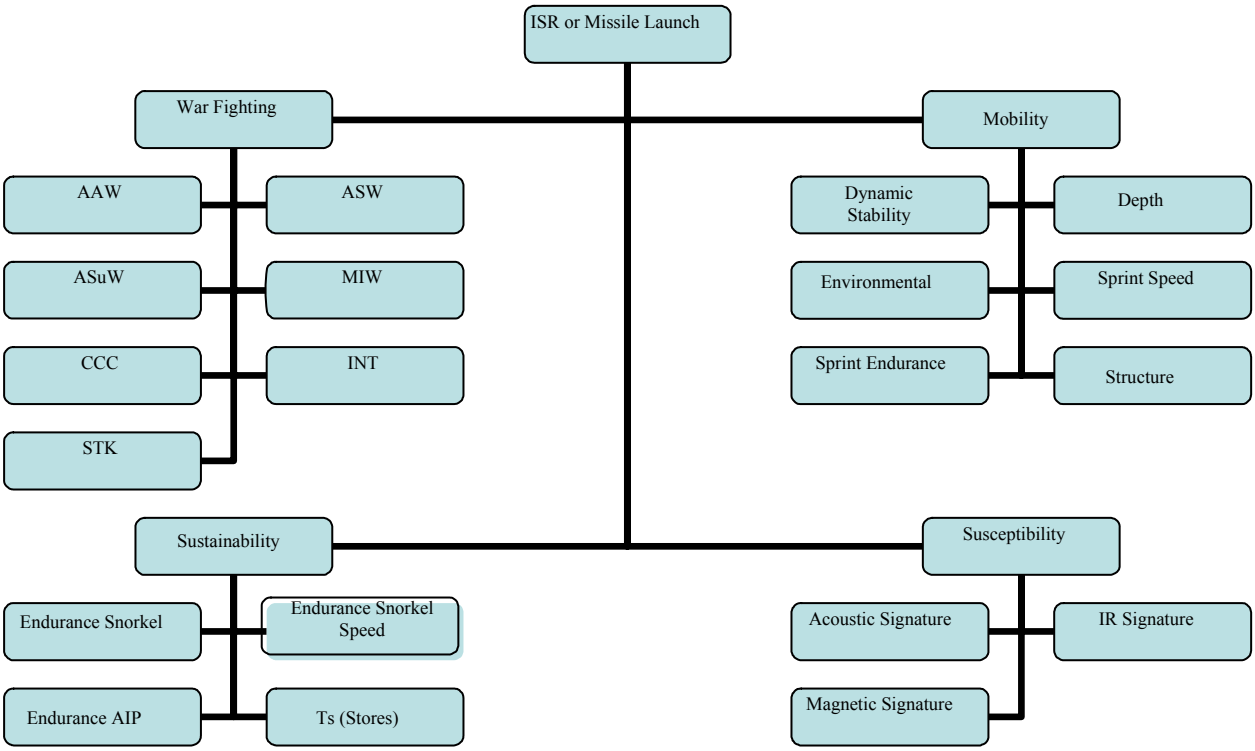

Figure 67 . OMOE Hierarchy

6.2 Submarine Synthesis Model [1]

The submarine synthesis model shown in Figure 3 defines and balances designs selected by the optimizer and assesses their feasibility, effectiveness, risk, and cost. It is developed in ModelCenter.

The Ship Synthesis Model is organized into the following modules:

- Input Module: Stores the design variable values and other design parameters which are provided as input to the other modules.
- Combat Module: Sums payload characteristics (weights, vertical centers of gravity (VCGs), arrangeable areas, and electric power consumption) using the combat system alternatives selected and an Excel file containing data for each system. The weights, arrangeable areas, and electric power consumption are simple summations; vertical centers of gravity are calculated using moments of weights. The combat module

outputs weights summarized by SWBS groups as well as a total, arrangeable area, power consumption, and the required payload outboard volume.

- Propulsion Module: Calculates propulsion and generator system characteristics (weights and stowage volumes) using the propulsion "subsystems" (propulsion system, propulsor type, battery type) alternatives and capacities (battery capacity, fuel weight (AIP), fuel weight (snorkel)) and an Excel file containing data (stowage and machinery room volumes, fuel consumption rates, and transmission efficiency). It also uses the battery type to determine battery and performance characteristics. The Propulsion Module outputs the battery power, weight and volume of the basic propulsion machinery, batteries and fuels, the volume of the prop, specific fuel consumption (SFC), power provided by AIP and snorkeling, AIP diesel fuel energy capacity, overall propulsive coefficient (PC), and transmission efficiency.
- Hull Module: Calculates hull characteristics (volumes and lengths of the three hull parts and the total bare hull surface area) using hull input quantities (diameter, beam-to-diameter ratio, length-to-diameter ratio and forward and aft fullness exponents). These quantities are used to find a shape defined using an MIT model (see Figure 24) which is composed of an ellipsoidal forebody, parallel midbody, parabolic aftbody, and transverse midbody; this hull form is a modified form of the hydrodynamically optimized teardrop hullform which adds parallel midbody (length) and transverse midbody (beam) to provide more arrangeable area. The Hull Module calculates lengths and offsets based on this model and integrates over the lengths to determine the volumes of each part. The module outputs the width of the transverse insertion, the bare hull surface area, the envelope volume, the length of each part of the hull, the beam, and the length overall.
- Tankage Module: Calculates the tankage volumes and liquid weights and crew manning numbers. The diesel fuel is split between clean (17%) and compensated (83%) tanks. Compensated tanks external to the pressure hull use ballast water to replace diesel fuel as it is used; this allows easier management of ballast and an overall more efficient design. Soft tanks ballast open to the sea and have a lower weight. The tankage weights (including AIP liquids) are based on the specific volumes for the tankage contents. The Tankage Module calculates manning numbers

using a parameterized model based on the ship size, power consumption, and manning and automation factor; these are calculated in the Tankage Module as this is a convenient place (the Hull Module is the first module to use these numbers). Additional (habitability) tankage volumes and weights are calculated using the crew numbers. The tankage module outputs the total inboard tankage volume and the outboard compensated tankage volume, enlisted and total crew numbers, and the weights for lube oil, fresh water, sewage, and clean and compensated fuel.

- Space Module: Calculates available and required arrangeable areas and hull volumes (including free flood and free flood min/max) using the stores and provisions duration, average deck height, crew numbers (enlisted, officers and total), the pressure hull arrangeable area margin, and the required area for payload (CCC and ordnance delivery system). The arrangeable area is calculated using parametric models; arrangeable area and average deck height are used to calculate the arrangeable volume; the hull volumes are based on their definitions and previously calculated volumes. The Space Module outputs various volumes (pressure hull, outboard displacement, everbuoyant, main ballast tank, submerged displaced, free flood (including min/max) and auxiliary space; it also outputs the total required and total available arrangeable area.

- Electric Module: Calculates (with applicable margins) the maximum electric power load and the 24-hour average load. It inputs the margins (electric functional margin factor, electric design margin factor and average electric power margin factor), payload weight, volumes of the pressure hull, machinery box and auxiliary box, the power provided while snorkeling, overall length and diameter, the required power for the payload, the total crew number and whether or not there is a degaussing system. It then calculates the power required using a parameterized model which uses the hull dimensions, the ship service power based on the total crew number and the total load.

- Resistance Module: Calculates sustained speed, ranges and endurances (sustained, snorkel and AIP), and the total mission length. The Resistance Module calculates resistance over a range of speeds using frictional resistance (from the bare hull surface area) form factor and a correlation allowance. The endurances are based on battery and fuel capacities and usage rates, the Propulsion Margin Factor (PMF),

Overall Propulsive Coefficient (PC), and the transmission efficiency (η). The mission length is based on the endurances that are calculated.

- Weight Module: Calculates total weights and VCGs for SWBS groups, overall VCG, stability (GB and GM), and minimum and maximum values for lead ballast. It calculates SWBS subgroups (systems, subsystems, shafting, cabling, etc.) weights and VCGs based on inputs. The group weights are found by summing the individual components and VCGs are calculated using weight moments. The hull geometry determines the center of buoyancy which is used with the overall VCG to calculate GB (the submerged stability condition). The surface stability condition (GM) is calculated using stability formula which considers the waterplane contribution to the stability. This module also calculates lead weight as difference between NSC weight and everbuoyant displacement. The feasibility module assesses the feasibility of this weight to satisfy minimum design and stability lead requirements.

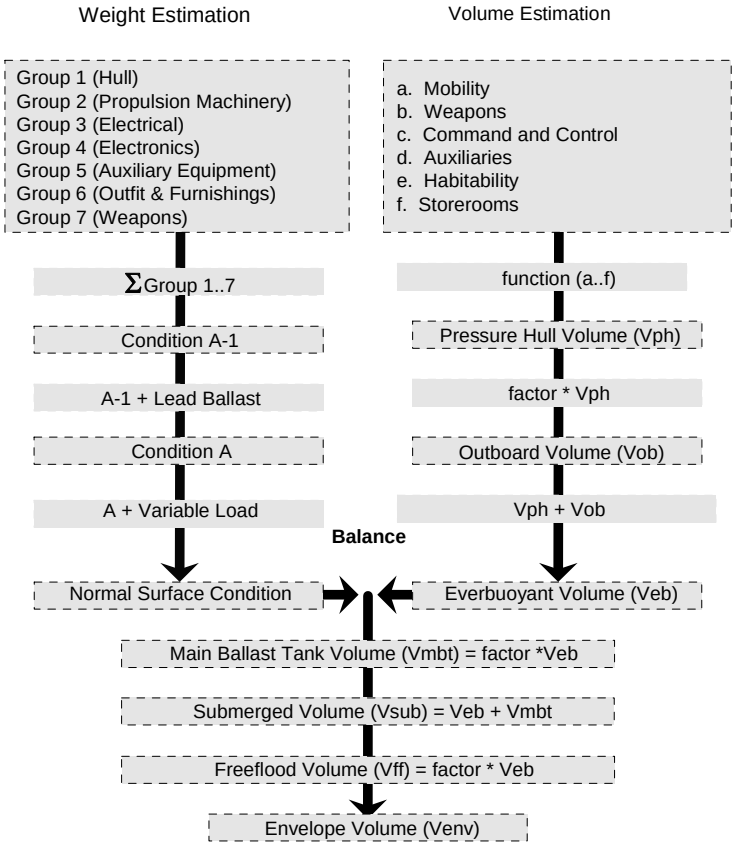

Figure 68: Submarine balance work flow diagram [1].

- Feasibility Module: Calculates ratios comparing the actual values of snorkel endurance range, AIP endurance duration, sustained speed, spring duration, submerged GB, surfaced GM, weight of lead, free flood, arrangeable area, and the stores and provisions duration to applicable minimums and/or maximums. Each ratio must be positive for a feasible design. It also checks if the values of the horizontal and vertical stability indices fall within the defined stability/maneuverability range. Each of these ratios and values are output to the MOGO Module to determine if the design is feasible.
- OMOE Module: Calculates a Value of Performance (VOP) for each Measure of Performance (MOP) using the actual values calculated and an Overall Measure of Effectiveness (OMOE). Each VOP is calculated based on weights provided by a previously-completed pair-wise comparison process. The OMOE (the only output) is calculated using each VOP added together using weights provided by the pair-wise comparison. The calculation of the OMOE is further described in Section 1.2.1.
- Cost Module: Calculates the basic cost of construction (CBCC), labor costs for each SWBS group using complexity factors and SWBS groups weights, material costs using SWBS groups weights, direct and indirect (using overhead) costs, and the basic cost of construction using the direct and indirect cost and a profit margin. The calculation of cost is further described in Section 1.2.2.
- Risk Module: Calculates an Overall Measure of Risk. The OMOR is found by first calculating a performance, cost, and schedule risk for each system (DVs) based on risk factors previously determined. The OMOR is a weighted summation of each total risk for each risk type. The calculation of risk is further described in Section 1.2.3.
- MOGO Module: The Multi-Objective Genetic Optimizer maximizes the OMOE while complying with the constraints produced by the ratios found in the Feasibility Module and minimizing the CBCC and OMOR.

6.3 Implementation and Integration of Dynamic Stability Models in the Submarine Synthesis Model in ModelCenter

The response surface models created in Chapter 5 are implemented into the OMOE and feasibility modules of the submarine synthesis model. The values of the horizontal and vertical stability indices are calculated in the OMOE module using the created response surfaces. These values are input into the feasibility module and assessed to determine if they fall in the ranges set in chapter 2 to ensure a tradeoff in stability and maneuverability (G_H should vary between 0.15 and 0.30, G_V should vary between 0.5 and 0.7). If the designs do not fall within these ranges then the design is infeasible.

The stability indices are also implemented in the OMOE module. As shown in Table 23 the stability indices are defined as a MOP (MOP 12). A VOP function is determined for each index and is shown in Figure 69 and Figure 70. The VOPs created for the stability indices do not follow the traditional s-curve used by other VOPs. This is because the ranges defined for the indices were developed to ensure a tradeoff between stability and maneuverability. Therefore, it was determined that the midpoint of each range would be the most desirable tradeoff and would correspond to a VOP of 1, this is the goal value. The threshold values are the upper and lower bounds of the two ranges. They represent the minimum and maximum tolerable values for the indices. An overall VOP is calculated as a function of the two stability indices VOPs. For each index a VOP is determined based on the VOP functions in Figure 69 and Figure 70. Each VOP contributes to 50% of the overall stability VOP. This overall VOP is used in the OMOE calculation for each design.

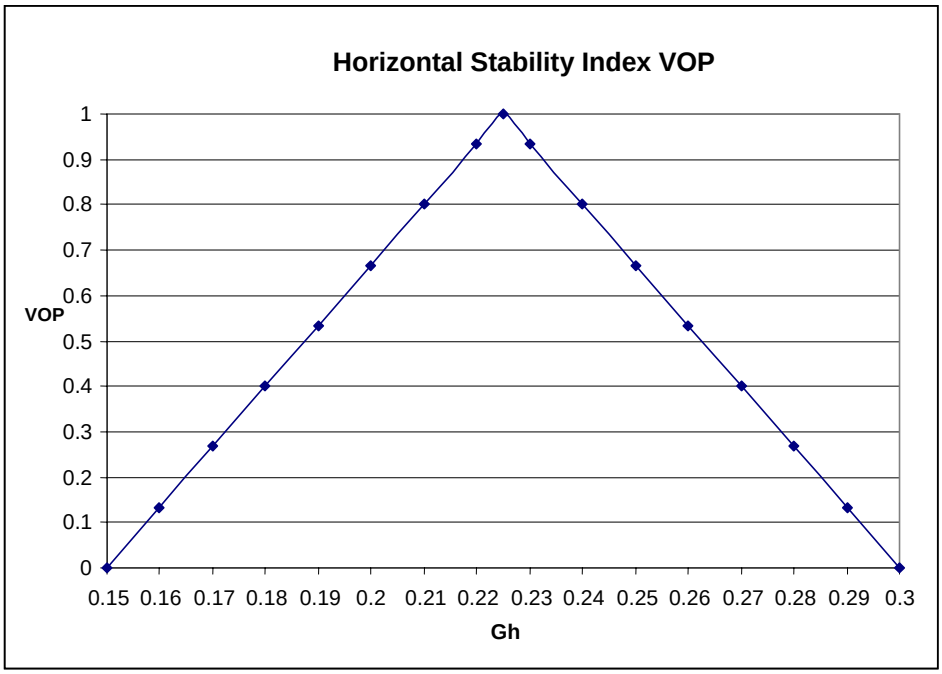

Figure 69. VOP for Gh.

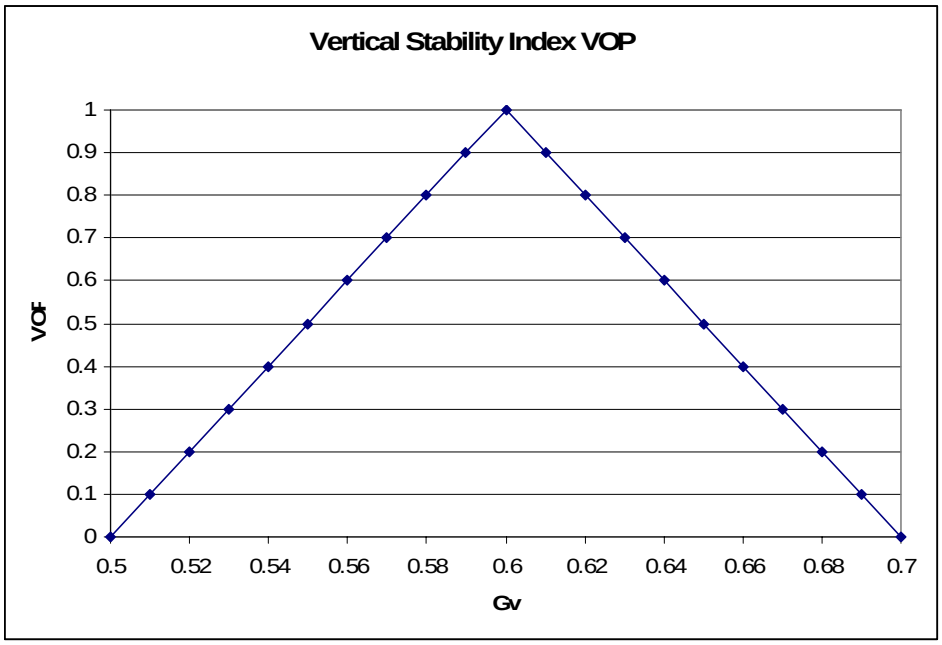

Figure 70. VOP for Gv.

6.4 Optimization

The design space is defined by twenty design variables listed in Table 24. The optimizer chooses values for each variable in the allowable range and the submarine synthesis model uses these values to balance the design, checks for feasibility, and calculate the measures of effectiveness, risk, and cost. The optimization utilizes the Darwin optimizer defined in Section 4.1.5 and the optimization is performed as outlined in Section 1.2.4.

Table 24. SSG(X) Design Variables (DVs)

DV #	DV Name	Description	Design Space
1	D	Diameter	24-34ft
2	LtoD	Length to Depth Ratio	7-10
3	BtoD	Beam to Depth Ratio	1-1.2
4	n_a	Fullness factor aft	2.5-4
5	n_f	Fullness factor forward	2.0-3.5
6	Depth	Diving Depth	500-1010ft
7	PSYS	Propulsion system alternative	Option 1) CCD, CAT 3512 V12 x2 Engines Option 2) CCD, CAT 3516 V16 x2 Engines Option 3) CCD, 2xCAT3516V16 + 2xCAT3512V12 Option 4) CCD, 2xCAT 3608 IL8 Option 5) OCD/AIP, 2xCAT 3512 V12 + 2x250KW PEM Option 6) OCD/AIP, 2xCAT 3512 V12 + 2x500KW PEM Option 7) OCD/AIP, 2xCAT 3516 V16 + 2x250KW PEM Option 8) OCD/AIP, 2xCAT 3516 V16 + 2x500KW PEM Option 9) OCD/AIP, 2x CAT 3608 IL8 + 2x250KW PEM
8	PROPtype	Propulsion Prop Type	Option 1) RDP, Rim Driven Prop Option 2) Shrouded
9	BATtype	Battery system type alternative	Option 1) Nickel Cadmium Option 2) Lead Acid Option 3) Zebra
10	Ebat	Battery Capacity	5000-12000 kwhr
11	Wfsnork	Weight Fuel Snorkel	50-150lton
12	Wfaip	Weight Fuel AIP	300-900lton
13	Ndegaus	Degaussing	0=none; 1=degaussing
14	Cman	Manpower Reduction	0.5-1.0
15	TORP	Torpedo system alternative	Option 1: Reconfigurable torpedo room, 6x21” tubes, 24 reloads Option 2: Reconfigurable torpedo room, 6x21” tubes, 18 reloads Option 3: Reconfigurable torpedo room, 6x21” tubes, 12 reloads Option 4: Reconfigurable torpedo room, 4x21” tubes, 16 reloads Option 5: Reconfigurable torpedo room, 4x21” tubes, 12 reloads Option 6: Reconfigurable torpedo room, 4x21” tubes, 8 reloads Option 7: No torpedo room, 24 external encapsulated Option 8: No torpedo room, 18 external encapsulated Option 9: No torpedo room, 12 external encapsulated
16	VLS	Vertical Launching System Alternatives	Option 1: 24 Cell VLS Option 2: 18 Cell VLS Option 3: 12 Cell VLS

DV #	DV Name	Description	Design Space
17	SONARSYS	Sonar/Combat System Alternatives	Option 1: BQQ-10 Bow Dome Passive/Active, LWWAA, high frequency sail and chin-array (mine and obstacle avoidance), TB-16, TB-29A; CCSM Option 2: BQQ-10 Bow Dome Passive/Active, AN/BQG-5 WAA, high frequency sail and chin-array (mine and obstacle avoidance), TB-16, TB-29A; BSY-2 Option 3: BQQ-10 Bow Dome Passive/Active, AN/BQG-5 WAA, high frequency sail and chin-array (mine and obstacle avoidance), TB-16, TB-29A; BSY-1 CCS MK 2 Block 1C Option 4:SUBTICS (Thales): Passive Cylindrical bow array, PVDF planar flank arrays, sail array, hydrophones
18	SPW	SPW Alternatives	Option 1: 4 Man Lock out chamber Option 2: None
19	SAIL	Sail (Radar, Masts and Periscopes, and communication)	Option 1: Virginia Class Sail plus: BPS-16 Radar; 2xAN/BRA-34 Radar; 2xAN/BVS-1 Photonics masts; 2xEHF/SHF HDR Multiband; Snorkel; IEM; Sea Sentry; Seal Locker; OE-315 HSBCA Option 2: Virginia Class Sail: BPS-16 Radar; 2xAN/BRA-34; 2xAN/BVS-1 Photonics Masts; 2xEHF/SHF HDR Multiband; Snorkel; IEM; Sea Sentry; OE-315 HSBCA Option 3: Seawolf Class Sail: BPS-16 radar; 2xAN/BRA-34; 2xAN/BVS-1 Photonics Masts; Type 8 Mod 3 Periscope; Type 18 Mod 3 Periscope; Sea Sentry; Snorkel; OE-315 HSBCA Option 4: 688I Class Sail: BPS-16 Radar; 2xAN/BRA-34; Type 8 Mod 3 Periscope; Type 18 Mod 3 Periscope; Snorkel; Sea Sentry; OE-315 HSBCA
20	ESM	Electronic Support Measure Alternatives	Option 1: Shrike ESM; WLY-1 acoustic interception and countermeasures system; AN/BLQ-10 Electronic Support Measures (ESM) system; 2x3” Countermeasure Launcher w/ Reloads, 2x6.75” Countermeasure Tube Option 2: Shrike ESM; AN/BRD-7/BLD-1; WLR-8(v)2 interceptors; 2x3” Countermeasure Launcher w/ Reloads, 2x6.75” Countermeasure Tube

6.5 Optimization Results

6.5.1 General Results

Figure 71 show the effectiveness-risk-cost frontier created from the genetic optimization. Each point represents a feasible submarine design. Figure 72 is an alternative view of Figure 71 showing the natural risk bands for all of the design. This was used to divided the data into four levels of risks to create Figure 73, a 2-D representation of the Non-Dominated Frontier (NDF). It shows the overall effectiveness versus cost for the four ranges of risk. Designs with the highest risk for a given cost also have the highest overall efficiency. Design points of most interest to the

customer are those that for a given range of risk offer an increase in effectiveness for only a small increase in cost.

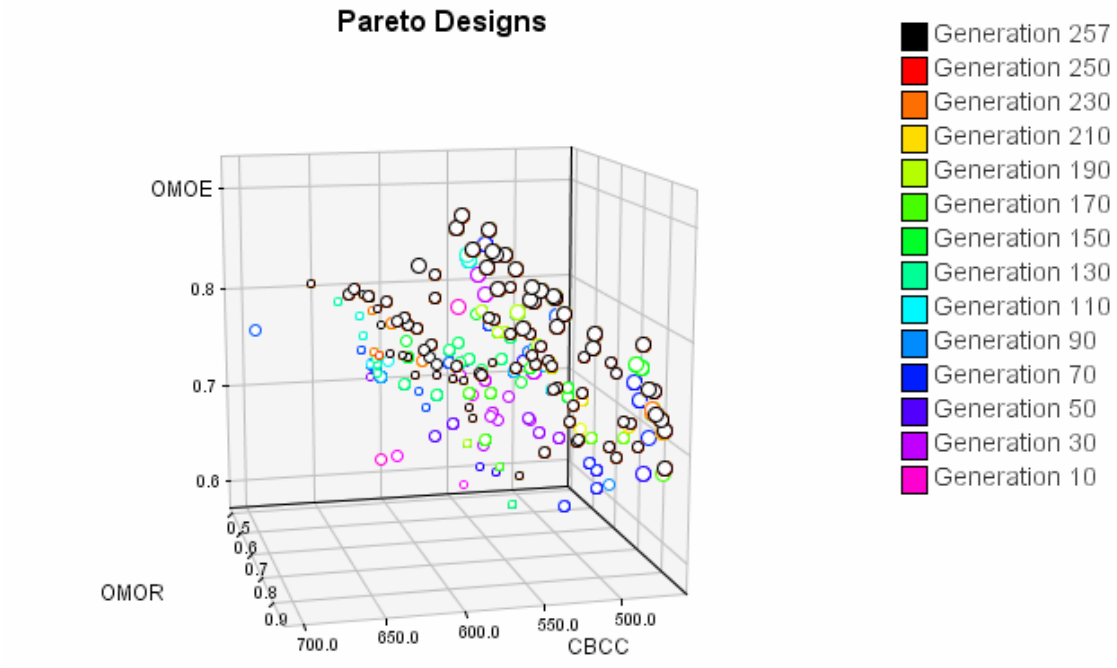

Figure 71. 3-D Non-Dominated Frontier.

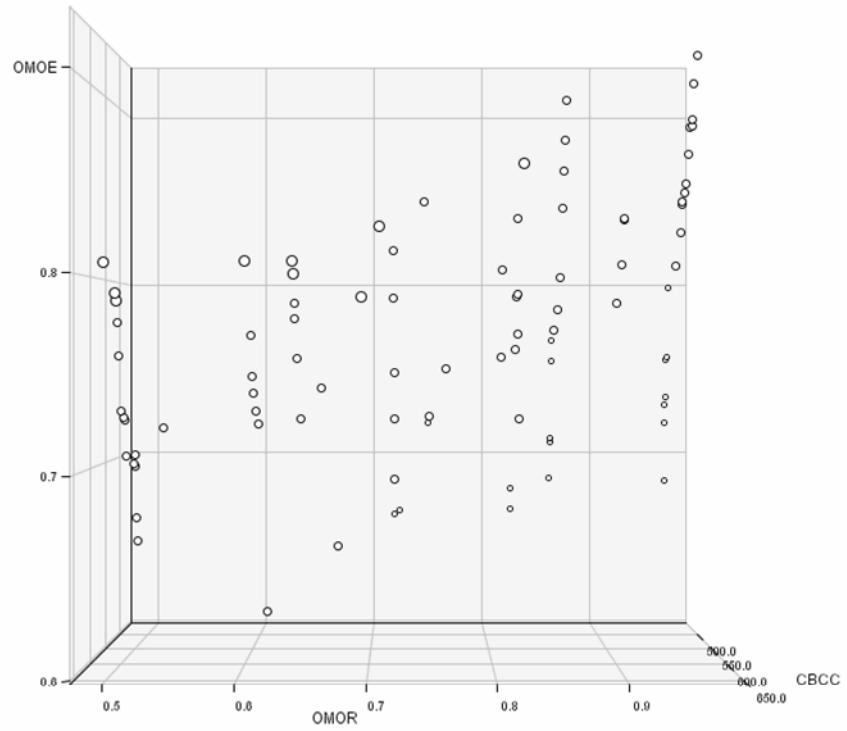

Figure 72. 3-D NDF showing risk bands.

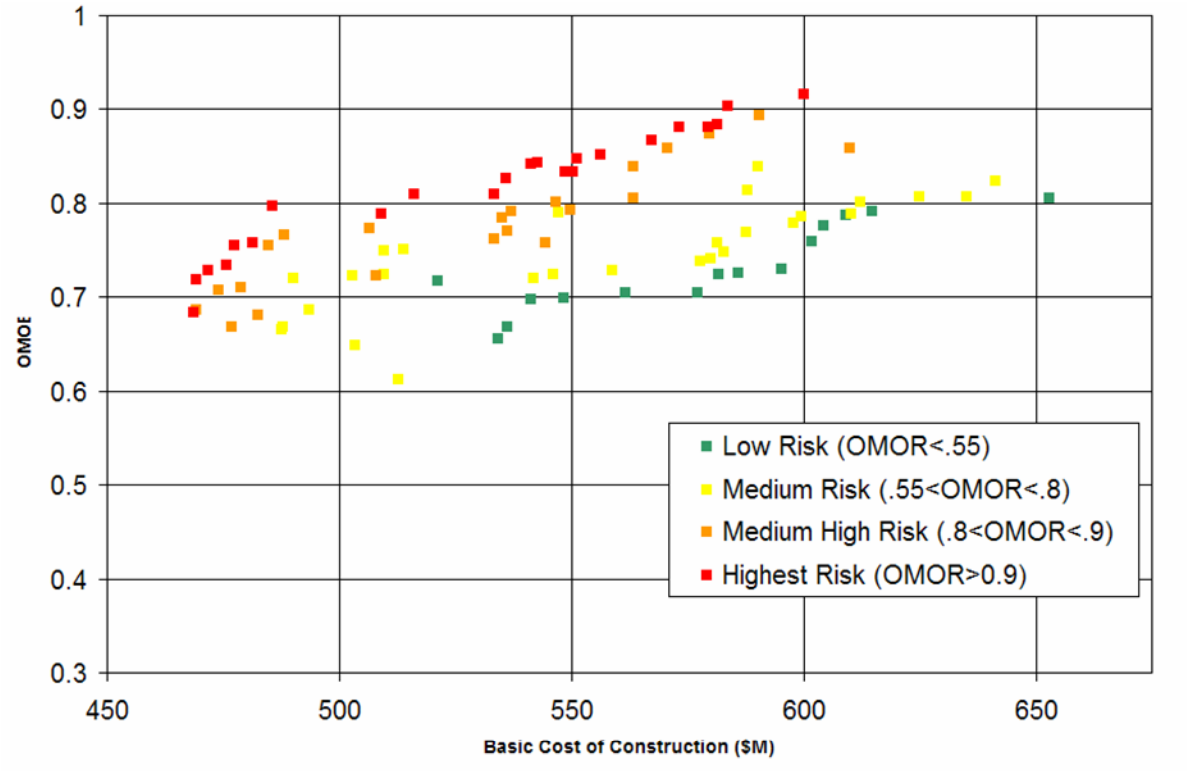

Figure 73. 2-D Non-Dominated Frontier.

6.5.2 Feasibility Results

Figure 74 shows the stability indices versus length to diameter ratio for the designs in the optimization. This graph shows that the only designs with a length to diameter ratio from 8.1 to 8.8 were feasible, meaning only these designs has stability indices in the ranges defined in Chapter 2 to ensure a tradeoff between stability and maneuverability. Figure 75 and Figure 76 show the forward plane and stern plane configurations for the designs in Figure 74. The majority of feasible designs have sail planes and all of the designs have a cruciform stern.

These results were not unexpected based on the results of the DOE shown in Chapter 5. Figure 74 indicates that by using the method outlined in Chapter 3 to size the control surfaces based proportional to the size of the submarine designs in this length to diameter range have the best tradeoff between stability and maneuverability. If designs with a length to diameter ratio above or below this range is desired then the size of the control surfaces need to be altered to allow for this tradeoff.

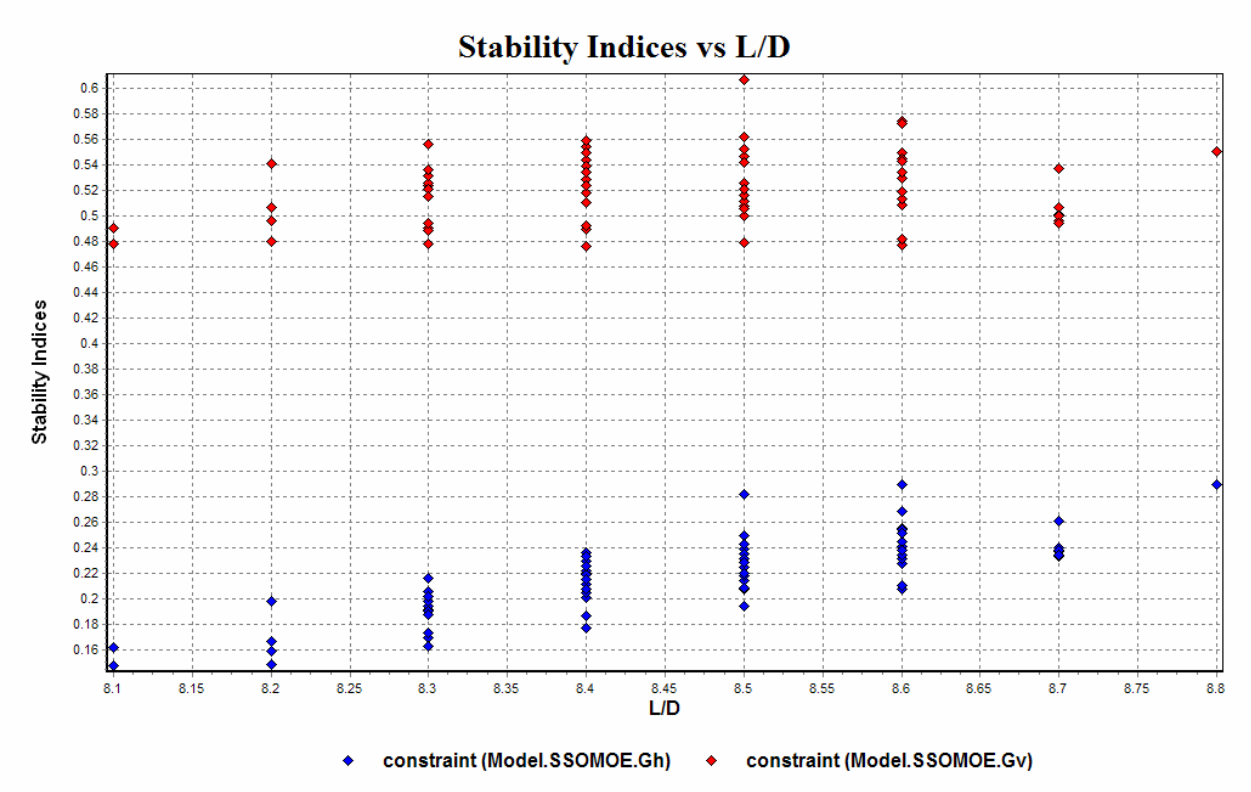

Figure 74. Optimization Results: Stability Indices vs. L/D

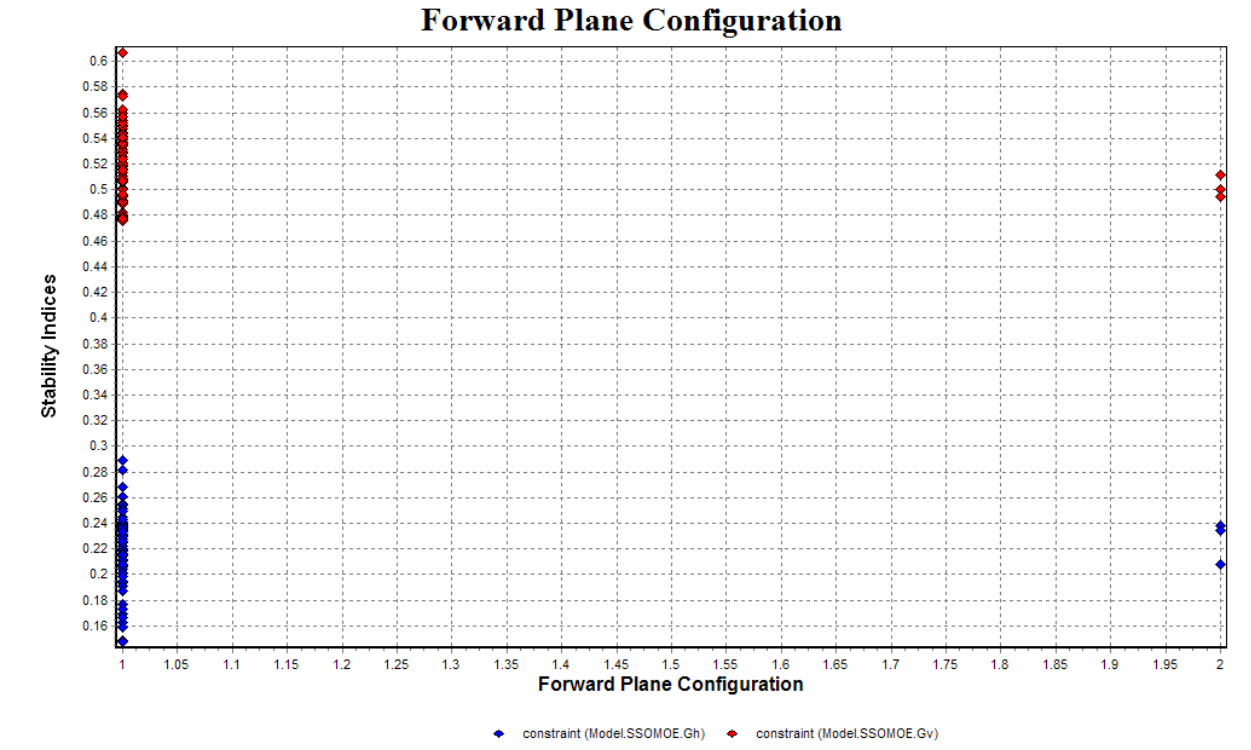

Figure 75. Optimization Results: Forward plane configuration.

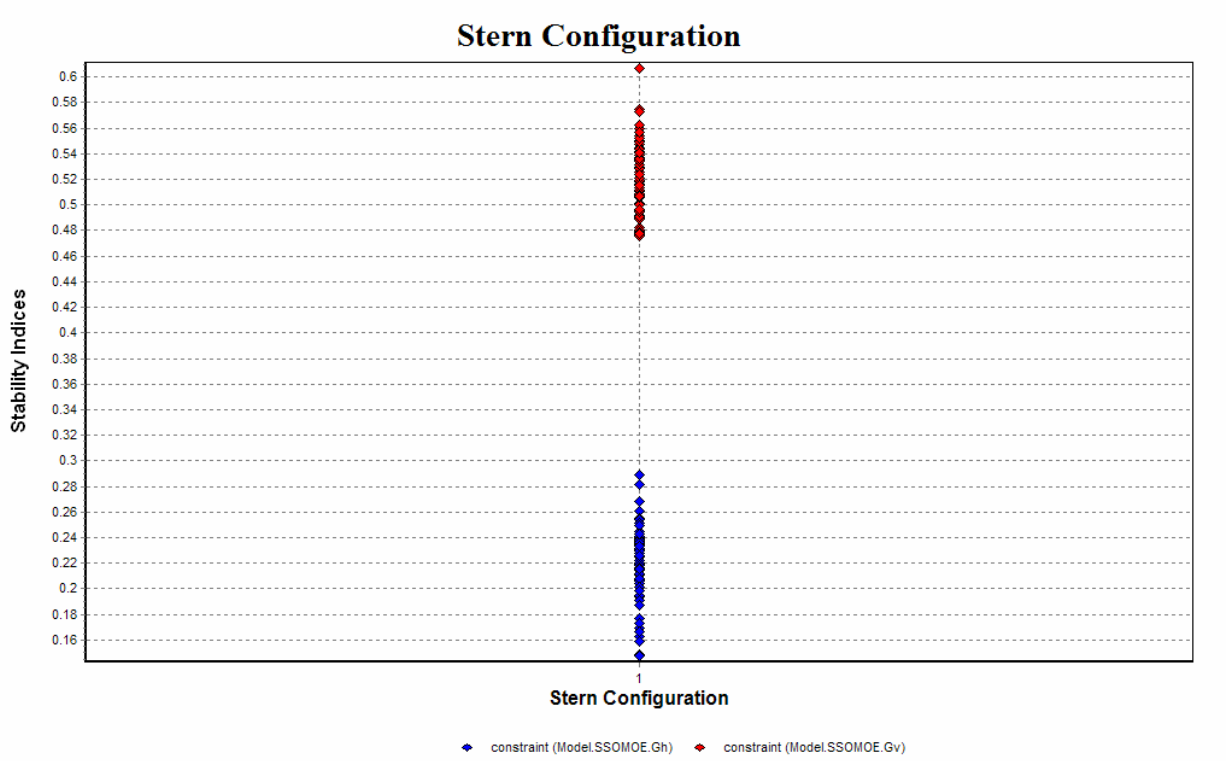

Figure 76. Optimization Results: Stern plane configuration.

CHAPTER 7 CONCLUSIONS

7.1 Dynamic Stability Model and Case Study Optimization Conclusions

Two tools, GEORGE and CEBAXI and LA_57, were used to analyze horizontal and vertical plane stability for a submarine during early stage design. Each tool required the hull offsets and geometry of the control surfaces as input for analysis. The hull offsets were generated based on an idealized teardrop shape and a control surfaces database was created based on past US Navy submarine designs to determine sizing trends. These methods were implemented as FORTRAN programs and integrated with the stability tools in ModelCenter to assess stability. The two tools were compared and it was determined that GEORGE and CEBAXI and LA_57gave more reliable results. A design of experiments was performed using GEORGE and CEBAXI and LA_57 to determine the level of importance of each design variable on the stability indices. From the data collected response surface models were generated for each configuration analyzed; sail planes with a cruciform stern, sail planes with an x-stern, bow planes with a cruciform stern, and bow planes with an x-stern. These response surfaces were implemented as part of the OMOE in the submarine synthesis model used in the concept exploration phase of the TSSE design philosophy used at Virginia Tech.

A case study using the SSG(X) design for the Virginia Tech senior design course was performed using the developed response surfaces and OMOE metrics. The results show that to achieve the tradeoff of stability and maneuverability specified in Chapter 2 a length to diameter ratio of approximately 8 to 9 is needed. In addition, a cruciform stern with sail planes was the best configuration. This process has been integrated into the Senior Design course at Virginia Tech and has proven to be successful in assessing dynamic stability and control in early stage design. Figure 77 is a Rhino model of the optimized SSG(X). The dimensions, control surface configuration, and control surface geometry are all characteristics determined using the process defined in this thesis.

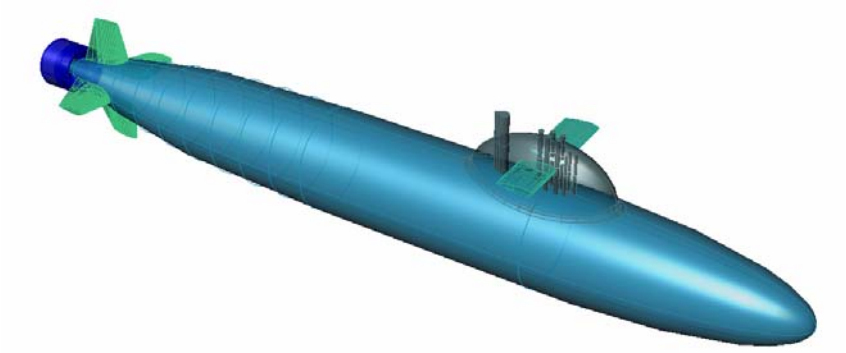

Figure 77. SSG(X) Rhino drawing [1].

7.2 Suggestions for Future Work

The developed process and generated response surfaces have proven to be a good tool to provide a baseline indication of dynamic stability and control early in the design process. This section outlines some modifications that can be made to the current process to increase its robustness and applicability.

As seen in Figure 49, Figure 54, Figure 59, and Figure 64 all designs analyzed during the design of experiments with a length to diameter ratio less than approximately 8 were unstable in both the horizontal and vertical plane. This may be a result of the designs used to create the control surface database. The designs used for the database had length to diameter ratios that varied from 8 to 13. No data was collected below a length to diameter ratio of 8. Therefore, the assumption of a linear trendline to model the control surface parameter may not be accurate at lower length to diameter ratios. A possibility for future study would be to use a quadratic fit to the data in the control surface database that would increase the size of the control surfaces at lower length to diameter ratios and see how it affects stability in that length to diameter range.

In addition, the data used to develop the control surface database only included designs with a cruciform stern configuration. Therefore the only difference between a cruciform stern and x-stern configuration was the value of the angle Φ as shown in Figure 11; both configurations had the same dimensions for the control surfaces. One of the advantages of an x-stern is the ability of the stern planes to have a larger span; therefore, varying the size of the control surfaces based on the stern configuration would be a possible improvement to the current method. In addition, to these modifications the presence of the discontinuity that appears in the GEORGE data will continue to be investigated.

REFERENCES

[1] Alemayehi, D, Boyle, R. Eaton, E, Lynch, T., Stepanchick, J, Yon, R., (2006) "SSG(X) Guided Missile Design Report." Virginia Tech Senior Design, Blacksburg, VA.

[2] Arentzen, E.S. Capt., Mandel, P. (1960) "Naval Architectural Aspects of Submarine Design", *SNAME Transactions*, Vol. 68, pg 622-692.

[3] Brown, A.J., Thomas, M. (1998), "Reengineering the Naval Ship Concept Design Process", From Research to Reality in Ship Systems Engineering Symposium, ASNE, September, 1998.

[4] Brown, A.J., Salcedo, J. (2002), "Multiple-Objective Optimization In Naval Ship Design", *Naval Engineers Journal*, Vol. 115, No. 4.

[5] Burcher, R., Rydill, L. (1994), Concepts in Submarine Design. Great Britain: University Press, Cambridge.

[6] Cann, G., Sullivan, P., Brooks, R., Reed, J. (1994), MIT Introduction to Submarine Design course packet, Cambridge, MA.

[7] Chang, M., Moran, T., Junghans, K., Lewis, J., Haussling, H., McCreight, K., Kim, Y., (2001) "The Theoretical Prediction of Forces and Moments Acting on an Appended Body of Revolution Performing Arbitrary Maneuvers," Report No. NSWCCD-50-TR-2001/055, July 2001.

[8] Demko, D., (2006), "Tools for Multi-Objective and Multi-Disciplinary Optimization in Naval Ship Design." Blacksburg, VA

[9] Fossen, T., (2002). Marine Control Systems. Marine Cybernetics AS, Trondheim, Norway.

[10] GEORGE User Manual, Hydromechanics Division, NCSL Panama City, FL

[11] Hover, F., Triantafyllou, M. "Maneuvering and Control of Marine Vehicles." MIT Open Courseware, Department of Ocean Engineering, Cambridge, MA.

[12] Jones, D., Clarke, D., Brayshaw, I., Barillon, J., Anderson, B., (2002) "The Calculation of Hydrodynamic Coefficients for Underwater Vehicles," DSTO Platforms Sciences Laboratory, Australia.

[13] Lewis, E. Ed. (1989). Principals of Naval Architecture, Volume III. SNAME Jersey City, NJ.

[14] ModelCenter Software (2004) Help Files, Phoenix Integration, Blacksburg, VA

[15] “US Sea Systems: Data Store-CAD models.” Feb. 2006.www.combatindex.com.

APPENDICES

Appendix A - Control Surface Database Designs (www.combatindex.com)

Figure A1. Top view of Benjamin Franklin class submarine.

Figure A2. Side view of Benjamin Franklin class submarine.

Figure A3. Top view of George Washington class submarine.

Figure A4. Side view of George Washington class submarine.

Figure A5. Top view of Ohio class submarine.

Figure A6. Side view of Ohio class submarine.

Figure A7. Top View of Lafayette class submarine.

Figure A8. Side view of Lafayette class submarine.

Figure A9. Top view of Permit class submarine.

Figure A10. Side view of Permit class submarine.

Figure A11. Top view of Seawolf class submarine.

Figure A12. Side view of Seawolf class submarine.

Figure A13. Top view of Skipjack class submarine.

Figure A14. Side view of Skipjackt class submarine.

Figure A15. Top view of Sturgeon class submarine.

Figure A16. Side view of Sturgeon class submarine.

Figure A17. Top view of Virginia class submarine.

Figure A18. Side view of Virginia class submarine.

Appendix B – Control Surface Database Plots

Control Surface Parameters vs. Length to Diameter Ratio

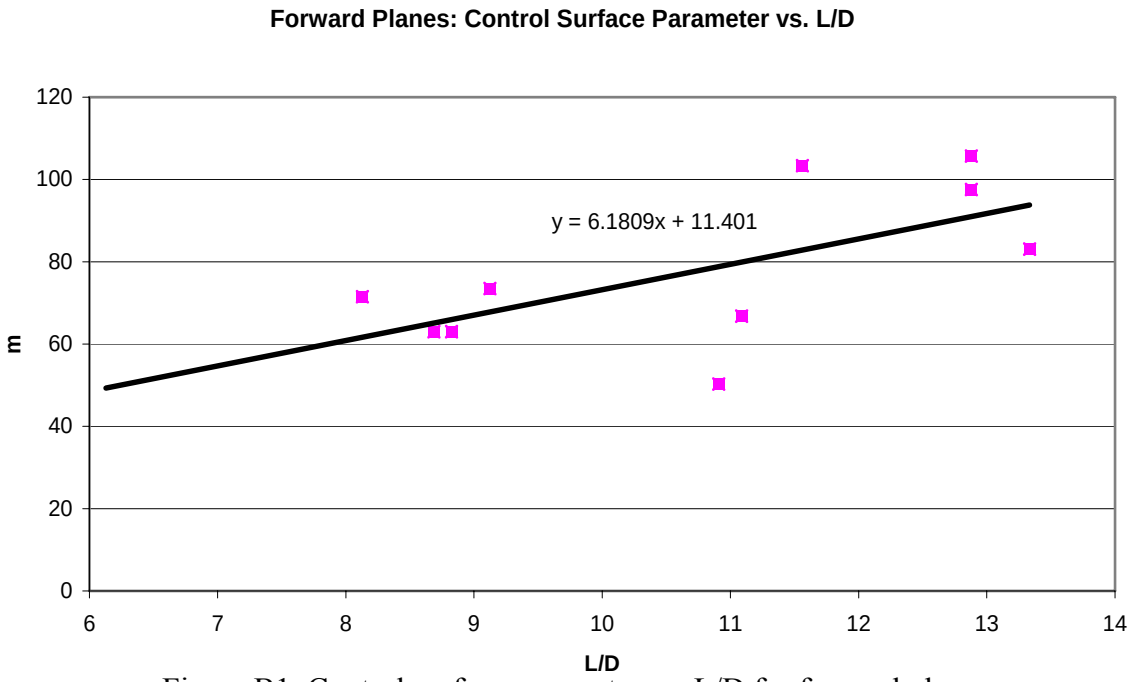

Figure B1. Control surface parameter vs. L/D for forward planes.

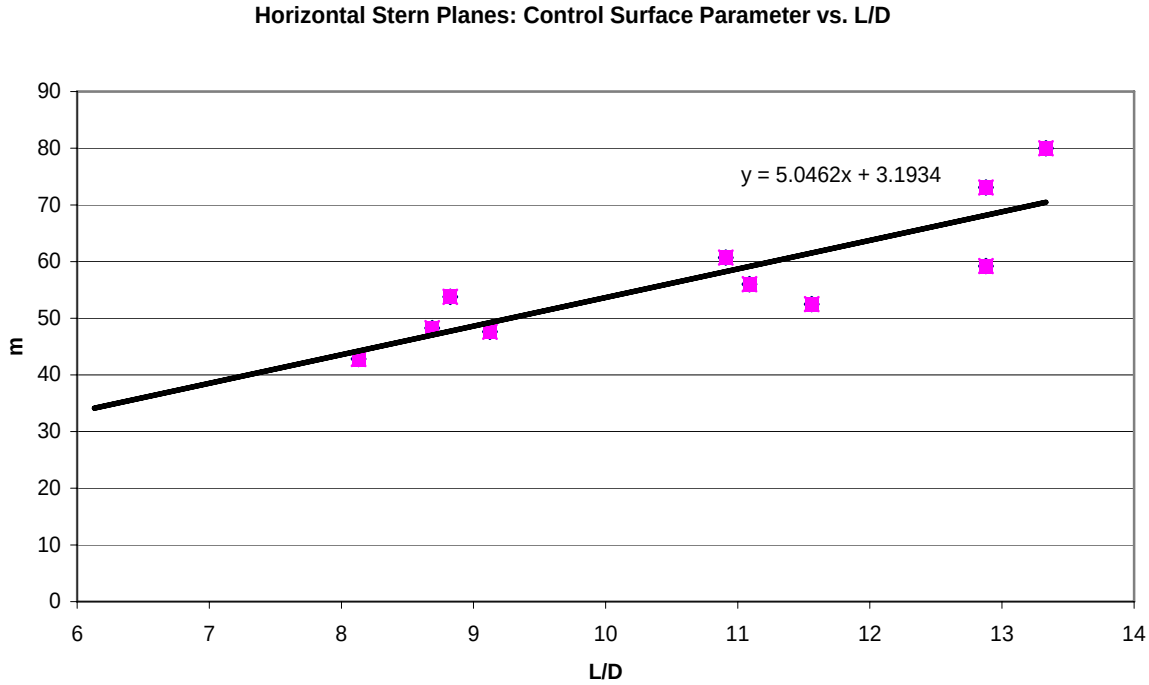

Figure B2. Control surface parameter vs. L/D for Horizontal Stern Planes.

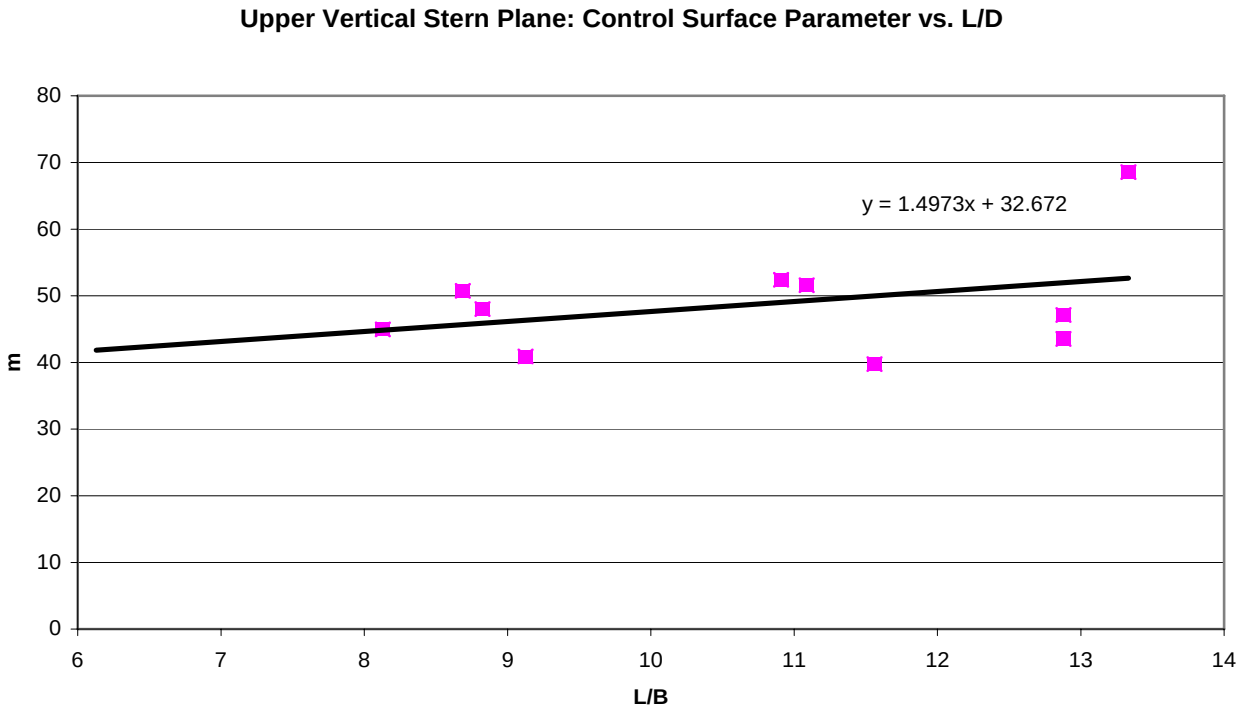

Figure B3. Control surface parameter vs. L/D for upper vertical stern planes.

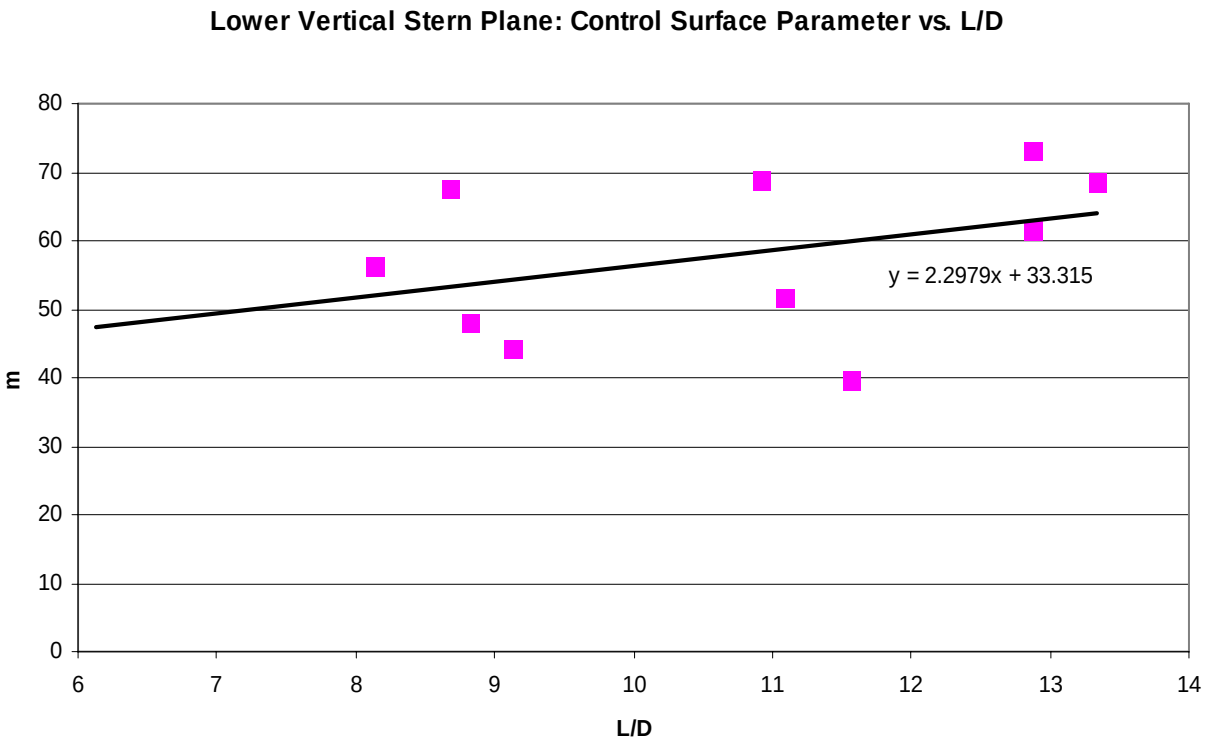

Figure B4. Control surface parameter vs. L/D for the lower vertical stern plane.

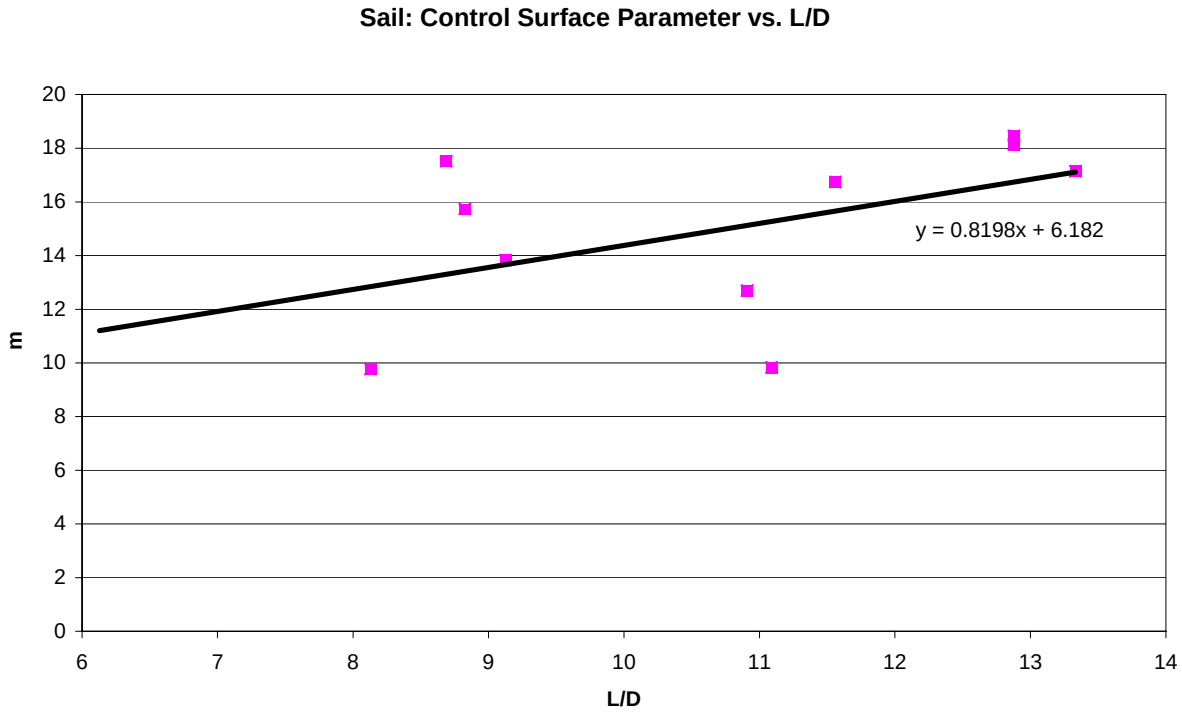

Figure B5. Control surface parameter vs. L/D ratio for the sail.

Aspect Ratio vs. Length to Diameter Ratio

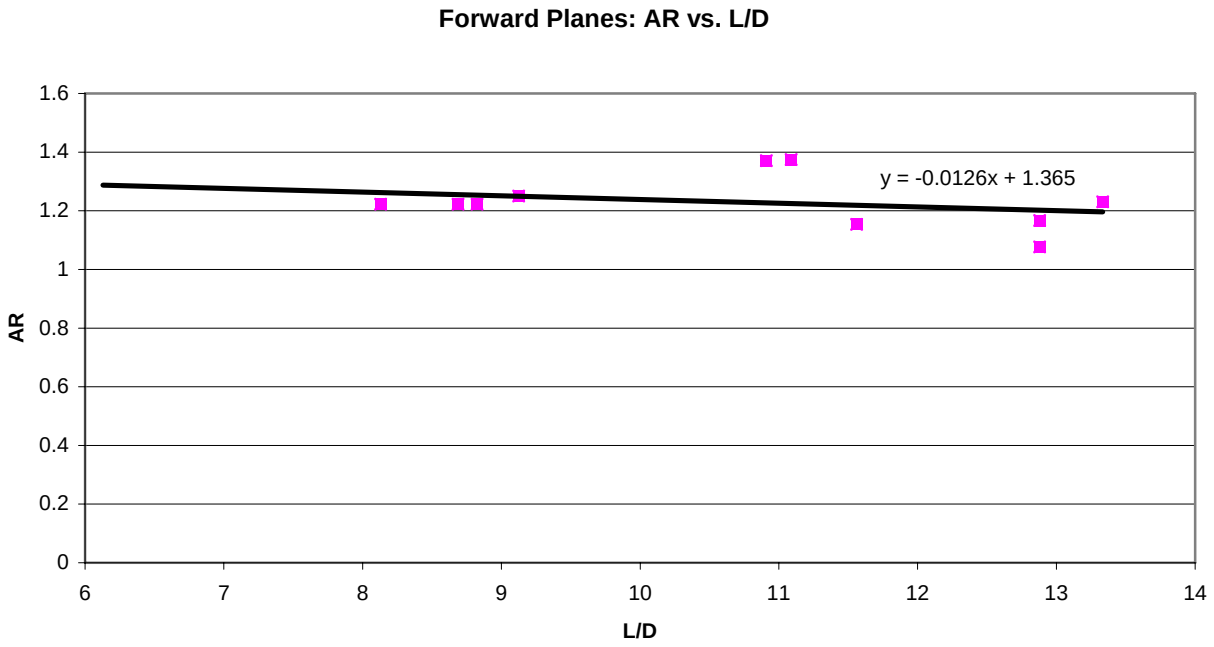

Figure B6. AR vs L/D for the forward planes.

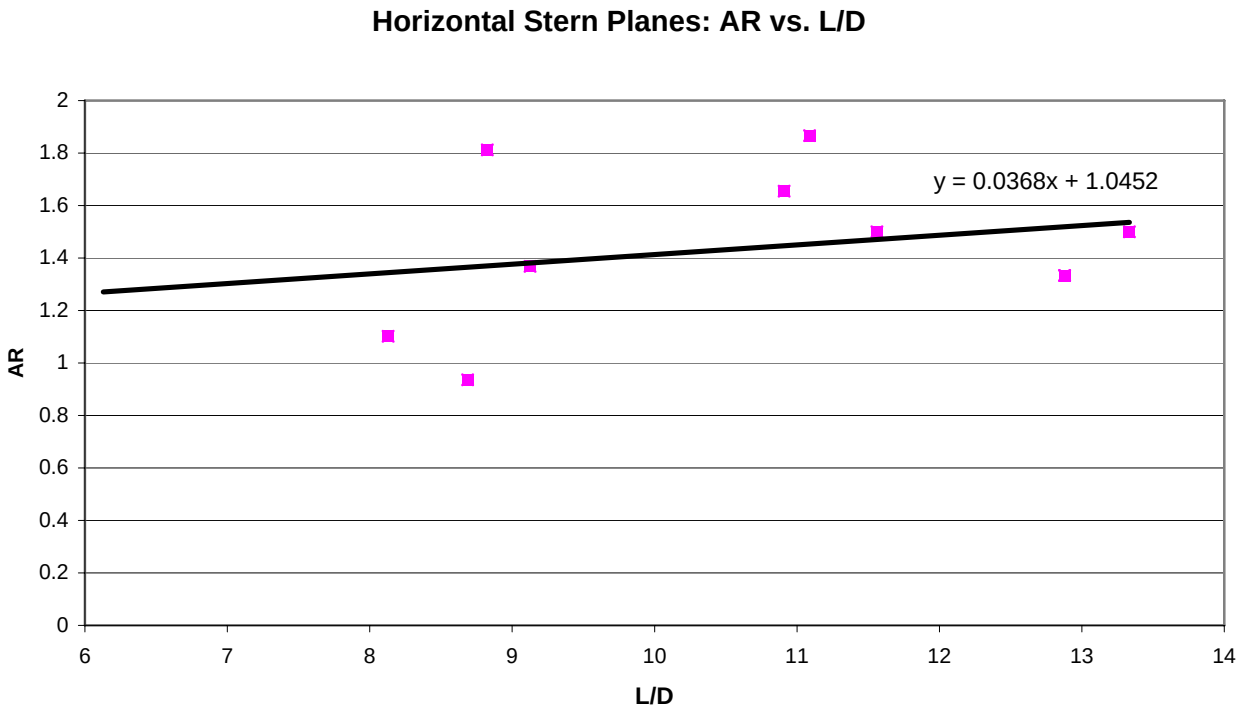

Figure B7. AR vs L/D for horizontal stern planes.

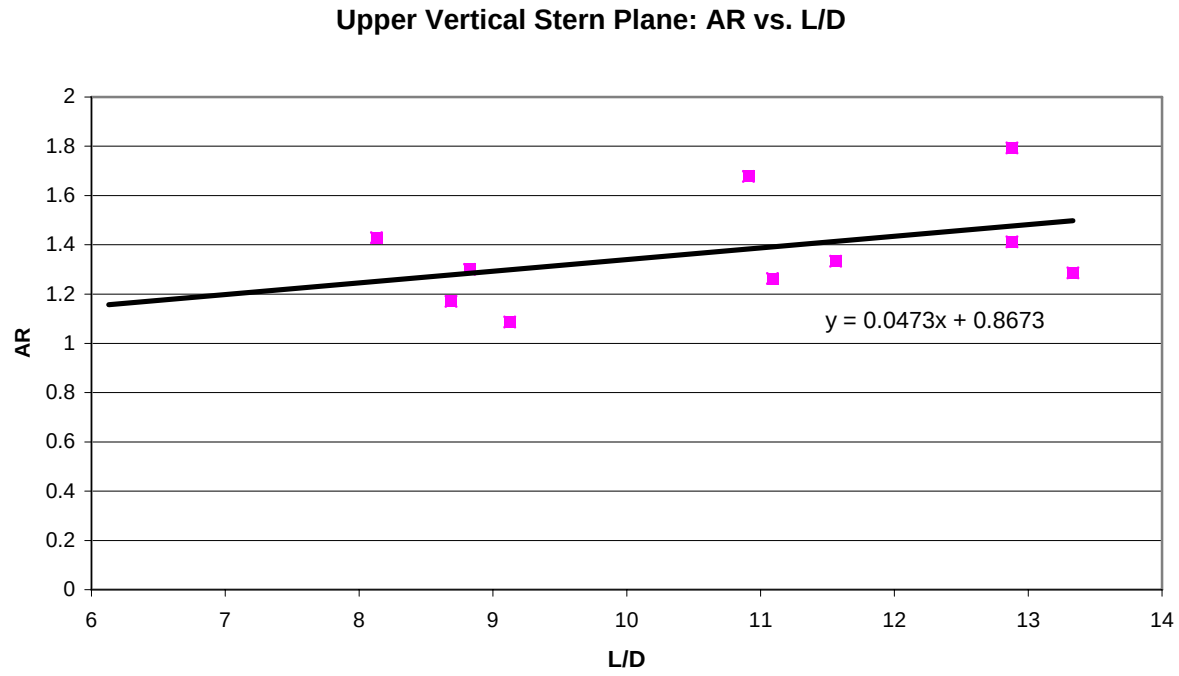

Figure B8. AR vs. L/D for upper vertical stern plane.

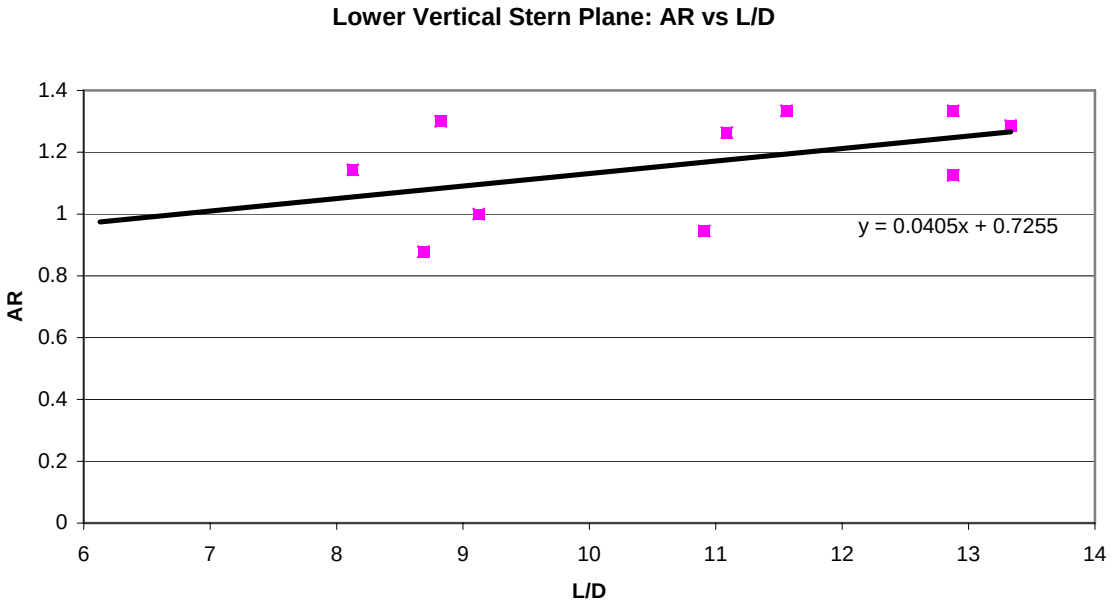

Figure B9. AR vs. L/D for lower vertical stern plane.

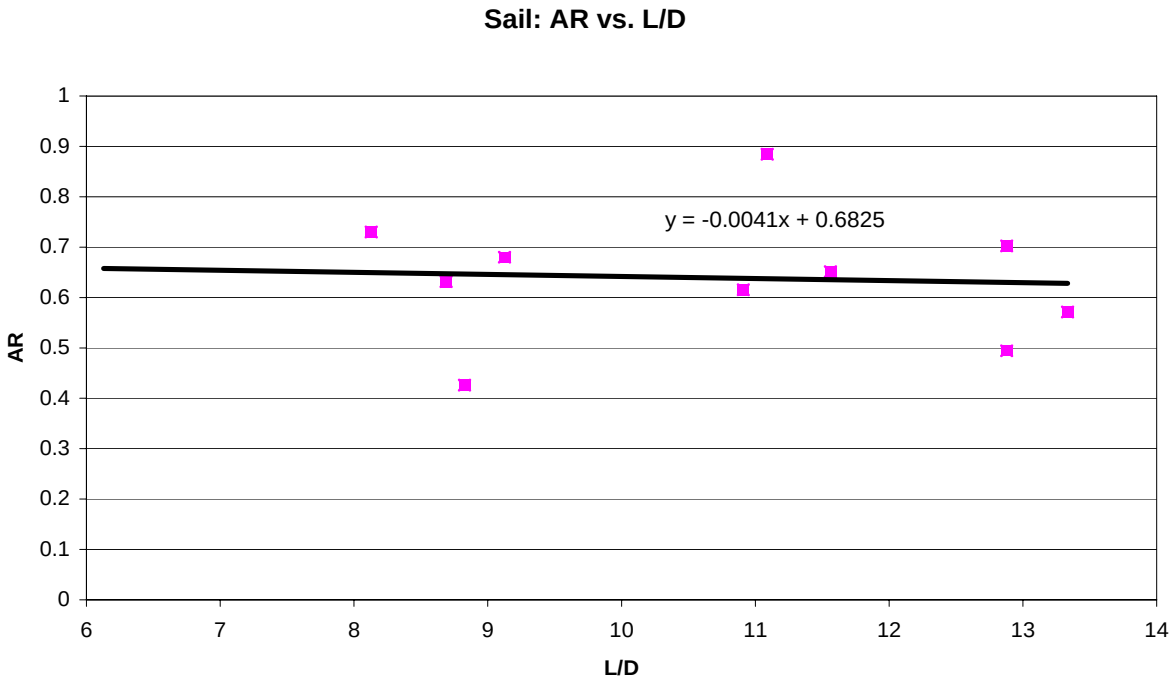

Figure B10. AR vs. L/D for the sail.

Non-Dimensional Delta Chord vs. Length to Diameter Ratio

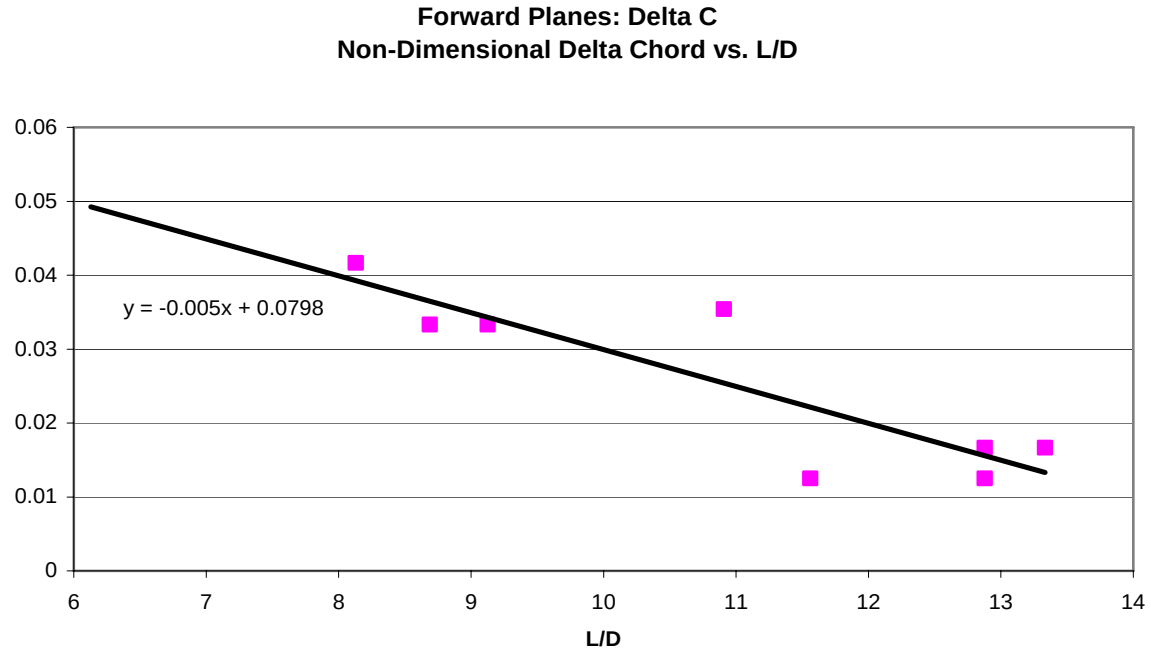

Figure B11. Non-dimensional delta chord vs. L/D for forward planes.

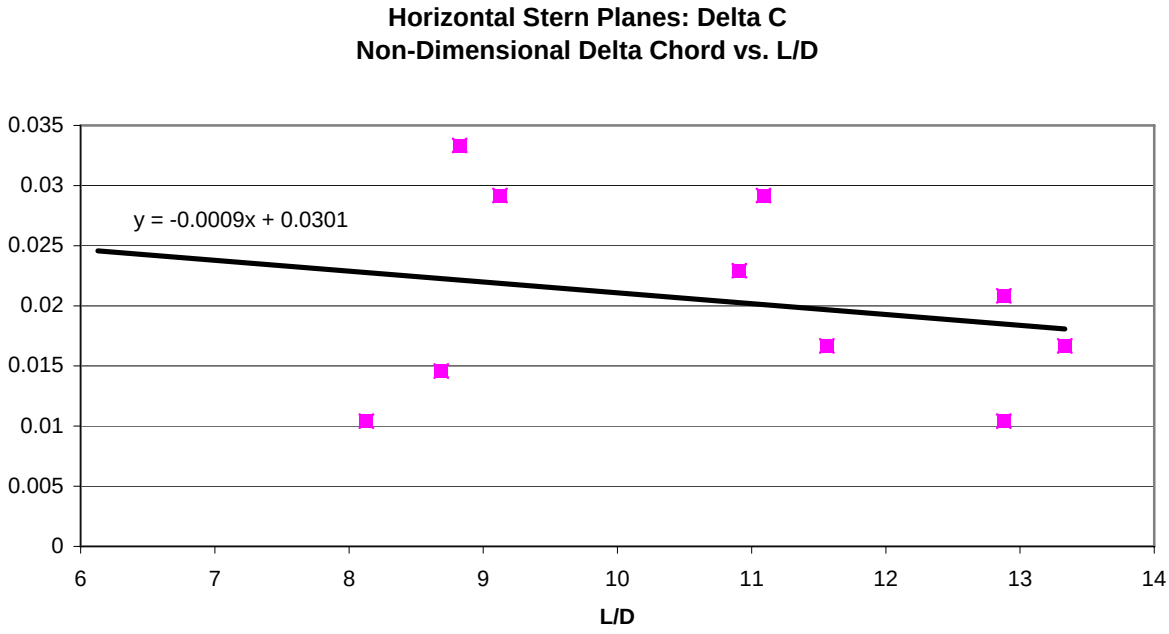

Figure B12. Non-dimensional delta chord vs. L/D for horizontal stern planes

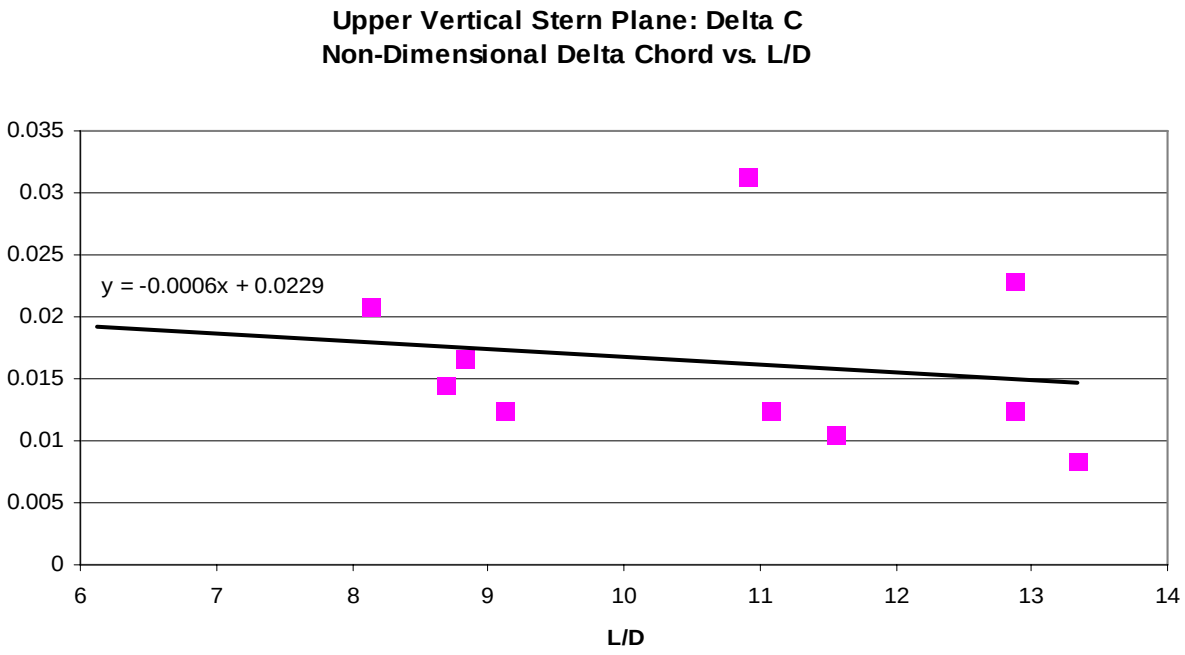

Figure B13. Non-dimensional delta chord vs. L/D for upper vertical stern plane.

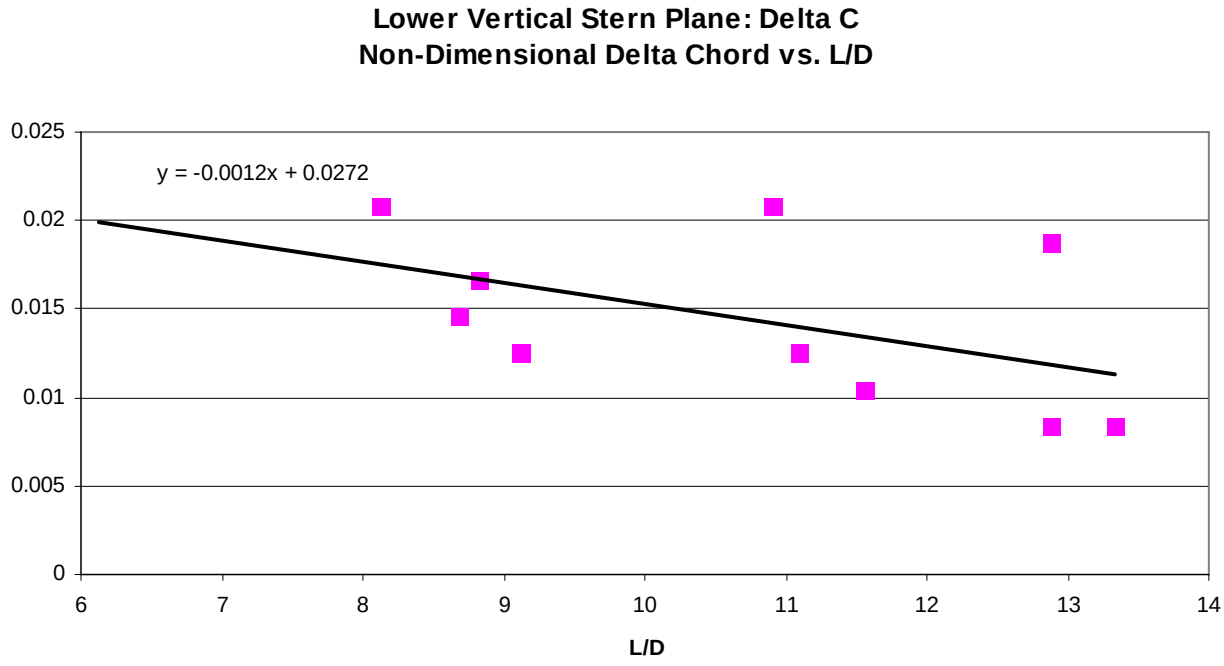

Figure B14. Non-dimensional delta chord vs. L/D for lower vertical stern plane.

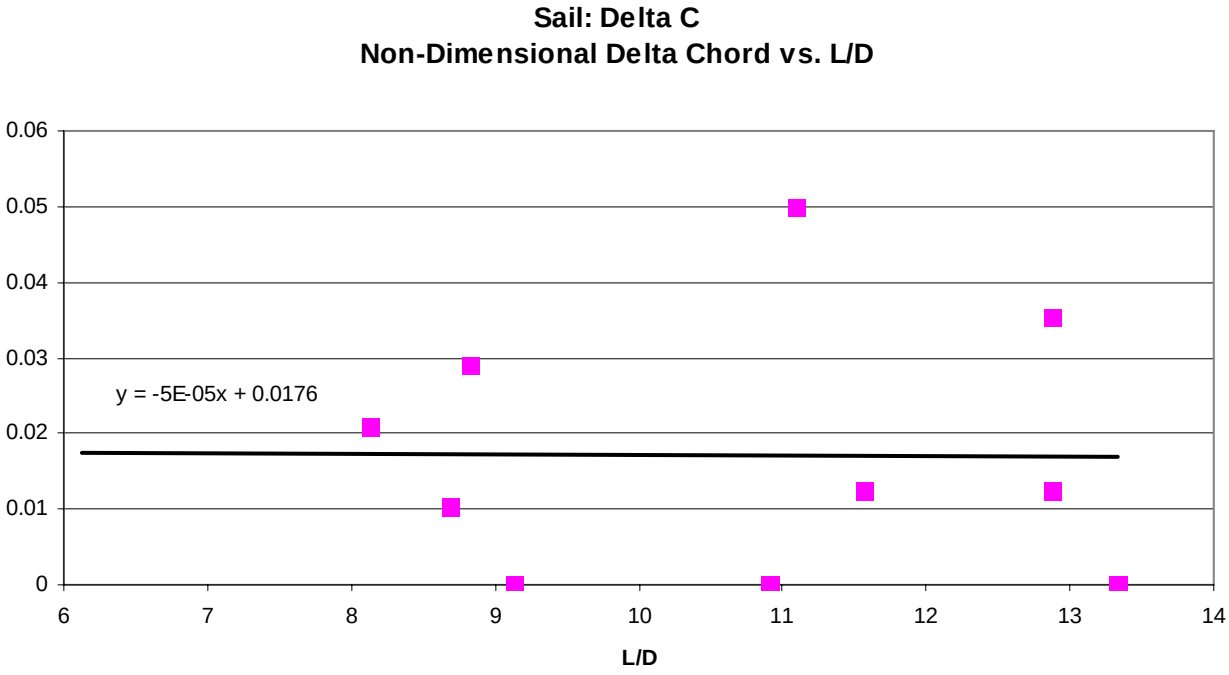

Figure B15. Non-dimensional delta chord vs. L/D for the sail.

VITAE

Education

Lisa Marie Minnick was born on May 1, 1982 in LaPlata, MD to Eileen and Thomas Minnick. She graduated from LaPlata High School in 2000. She earned a dual Bachelors of Science degree in Ocean and Aerospace Engineering from Virginia Polytechnic Institute and State University in May of 2004. Upon completion of her Bachelors degree Lisa stayed at Virginia Tech for her Masters of Science degree in Ocean Engineering.

Employment

Upon completion of her Masters degree Lisa will begin employment with the US Navy at the Carderock Division of the Naval Surface Warfare Center (NSWCCD). She will be working in the Maneuvering and Controls Division of the Hydromechanics Department.

Professional Affiliations

During Lisa's undergraduate and graduate career at Virginia Tech she was active in the Virginia Tech chapter of the Society of Naval Architects and Marine Engineers (SNAME) and American Society of Naval Engineers (ASNE). As an undergraduate she served as the Student Engineers' Council representative.

Lisa was also highly active in the Alpha Rho chapter of Phi Sigma Pi National Honor Fraternity. As an undergraduate she served on the executive board as Historian and Vice President of Internal Affairs.